VYSOKÉ UČENÍ TECHNICKÉ V BRNĚ
BRNO UNIVERSITY OF TECHNOLOGY

FAKULTA STROJNÍHO INŽENÝRSTVÍ
ÚSTAV PROCESNÍHO A EKOLOGICKÉHO INŽENÝRSTVÍ

FACULTY OF MECHANICAL ENGINEERING
INSTITUTE OF PROCESS AND ENVIRONMENTAL ENGINEERING

NEW ELEMENTS OF HEAT TRANSFER EFFICIENCY IMPROVEMENT IN SYSTEMS AND UNITS

NOVÉ PRVKY ZVÝŠENÍ EFEKTIVITY VÝMĚNY TEPLA V SYSTÉMECH A ZAŘÍZENÍCH

DIZERTAČNÍ PRÁCE
DOCTORAL THESIS

AUTOR PRÁCE
AUTHOR

Ing. VOJTĚCH TUREK

VEDOUCÍ PRÁCE
SUPERVISOR

doc. Ing. ZDENĚK JEGLA, Ph.D.

BRNO 2012

Abstract

Improved heat transfer efficiency leads to decrease in energy consumption which then results in lower equipment operational cost, reduced emissions, and consequently also lower environmental impact. However, common enhancement approaches such as adding fins or tube inserts may not always be suitable or feasible – especially in case of heat recovery from streams having a high fouling propensity. Since heat transfer rate depends also on flow field characteristics, fluid distribution, and fouling which can all be greatly influenced by the actual shapes of flow system components, several simplified models for fast and accurate enough prediction of fluid distribution as well as applications for shape optimization based on these models were developed. In addition, accuracy of one of the models was further increased by fine-tuning it using data obtained by evaluation of 282 flow systems in the fluid flow modelling software ANSYS FLUENT. The created applications can then be employed during the design of heat exchange units to improve their performance and reliability.

Keywords

flow distribution, fouling, heat transfer, shape optimization

Abstrakt

Zvýšení efektivity výměny tepla vede k poklesu spotřeby energie, což se následně projeví sníženými provozními náklady, poklesem produkce emisí a potažmo také snížením dopadu na životní prostředí. Běžné způsoby zefektivňování přenosu tepla jako např. přidání žeber či vestaveb do trubek ovšem nemusí být vždy vhodné nebo proveditelné – zvláště při rekuperaci tepla z proudů s vysokou zanášivostí. Jelikož intenzita přestupu tepla závisí i na charakteru proudění, distribuci toku a zanášení, které lze všechny výrazně ovlivnit tvarem jednotlivých součástí distribučního systému, bylo sestaveno několik zjednodušených modelů pro rychlou a dostatečně přesnou predikci distribuce a také aplikace pro tvarovou optimalizaci distribučních systémů využívající právě tyto modely. Přesnost jednoho z modelů byla dále zvýšena pomocí dat získaných analýzou 282 distribučních systémů v softwaru ANSYS FLUENT. Vytvořené aplikace pak lze využít během návrhu zařízení na výměnu tepla ke zvýšení jejich výkonu a spolehlivosti.

Klíčová slova

distribuce toku, přenos tepla, tvarová optimalizace, zanášení

TUREK, V. *New Elements of Heat Transfer Efficiency Improvement in Systems and Units.* Brno: Vysoké učení technické v Brně, Fakulta strojního inženýrství, 2012. 124 s. Vedoucí dizertační práce doc. Ing. Zdeněk Jegla, Ph.D.

I hereby declare that this thesis is the result of my own work and that all sources have been duly acknowledged.

Vojtěch Turek

I would like to express my gratitude to doc. Ing. Zdeněk Jegla, Ph.D., for supervising this thesis. His guidance, support, and friendly advice have been invaluable.

Special thank you is due to doc. Ing. Jiří Hájek, Ph.D., who provided many insightful comments and was always willing to help. His assistance during the CFD evaluations has been greatly appreciated.

I am grateful to prof. Ing. Petr Stehlík, CSc., whose numerous comments and suggestions were very helpful as well.

Last but not least, I would like to thank my family for their support during my studies and all my colleagues at the institute for creating an excellent working atmosphere.

Vojtěch Turek

Trademark Notice

The company and product names used in this thesis are for identification purposes only. All trademarks and registered trademarks are the property of their respective owners.

Contents

1

Introduction

Many processes involve exchange of thermal energy and as such require equipment capable of transferring heat from one medium to another. These heat exchange units – commonly called heat exchangers – can therefore be found not only in various industries from the chemical and petroleum ones through pulp and paper production to the food or beverage industries (condensers, evaporators, reboilers, heat recovery steam generators, etc.), but also in households (refrigerators, boilers, hot water radiators, air conditioners, heat pumps), transportation (HVAC and engine cooling systems), electronics (heat sinks for cooling of hot chips on printed circuit boards), and in many other areas. Since by improving heat transfer efficiency we can substantially decrease energy consumption, this will result in lower equipment operational cost, reduced emissions, and consequently also lower environmental impact.

In general, we must always start with the whole process in mind and first and foremost make sure that heat is utilized efficiently in the global sense. This involves heat transfer intensification in terms of a heat exchanger network (Klemeš and Varbanov, 2012), be it a grassroot design (Laukkanen et al., 2012) or a retrofit (Wang et al., 2012; Zhu et al., 2000). Methods such as process integration (Klemeš and Lam, 2011; Zhang et al., 2012) are of paramount importance as well and many tools are being developed for this purpose (see for instance Klemeš et al., 2009). Once this is done, we can proceed to analysis of possible improvements of heat transfer efficiency in individual heat exchange units. Here, heat transfer can be further enhanced in a number of ways from which the most common technique probably is adding fins to heat transfer surfaces. These can be of various shapes and sizes and their effect has been investigated both theoretically and experimentally. As for the former approach, e.g. Torabi and Aziz (2012) studied T-shaped fins, Sabbaghi et al. (2011) semi-spherical fins, and Kundu and Lee (2012) or Sharqawy et al. (2012) provided models of fins with variable cross-sections. A relatively complex non-linear model dealing with temperature-dependent heat transfer coefficient was described by Khani et al. (2009). Islam et al. (2009) or Liang and Wong (2010), on the other hand, investigated constant cross-section fins experimentally.

By adding fins we primarily increase heat transfer area, but increasing turbulence results in enhanced heat transfer as well. This can be achieved for example by using corrugated (Hasan et al., 2012; Pethkool et al., 2011), dimpled (García et al., 2012), wavy (Castellões et al.,

2010; Guzmán et al., 2009), twisted (Tan et al., 2012), or otherwise deformed tubes (Tang and Zhu, 2012). In plate-type heat exchangers, a vast array of different plate corrugation patterns (Arsenyeva et al., 2011; Yin et al., 2012) and plate-fin designs (Fernández-Seara et al., 2012; Sheik Ismail et al., 2010) are used. Turbulence can also be increased by various types of tube inserts – wire mesh packings (Dyga and Płaczek, 2010), plain wire coils (Jafari Nasr et al., 2010), triangular cross-section wire coils (Gunes et al., 2010), twisted wire brushes (Naphon and Suchana, 2011), helical tapes with central supporting rods (Bhuiya et al., 2012), plain twisted tapes (Bas and Ozceyhan, 2012), twin twisted tapes (Eiamsa-ard et al., 2010a), twisted tapes with delta-winglets (Eiamsa-ard et al., 2010b), or twisted tapes of other shapes (Rahimi et al., 2009; Wongcharee and Eiamsa-ard, 2011b). Vortex generators have an analogous effect, as verified for example by Cheng et al. (2012), He et al. (2012), or Du et al. (2013). We must, however, consider the fact that enhanced surfaces, flow channel inserts, and other similar design modifications are not suitable if working fluid has high fouling propensity.

Another way of enhancing heat transfer is by using nanofluids, i.e., heat transfer fluids enriched with nanoparticles made of silicon dioxide (Timofeeva et al., 2011), aluminium oxide (Noie et al., 2009; Sundar and Sharma, 2010), copper (Ahmed et al., 2011), or cupric oxide (Wongcharee and Eiamsa-ard, 2011a). Elements such as multi-walled carbon nanotubes (Lotfi et al., 2012) can be added into the fluid as well. We could even employ oscillatory flows (Cheng et al., 2009; Lambert et al., 2009), but this approach is not common due to the detrimental effect of vibrations on the equipment.

The above methods of local heat transfer efficiency improvement, however, may not always be suitable or feasible – especially in case of heat recovery from polluted streams (waste-to-energy plants etc.; see e.g. Stehlík, 2011). Nevertheless, efficiency depends also on the actual character of flow in the unit which, in turn, significantly affects fouling (Jegla et al., 2010; Kukulka and Devgun, 2007) and in consequence the overall heat transfer coefficient. Additionally, since heat transfer rate is largely dependent on the available heat transfer area, massive flow parallelisation inside heat exchangers is very common. Therefore, with respect to the fact that flow field characteristics, fluid distribution, and fouling can be greatly influenced by the actual shapes of flow system components (splitting and collecting manifolds, ducts, etc.), in this thesis we will deal with shape optimization of such components. As will be clear later on, this should also increase equipment reliability and lower maintenance cost.

1.1 Goals and Overview

The aim of this thesis is to provide mathematical models of flow systems applicable in shape optimization algorithms and also computer implementations of these models. Obviously, such models must be simple and easy to evaluate yet robust and accurate enough otherwise either the results would be useless or the optimization times necessary to obtain them would be unacceptably long.

We will first discuss common types of heat exchange units (Chapter 2) and then we will proceed to simplified modelling of fluid flow and analysis of flow distribution (Chapter 3). Three different mathematical models and optimization tools based upon them will be presented. We will also shortly mention flow instabilities and backflow and, via two industrial examples, discuss the relationship between fouling and flow field characteristics. In addition, since heat transfer efficiency is closely linked to synthesis of heat exchanger networks, a very brief overview of this problem will be provided as well (Appendix A).

2

Heat Exchange Units

Heat exchangers, being one of the most widely used process equipment, transfer heat between two or more process streams and are essential to virtually any process plant. For a two-stream heat exchanger, one of the streams requires heating or cooling while the other is either also a process stream that needs cooling or heating, respectively, or it may be a utility stream. Steam is routinely used as a hot utility stream. As for coolants, water or air are commonly utilized. Considering multiple-stream exchangers, these are becoming more and more common due to their higher efficiency and overall compactness (Lunsford, 1996).

There are many different types of heat exchangers and it is customary to call units serving specific purposes differently, e.g. economizers, condensers, fired heaters, reboilers, evaporators, superheaters, etc. Since each of them has its advantages and disadvantages, selection of a suitable type and subsequent design of such a unit largely influence its reliability and service life. This is especially true for high-temperature and fouling-intensive applications.

2.1 Classification of Heat Exchange Units

According to Hewitt et al. (1994), heat exchangers can be classified using four different criteria, namely the way in which heat is transferred from one fluid to the other, flow arrangement, geometry of construction, and heat transfer mechanism.

Classification based on the way in which heat is transferred from one fluid to the other produces three sub-classes. In recuperative heat exchangers, fluids are separated by a relatively thin solid wall and thus cannot mix. Heat then passes from one fluid through the wall into the other fluid. Regenerative heat exchangers, on the other hand, contain a matrix that is either fixed of rotary. Heat is temporarily transferred from the hot stream into the matrix which, at a later time, heats the cold stream. Although fluids are separated, limited leakage through seals may be observable if the matrix is not fixed. In direct-contact heat exchangers, no solid heat transfer surface separating fluids is present. Both fluids are being

mixed (e.g. when water is injected into steam or hot gas bubbles through cooler liquid) and therefore heat and mass transfers may occur at the same time.

Classification by flow arrangement yields four sub-classes. Velocity vectors have both the same direction when the flow is concurrent while for countercurrent flow the directions are opposite (see Figure 2.1). In cross-flow, one fluid flows perpendicular to the other. Nevertheless, in many heat exchangers the arrangement is a combination of the above rather than pure concurrent, countercurrent, or cross-flow.

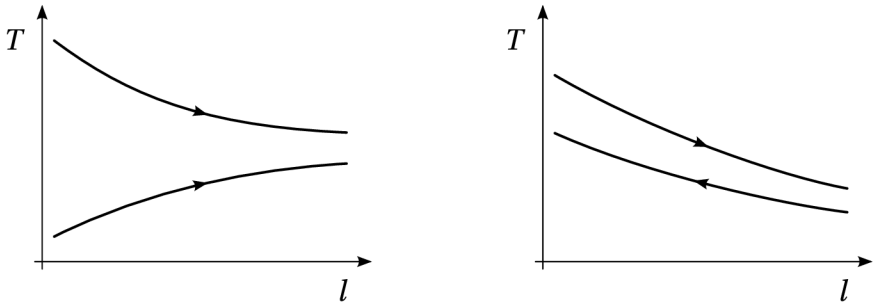

(a) concurrent (b) countercurrent

Figure 2.1. Typical temperature profiles for concurrent and countercurrent flow arrangements

Classification according to geometry of construction contains three sub-classes. Here we have units with tubes, plates, or enhanced heat transfer surfaces (e.g. tubes with fins).

Classification using heat transfer mechanism is rather straightforward and produces three sub-classes as well – units in which no phase change occurs (single-phase convection on both sides), units in which only one of the fluids changes phase (single-phase convection on one side, two-phase convection on other side), and units in which both fluids change phase (two-phase convection on both sides). The latter two types therefore involve evaporation or condensation.

In the following text, we will discuss conventional heat exchange units in a bit more detail. Special (made-to-measure) heat transfer equipment will be mentioned as well. It will be clear from functioning principles of all these units that their efficient and reliable operation is – among other factors – conditioned by uniform flow distribution. What is more, since flow characteristics such as velocity field greatly influence deposition of particles inside an exchanger's flow system, by adjusting distribution we can also significantly reduce fouling rate (industrial examples will be discussed later in Section 3.5). This, of course, prolongs service life and brings substantial savings due to lower frequency of service shutdowns.

2.2 Conventional Heat Exchange Units

Conventional heat exchange units provide the benefit of standardized and well-tested designs for which operating conditions guaranteeing reliable operation are available. Such units are being manufactured in large quantities according to specifications given e.g. by Tubular

Exchanger Manufacturers Association, Inc. (2007) and because no additional research and development is necessary, they also tend to be relatively inexpensive. The general trend therefore is to first evaluate whether a conventional heat exchange unit can be used for a given purpose and only if this is not possible then a new unit is designed.

2.2.1 Tubular Heat Exchangers

A tubular heat exchanger can either consist of a smaller-diameter tube mounted inside a larger-diameter tube ("double-pipe exchanger", see Figure 2.2) or, more commonly, a tube bundle inside a shell ("shell-and-tube exchanger", see Figure 2.3). Thus, heat transfer surfaces are plain or enhanced tubes. Additionally, shell-and-tube heat exchangers can contain multiple-pass tube bundles, i.e., for double-pass we have a bundle of U-tubes, for triple-pass the tubes in the bundle bend twice, etc. Multiple-pass shells are common as well. Baffles, either segmental or doughnut and disc ones, present in the shell direct fluid flow in shell-side, support the tubes, and limit possible tube vibrations.

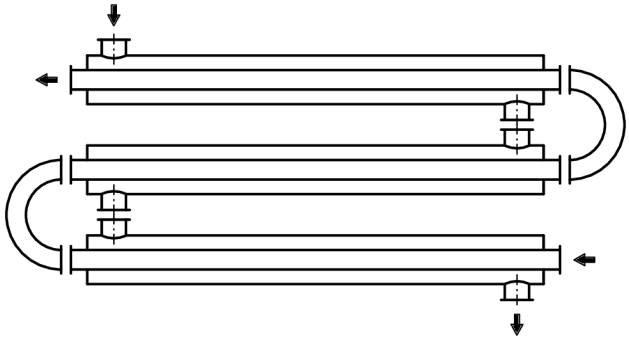

Figure 2.2. Countercurrent double-pipe heat exchanger

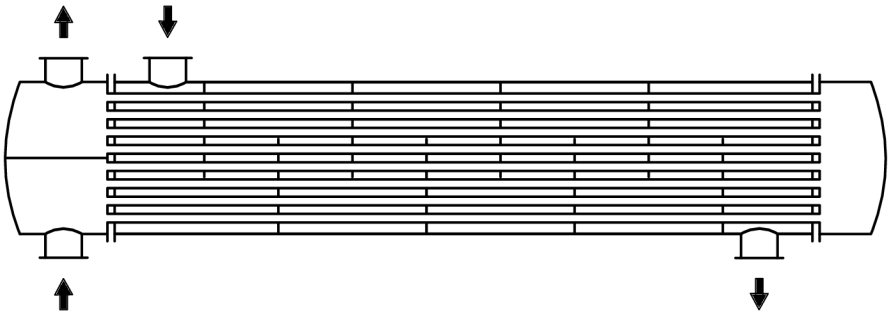

Figure 2.3. Segmentally baffled one-pass shell and two-pass tube shell-and-tube heat exchanger

Flow in shell-side can be improved by suitable adjustments of baffle design as is done in helixchangers (Král et al., 1996) – see Figure 2.4. Such an arrangement also increases the heat transfer rate vs. pressure drop ratio, reduces leakages (baffle bypass effect), flow-induced vibrations, and limits creation of stagnation zones thus decreasing fouling rate (CB&I Lummus Technology, 2012).

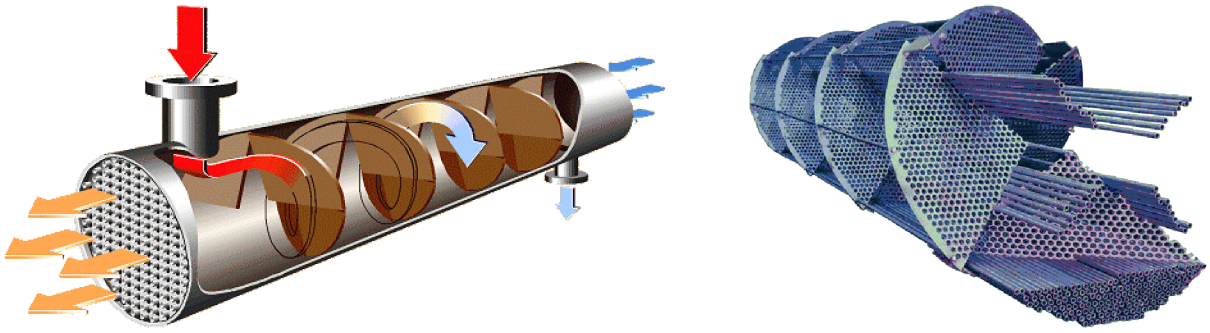

(a) scheme (b) tube bundle

Figure 2.4. Helixchanger: shell-and-tube heat exchanger with helical baffles (CB&I Lummus Technology, 2012, reprinted with permission)

Another sub-type of shell-and-tube heat exchangers is the lamella exchanger employing hollow lamellae instead of tubes while no baffle plates are present. This, combined with pure countercurrent and highly turbulent flow, guarantees a high heat transfer rate and low pressure drop (Hewitt et al., 1994, Sec. 4.2.5).

It is obvious that a smaller tube diameter will yield higher heat transfer surface area. The lower limit on tube outer diameter, however, is around 20 mm to ensure cleaning can be performed (Hewitt et al., 1994, Sec. 6.2.3). Considering shell-side, the minimum recommended tube pitch is approximately 1.25 times the tube diameter (Hewitt et al., 1994, Sec. 6.2.5). As for thermal expansion, it can be dealt with by using a U-tube bundle, a toroidal expansion joint on the shell, or a floating head.

Generally, pure countercurrent flow arrangement is preferred (Hewitt et al., 1994, sec. 3.7). If necessary, heat transfer can be intensified by using twisted tubes (see Figure 2.5), twisted tube inserts, enhanced tube surfaces, etc. Of course, such enhancements should be avoided when fouling is a real possibility.

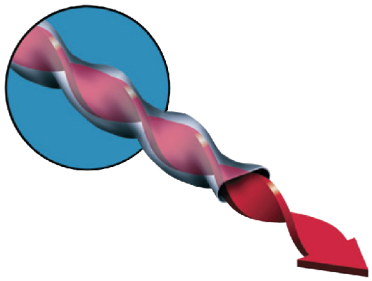

Figure 2.5. Twisted tube (Koch Heat Transfer Company, LP, 2012, reprinted with permission); this design is reported to improve shell-side distribution and increase tube-side heat transfer coefficient by 40 % compared to plain tubes

The advantages of tubular exchangers are the ease of manufacturing and maintenance and the possibility of using tube enhancements. As for disadvantages, these units provide relatively small heat transfer surface area per unit volume.

2.2.2 Plate Heat Exchangers

In plate heat exchangers fluids flow alternately between stacked plain or cross-corrugated plates that can be sealed and held together in two different ways. Either gaskets are placed near the plate edges as shown in Figure 2.6 and the stack is held together by a frame or the plates are brazed or welded thus forming a single element. Spiral heat exchangers (see Figure 2.7), being fundamentally identical, generally contain only two coiled plates.

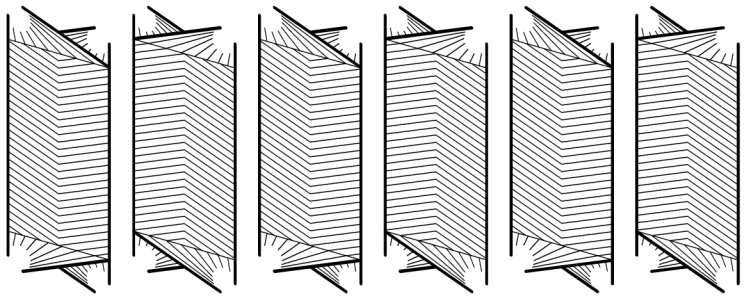

Figure 2.6. Gasketed plates; flow directions of hot and cold fluids are marked by arrows and gaskets by a thick line (the two rightmost plates are end plates – one for the hot fluid and one for the cold fluid)

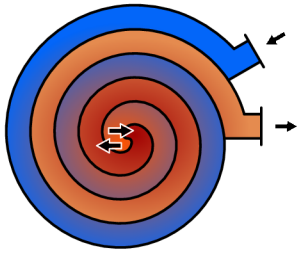

Figure 2.7. Cross-section of a spiral heat exchanger – hot stream inlet and cold stream outlet are near the exchanger axis while cold stream inlet and hot stream outlet are on the outer wall

With plate exchangers we are able to reach very high compactness, that is, a very large heat transfer area with a small exchanger footprint. Also, heat transfer tends to be more efficient than in shell-and-tube exchangers due to more complex flow passage geometry leading to higher degree of turbulence (Hewitt et al., 1994, Sec. 7.2.1). Since flow arrangement of these heat exchangers can be considered to be almost pure countercurrent, with a certain temperature difference we get higher heat duty than for a shell-and-tube exchanger under equivalent conditions. Alternatively, to get the same heat duty as in case of a shell-and-tube exchanger a lower temperature difference is necessary.

The gasketed plate-and-frame variant is easy to clean and highly scalable – we can easily append additional plates or remove some of the existing ones. These advantages, however, come with the cost of restricted pressure and temperature ranges. Furthermore, we are limited by gasket/fluid compatibility since otherwise the gaskets may deteriorate. Of course, should the plates be brazed or welded together then we get a compact high-pressure and high-temperature heat exchanger capable of working with almost any fluid, but without the added benefits of scalability and easy cleaning. If only one of the fluids is incompatible with

the gasket material, partially welded plate exchangers provide a reasonable trade-off between scalability and usability. Here, welded pairs of plates are stacked and sealed with gaskets. The aggressive fluid then flows through the welded pairs while the other, less aggressive fluid flows through gasketed channels. Should both fluids be aggressive, special materials such as graphite, ceramics, or polymers can be employed, but then the pressure and temperature limitations apply again.

Plate-and-shell heat exchangers, consisting of a stack of welded circular cross-corrugated plates fitted into a shell, originate in the concept of a shell-and-tube heat exchanger applied to plate-type exchangers. One of the streams then flows inside the welded plate pairs and the other between these pairs while being directed by shell baffles. Similarly as in case of welded plate heat exchangers, high-pressure and high-temperature streams can be treated in these units. What is more, thermal cycling is not an issue here due to thermal expansion of the plate pack being possible inside the shell. In another but similar type of welded compact heat exchangers, a single plate pack consisting of many large plates welded together is placed into a cylindrical shell.

Plate-fin heat exchangers are built by stacking fins separated by partition plates. Commonly, fins are made of aluminium, steel, or titanium and are plain, serrated, perforated, or wavy. The stack is then welded or brazed together at the edges thus making the exchangers capable of withstanding significant pressures and temperatures.

As for extreme operating conditions (up to 65 MPa and 900 °C; Heatric Ltd., 2012), printed-circuit heat exchangers can be employed. These consist of diffusion-bonded plates with semi-circular flow passages usually between 0.5 and 3.0 mm deep being etched into them (Heatric Ltd., 2012). In this case, various combinations of countercurrent and cross-flow arrangements can be obtained.

Fouling is a serious issue in all the above heat exchangers due to small plate spacing or cross-sectional areas of the flow passages. This must be considered especially if the exchanger cannot be dismantled for cleaning. Other disadvantages of plate-type heat exchangers are the possibility of leakages between plates and relatively high pressure drop (Hewitt et al., 1994, Sec. 8.3.5).

2.2.3 Air-Cooled Heat Exchangers

Air-cooled heat exchangers, commonly employed e.g. for condensing vapours, have several major advantages. They are cheap and very simple, thus little maintenance is necessary. No intricate piping or pumping system is required and, in most cases, fouling or corrosion do not occur at a significant rate (Hewitt et al., 1994, Sec. 9.2.1). On the other hand, there are disadvantages that must be considered, namely heat transfer coefficient being relatively low and hence these exchangers tend to be larger (Hewitt et al., 1994, Sec. 9.2.2). We must also bear in mind that embedded fans may be noisy and that temperature difference available for cooling may be lower in some locations due to warmer climate.

Figure 2.8 shows two common arrangements of these exchangers – forced draft and induced draft. In both cases, air passes over tubes in a tube bundle in which cooled fluid is flowing. These arrangements can be either horizontal as shown in the figure, vertical, or inclined. Additionally, tubes may be finned to enhance air-side heat transfer. With induced draft we obtain a more uniform air distribution while with forced draft less electrical power is required by the fan (cooler air has lower density; Hewitt et al., 1994, Sec. 9.3.1.1). If there is no fan then the exchanger works with natural draft – a cooling tower is a typical example of

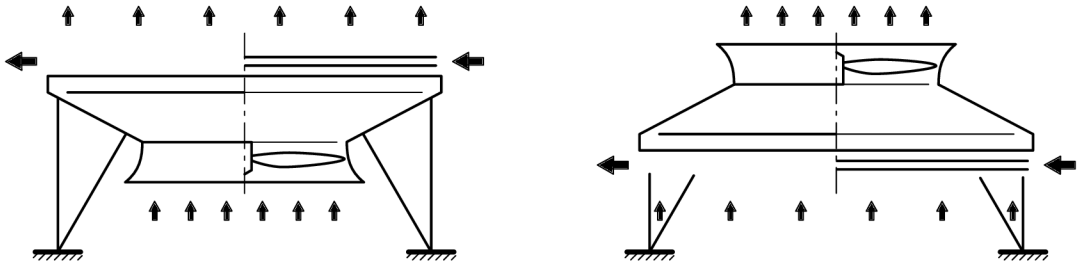

(a) forced draft (b) induced draft

Figure 2.8. Forced and induced draft arrangements of air-cooled heat exchangers

such a design. Driving force for air flow is then given by density difference and therefore the construction must be tall enough.

Tube bundles usually consist of several rows of tubes either connected to common headers (a splitting and a collecting manifold) or forming a single coil. In some cases a set of several smaller coils connect the inlet and outlet common headers. From this it is obvious that the headers must be designed properly and fluid velocity inside the flow system must be large enough to prevent fouling.

2.2.4 Evaporators and Condensers

Both evaporators and condensers are units used when a phase change is required from liquid to gas or from gas to liquid, respectively. Evaporators can also be employed for instance to crystallize or concentrate a solution. Additionally, unlike for condensers, a few other names for evaporation units exist, e.g. vapour generators which generate pure fluids or revapourize liquefied gas, chillers used for cooling of process streams, etc.

Design of these units can in many cases be almost identical to shell-and-tube heat exchangers discussed in Section 2.2.1 (as can be seen in Figure 2.9 showing a horizontal shell-side evaporator) or plate-type heat exchangers from Section 2.2.2. In film evaporators a thin falling or climbing liquid film is present on heated surfaces. Rate of evaporation may be increased by

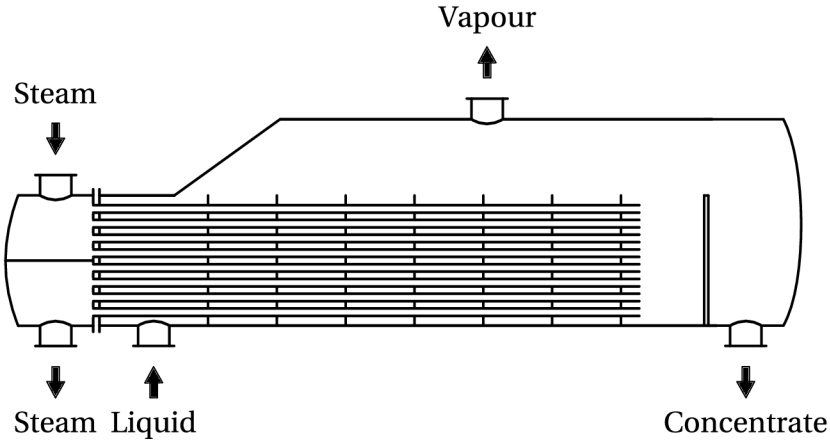

Figure 2.9. Horizontal shell-side evaporator (sometimes also called kettle reboiler)

increasing heated surface temperature, by reducing (partial) pressure of the vapour which reduces liquid surface temperature, or by increasing the film heat transfer coefficient (Hewitt et al., 1994, Sec. 15.3.2). For correct functioning of any falling film evaporator, a distribution section at the top of the bundle must maintain uniform and sufficient film thickness so that it does not break into several individual streams. As for climbing film evaporators, these do not require much care except for adequate inlet flow rate of the liquid to be evaporated. Since boiling occurs only along a very limited length of the lower tube bundle end, such evaporators are suitable for concentrating heat sensitive liquids.

In case of evaporators in which boiling is prevalent, e.g. short-tube, basket-type, and long-tube evaporators, or the kettle reboiler from Figure 2.9, two-phase mixture exits into a larger space or a vessel where the two phases are separated (Hewitt et al., 1994, Sec. 15.4.1).

Condensers serve exactly the opposite purpose – they are necessary when vapour from a distillation column, a turbine exhaust stream, a reactor effluent, or the like must be converted to liquid. Condensate can then develop in four different ways, namely by forming a continuous liquid film on a cooled heat transfer surface ("film-wise condensation"), by forming droplets if wettability of the heat transfer surface is low ("drop-wise condensation"), homogeneously in a bulk vapour caused by decrease in temperature of increase in pressure ("homogeneous condensation"), or by producing two separate liquid phases ("immiscible-liquid condensation") (Hewitt et al., 1994, Sec. 16.2).

Direct-contact condensers in which coolant is injected into the vapour stream or vice versa are usually used when corrosive or fouling streams pass through the equipment (Hewitt et al., 1994, Sec. 17.3.5). Air-cooled condensers are virtually the same as air-cooled heat exchangers described in Section 2.2.3. As for plate-type condensers, these are less common but, construction-wise, they are identical to the respective plate-type heat exchangers (see Section 2.2.2). A sample shell-and-tube condenser is shown in Figure 2.10.

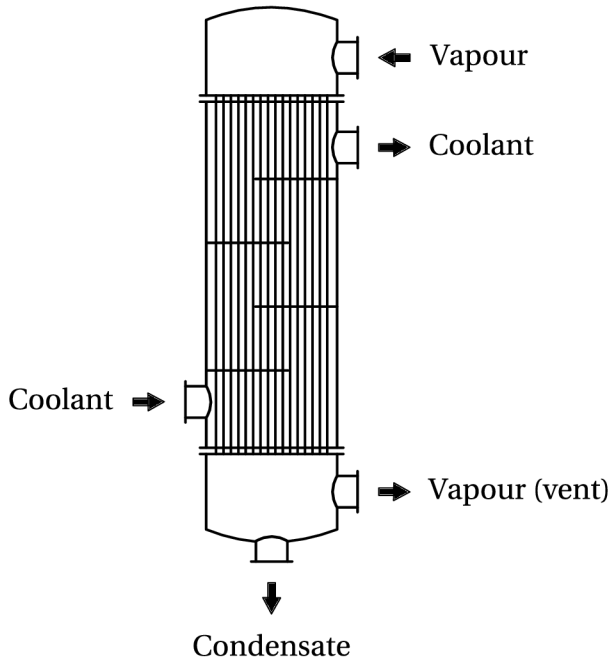

Figure 2.10. Vertical tube-side condenser

2.2.5 Fired Heaters

Fired heaters are equipment used for heating of process streams by flue gases produced during combustion of gaseous, liquid, or solid fuels. These units operate under high temperatures and can withstand high fluid pressures. Usually, they consist of a refractory lined chamber containing burners and tube banks through which flows the heated fluid. They are routinely used in the petroleum industry for cracking, fractionation, and high-temperature processing. In some plants they are also utilized for reheating of an auxiliary hot stream which is then fed into regular exchangers (shell-and-tube etc.) heating fluids that are prone to deterioration under higher temperatures common in radiant and convection sections.

In these units, heat is transferred into the tubes by radiation, reradiation, and convection. The (re)radiation heat transfer rate then depends on emissivity of the surface of the tubes, emissivity of the gas, and on relative size of the radiant chamber (Hewitt et al., 1994, Sec. 2.4). It is obvious that sufficiently long fluid residence time must be ensured while avoiding excessive heating that may lead to equipment damage, increased fouling rate, and fluid degradation. A typical vertical cylindrical fired heater is shown in Figure 2.11, however, cabin and box fired heaters with differently shaped or placed tube coils and sometimes rectangular cross-section of the radiant chamber are common as well. Possible design modifications for improved heat transfer efficiency were discussed e.g. by Jegla (2008) or Tucker and Ward (2012).

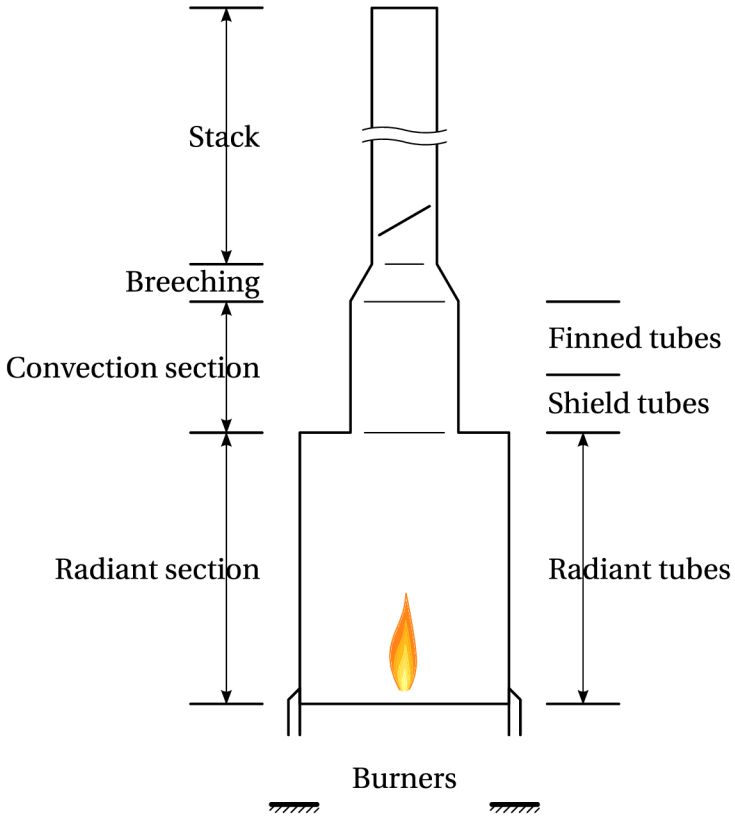

Figure 2.11. Vertical cylindrical fired heater

2.3 Special Heat Exchange Units

In situations when common heat exchangers cannot be used or are not sufficient considering the achievable heat duties, new heat exchange units must be designed. Specific conditions under which the new exchanger will operate must then be taken into account to ensure low-maintenance and reliable operation. Also, tools such as computational fluid dynamics, virtual prototyping, or optimization can provide valuable information leading to substantial design improvements.

Figure 2.12 shows a sample made-to-measure channel-type recuperator for high temperature applications. This exchanger is a part of a waste incineration unit in a pulp and paper production plant and is used for preheating of fluidizing and combustion air by flue gas. The six pairs of headers visible at the top of the exchanger feed cold air into and collect hot air from U-tube banks inside the shell. Due to the fact that uniform air distribution into U-tubes of each individual bundle is desirable, shape optimization of these headers is necessary (see Section 3.4.3).

Figure 2.12. Made-to-measure heat exchanger for preheating of fluidizing and combustion air (Stehlík, 2011, reprinted with permission of EVECO Brno, Ltd.)

2.4 Heat Recovery Systems

In general, the aim is to maximize heat utilization within a process or a group of processes and thus lower energy consumption due to external heating or cooling. Hence, heat recovery is closely linked to synthesis of heat exchanger networks (see e.g. Kemp, 2006, Chap. 4; a short description of the issue is also available in Appendix A) which, for a known set of hot and cold process streams, finds optimum placement of heat exchangers and their heat duties. Nonetheless, suitable heat exchanger types must still be selected and each of them must then be carefully designed to make sure the network will perform optimally.

Considering individual units, a wide range of equipment is available for recovery of waste heat from process streams. Since their main uses are preheating of combustion or fluidizing air by hot flue gases and heating of chemical reactor feeds by hot effluents, particular attention must be paid to likely problems such as high-temperature corrosion, fouling, and condensation of acidic compounds that may be present in the hot stream. In any case, heat recovery systems usually consist of a shell and a tube bank with plain or finned tubes and are designed to be able to operate under high temperatures so that extraction of heat from flue gases is possible.

Plain tube banks with tubes made of stainless steel are prevalent in both gas/gas and gas/liquid applications while flat stainless steel tubes are employed to obtain a more compact solution. Should the equipment operate under high temperatures, a higher-grade corrosion-resistant stainless steel is used. The same applies if a corrosive fluid flows through the system with the exception of lower temperatures when tubes made of glass (up to 250 °C) or PTFE/PVC-C (up to 100 °C) are preferred (Hewitt et al., 1994, Sec. 4.2.8). If plate-type banks are chosen then the plates are widely-spaced with straight-through flow passages for easier cleaning. Also, sometimes the units are modular which introduces the benefit of scalability and lowers capital cost. Another advantage of a modular design is the possibility to heat several streams to required temperatures at the same time.

2.4.1 Heat Recovery in Waste-to-Energy Applications

The above mentioned concept is characteristic of regular process plants. In waste-to-energy (WTE) process plants, however, we must take their specific requirements and limitations into account. First of all, the amount and type of waste to be incinerated must be considered including combustion regime of the burner (oxidation or gasification). The reason is simple – as was demonstrated by Bébar et al. (2002), operation in gasification regime produces less flue gas of the same temperature at the exit from an after-burner chamber than if the burner operated in oxidation regime. In other words, the regime determines the temperature and flow rate of the single hot process stream. Also, a narrow temperature range is required by each flue gas cleaning method (wet scrubbing, dry/semi-dry scrubbing, removal of heavy metal oxides, etc.) to be effective, thus affecting temperature range available for heat recovery. This particular issue was studied by Pařízek (2009). As for design and heat transfer efficiency improvements, these were discussed for example by Hájek (2008) or Stehlík (2011).

Since, by default, there are virtually no cold process streams, project engineers usually incorporate production of steam (which can be sold to an external consumer or used to generate electricity), preheating of combustion air if necessary, etc. Essentially, the selected set of cold process streams depends on the needs of waste incineration plant operator and local demand for heat.

Another issue that must be dealt with here is that flue gas has a high fouling propensity and contains large amounts of aggressive compounds. Using heat transfer equipment that is difficult to clean or contains enhanced surfaces is therefore undesirable.

2.4.2 Common Configurations of Industrial Heat Recovery Units

Heat recovery units used in industrial applications can be as simple as a single cross-flow heat exchanger heating supply air by extract air or as complex as a ten-exchanger heat recovery steam generator consisting of a high-pressure and intermediate-pressure super-heaters,

evaporators, and economizers, low-pressure super-heater and evaporator, a reheater, and a feedwater heater. They are usually classed into low and high temperature ranges with the boundary temperature between these two classes being around 450 °C (The Carbon Trust, 2012, p. 42), High-temperature units can therefore typically be found in processes employing kilns, furnaces, or fired heaters.

A mechanism delivering the recovered heat to another process or processes is necessary in any heat recovery application. Steam, being the most common process heat delivery medium, is commonly generated in heat recovery steam generators since these can extract more waste heat than a single heat exchanger. Thermal oil is suitable as well should the heat transfer medium be required to withstand high temperatures. Hot air generally tends to be used in lower-temperature application such as drying where it also acts as a carrier for the extracted liquid. Sometimes also hot water is used, but here the temperature limit is rather low since – if not pressurized – water will boil when heated above 100 °C.

Heat Recovery Steam Generators

The advantages of steam are its flexibility and high heat capacity. Heat recovery steam generators (HRSG) are thus very popular when waste heat is extracted from process streams. An HRSG usually consists of one or more modules comprising a super-heater, an evaporator, and an economizer (see Figure 2.13). Other heat exchangers may be present as well, e.g. various reheaters, air preheaters, etc. Considering modular generators, they produce steam at multiple pressure levels denoted as HP (high pressure), IP (intermediate pressure), and LP (low pressure). Each of the modules then has its own steam drum and the units are called double-pressure or triple-pressure HRSGs. Commonly, heat is recovered from a flue gas stream and such systems therefore contribute to maximum utilization of energy stored in the fuel, which obviously reflects in lower operational costs. Produced steam can then be used on site, sold to an external consumer, or used to generate electricity.

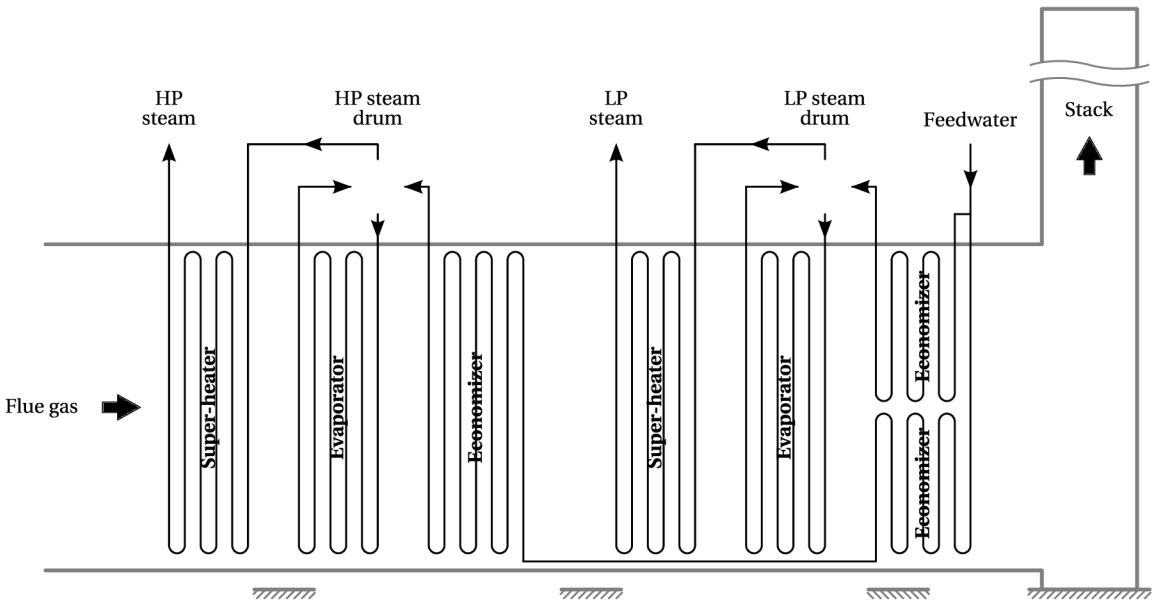

Figure 2.13. Typical arrangement of a double-pressure heat recovery steam generator

HRSGs can also be categorized according to their layout. In horizontal generators the hot stream flows horizontally over vertical tube banks while vertical HRSGs contain horizontally mounted tube banks and the hot stream flows vertically.

Thermal Oil Systems

Thermal oil systems (see flow-sheet in Figure 2.14) feature two main advantages over systems using steam as the heat transfer medium. First, they can operate under relatively high temperatures while keeping the whole process safer as lower pressures are necessary. The other major advantage is the fact that corrosion and scaling, largely occurring when steam is used, are virtually non-existent here. As a result, operating and maintenance costs are lower and these systems are more reliable.

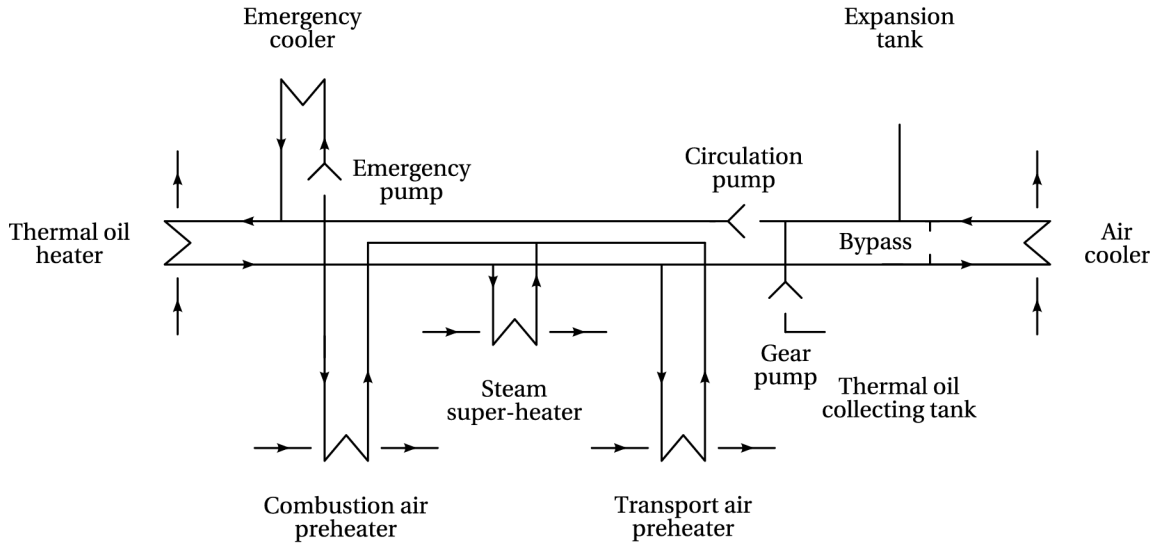

Figure 2.14. Flow-sheet of a thermal oil system recovering heat from flue gas for production of super-heated steam and preheating of combustion and transport air

Air Preheaters

In industrial processes, heat is usually recovered from flue gas to increase temperature of combustion or fluidizing air before it enters combustion chamber. This increases thermal efficiency of the process by lowering the amount of auxiliary fuel being necessary. Heat can be recovered in two types of units – a recuperative tubular type with tubes mounted in the flue gas duct (such as the one in Figure 2.12 discussed previously) or a regenerative type, for example the Cowper stove (see Hewitt et al., 1994, p. 897, Fig. 29.3). In case heat is to be recovered from an extremely high-temperature stream, ceramic tube recuperators can be employed.

The simplest configuration for a convective recuperator is a single tube bundle mounted perpendicularly to flue gas flow direction, i.e., a cross-flow arrangement. Air then usually flows inside the tubes, but configuration in which air flows past the bundle and flue gas flows through the tubes exist as well. The second variant are radiation recuperators. These can either be similar to double-pipe heat exchangers and thus comprise two concentric

segments or consist of a circular or rectangular array of tubes mounted axially in a flue gas duct (see Figure 2.15). Hybrid designs with radiation and convective section can, too, sometimes be encountered. Considering high-temperature applications, flow distribution, tube deformations, and possible related failures must be taken into account when the unit is being designed. Enhanced tubes are to be avoided if heat is recovered from a fluid with a high fouling propensity.

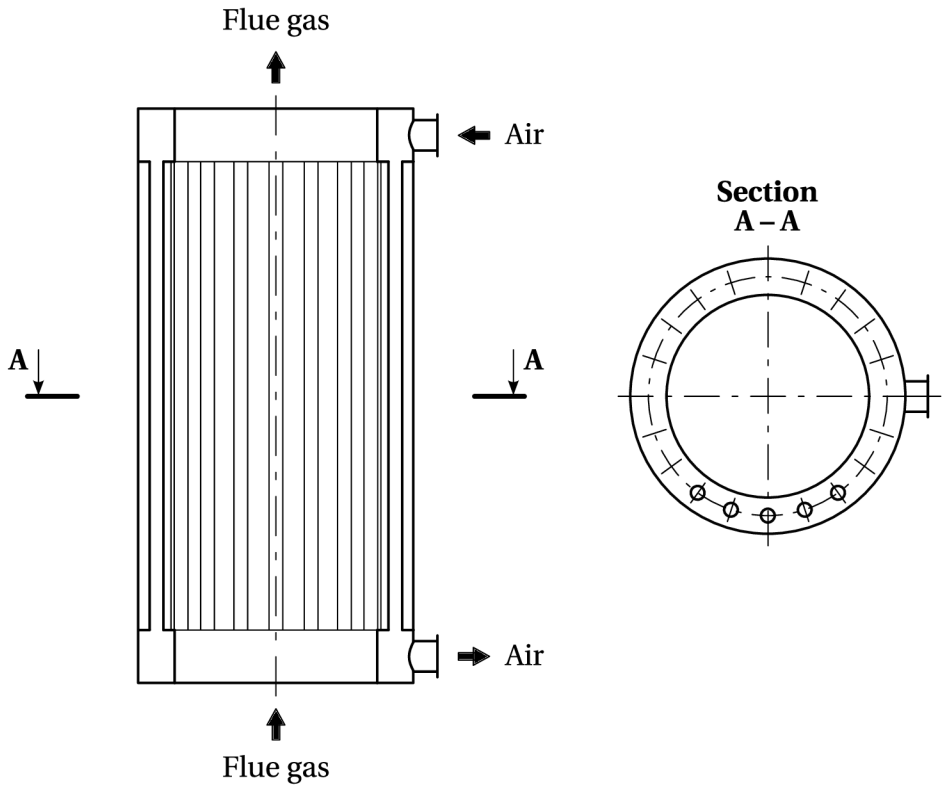

Figure 2.15. Countercurrent radiation recuperator with a circular array of tubes

As for regenerative heat exchangers, these are customarily used in pairs in smelting plants or steel mills. They work in an alternate fashion with matrix – ordinarily made of refractory bricks – in one of the exchangers being heated e.g. by a blast furnace gas ("hot period") while hot matrix in the second exchanger preheats the air stream ("cold period"). After a certain amount of time, the operation is reversed (see Hewitt et al., 1994, p. 896, Fig. 29.1).

Reheating of Polluted Streams

Flue gases commonly contain large amounts of pollutants such as heavy metals, sulfur oxides, nitrogen oxides, hydrogen halides, polychlorinated dibenzo-p-dioxins and dibenzofurans (PCDD/F), or fine solid particles upon exiting secondary combustion chamber (Jecha et al., 2008). In waste-to-energy applications, concentrations of these compounds tend to be especially high. To meet environmental regulations, a number of various units is integrated into each plant, e.g. dry, semi-dry, or wet scrubbers, adsorbers, fabric filters, or electrostatic precipitators. These then employ processes which in some cases require the temperature of

the polluted stream to be in a certain narrow range for the particular chemical reactions to happen as designed.

Flow-sheet of an industrial incinerator with integrated flue gas cleaning equipment is shown in Figure 2.16. We can see that flue gas leaving the secondary combustion chamber first preheats secondary combustion air, then goes through the heat recovery steam generator and after that it enters the cleaning process starting with the fabric filter removing fly ash. Afterwards, flue gas continues to the wet scrubber where sulfur oxides, hydrogen halides, and – in part – also the contained heavy metals are removed. Remaining heavy metals are separated from the stream in the adsorber. However, cold flue gas leaving the wet scrubber must be reheated (see the heat exchanger 8 in the figure recovering heat from flue gas stream just before it enters the venturi scrubber) to ensure the adsorption is efficient.

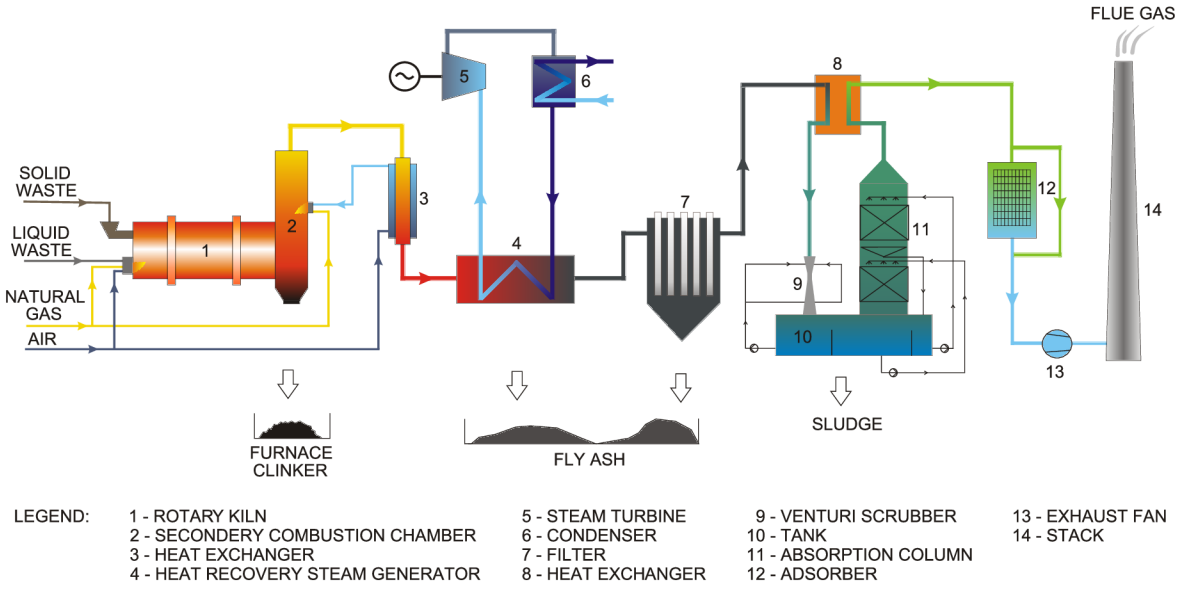

Figure 2.16. Flow-sheet of an industrial incinerator with integrated flue gas cleaning equipment (Jecha et al., 2008, reprinted with permission)

We must always bear in mind that as long as flue gas contains any highly corrosive acidic compounds, its temperature must stay above the respective acid dew point. Reheating of the flue gas stream thus prevents condensation of such compounds and subsequent damage to the downstream ducts, fans, etc. If no waste heat for reheating is available and reheating with utilities is economically infeasible in the long run, then the equipment must be made of materials able to withstand the corrosive conditions. Nevertheless, this issue must be decided upon on a per-site basis.

2.4.3 Recommended Approach to Heat Recovery Systems Design

When designing a heat recovery system, we need to consider the entire process flow-sheet and integrate individual heat transfer units in such a way that, first, demands of sub-processes are met – preferably by inter-process heat transfers. Only after that we can perform an economic evaluation to determine whether heat recovery would be feasible and profitable. If so, design and optimization of heat recovery systems is the next step. Finally, we select, design, and

optimize individual heat exchangers. Since in many cases heat recovery involves flue gas or other streams with a high fouling propensity, this issue must be taken into account so that the risk of equipment malfunction or failure is minimized – see for example (Stehlík, 2011) or (Kilkovský et al., 2011). Here, tools such as the HGA Database (Kilkovský et al., 2007) may be of significant help.

In general, for each unit we can decide on an energy utilization strategy respecting several inter-related and mutually complementary points provided by Pavlas et al. (2007):

- energy rejected from hot flue gas is only a by-product of heat releasing combustion processes;
- recovered energy should be utilized by the process to lower the consumption of utilities;
- any surplus energy should be exported to external customers so that economic profit is generated;
- wasting heat by injection of water or cold air into flue gas stream before it enters the cleaning system is the fallback cooling option.

3

Flow Distribution

Heat exchanger duty depends largely on the actual heat transfer area since properties of both hot and cold streams and hence also the temperature difference are given by plant flow-sheet and are more or less fixed. Increasing heat transfer area by massive flow parallelisation is therefore a very common way of increasing heat duty while retaining compact heat exchanger design. Typical examples of exchangers with parallelised flows are the shell-and-tube heat exchanger or the plate-type heat exchanger discussed in Chapter 2.

One of the first papers on flow distribution in parallelised systems (Acrivos et al., 1959) described the analytical successive branch-by-branch approach decomposing an entire splitting or combining constant cross-section manifold into control volumes around the discharge ports and dealing with each of them separately. Nevertheless, only manifolds with uniformly spaced lateral pipes and circular cross-sections distributing fluid into (or collecting fluid from) atmosphere or some other constant-pressure environment were discussed. Another paper (Bailey, 1975) dealing with uniformly perforated manifolds having constant circular cross-sections investigated the influence of axial velocity of fluid on the actual direction of discharge. Here, friction coefficients were assumed to be calculated rather than given as constants in advance. Other existing algebraic models describe either mere division or combination of flows in manifolds with circular (Lu et al., 2008) or rectangular (Fu et al., 1994) cross-sections, or parallel flow systems with these manifolds, e.g. in solar panels alone (Jones and Lior, 1994) or in solar panels combined with thermal collectors (Ghani et al., 2012).

Considering micro-scale applications, flow distribution in constant cross-section microchannels was investigated for example by Toh et al. (2002) or Kumaraguruparan et al. (2011). Flow distribution in such manifolds in micro-reactors was studied by Rebrov et al. (2007, 2011) and Saber et al. (2010), but these authors worked with more complex plane-bifurcated flow system. Micro-reactors with linearly tapered manifolds were described by Commenge et al. (2002) while similar geometries employed in electronics cooling modules (heat sinks) were analysed by Choi et al. (1993a,b) or Kim et al. (1995). Another micro-scale application where flow distribution plays a paramount role are fuel cells. Here, differential models of constant cross-section flow systems were presented among others by Kee et al. (2002), Maharudrayya et al. (2005), or Chen et al. (2007), and differential models along with analytical solutions were provided e.g. by Wang (2008), Wang (2010), or Wang and Wang (2012). In addition, a finite

difference model was presented by Koh et al. (2003). Models of flow systems based on the concept of electrical resistance networks are available as well (Amador et al., 2004; Zhang et al., 2009). In spite of the fact that these models could be used in the usual process industry design problems, their complexity owing to the differential nature is quite restrictive (the utilized equations – momentum conservation law etc. – contain differential and integral terms). As for two-phase flow in such micro-devices, various experimental studies involving different media and geometries were performed by Nie and Chen (2010), Bi et al. (2010), Kim et al. (2011), or Kim et al. (2012). Besides the above mentioned models, some authors, e.g. Tondeur and Luo (2004), Tondeur et al. (2009), Escher et al. (2009), Liu et al. (2010a,b), or Liu et al. (2012), also dealt with highly bifurcated spatial distribution structures. Although such a concept is interesting regarding fuel cells, micro-reactors, or electronics cooling modules, from the process heat exchange units point of view it is of a very limited use because cleaning of a fouled distribution system of this type would be rather difficult.

More advanced models of distribution systems in common process equipment cover division or combination of flows in case of manifolds with circular (Chandraker et al., 2002) or rectangular (Habib et al., 2009) cross-sections. As for complete parallel systems, both finite-difference (Datta and Majumdar, 1980) and differential (Bajura and Jones, 1976; Miao and Xu, 2006) models have been developed. Models supporting two-phase flow were presented e.g. by Ablanque et al. (2010), Pustylnik et al. (2010), El Achkar et al. (2011), Byun and Kim (2011), Zhang et al. (2011), Marchitto et al. (2012), or Yuan et al. (2012). Many authors also published experimental studies based of computational fluid dynamics (CFD) evaluations. Common distribution systems consisting of a splitting and a collecting manifold connected by many branches were investigated e.g. by Heggemann et al. (2007), Kulkarni et al. (2007), Tong et al. (2009), Khadamakar et al. (2011), Zhang et al. (2011), or Gandhi et al. (2012) while trickle-bed reactors were addressed for instance by Bazmi et al. (2012) or Martínez et al. (2012).

Since the amounts of fluid flowing through branches of a parallel flow system (i.e., the resulting distribution) depend on pressure differences between branch ends in splitting and collecting manifolds and these can be greatly influenced by longitudinal manifold cross-section variability, an appropriate design of the manifolds can result in a much more uniform flow distribution. This is due to the fact that the differences themselves are given by pressure profiles in the manifolds and any change of a pressure profile (caused, for instance, by a locally convergent or divergent shape of the manifold) must influence the lateral flow rates. All the models mentioned so far, however, either assume manifolds of constant cross-sections or are far too complex to be employed for shape optimization – they can be implemented directly using common programming languages (C++, Java, etc.), but a discretization of the respective governing equations is required which introduces a considerable amount of additional work. What is more, a computational tool based on one of these models would probably need significantly more time to yield a solution than a tool making use of the simpler successive branch-by-branch approach with algebraic equations. As for CFD, although it can be very useful (one obtains an extensive set of accurate data that would otherwise be unavailable), considering shape optimization such an approach is highly disadvantageous due to the amount of work associated with each individual geometry. That is, every geometry must be created, meshed, and then evaluated which, in total, can take from several hours up to several days.

Considering the lack of models that are computationally inexpensive, easy to implement, and can be readily modified to cover even made-to-measure flow systems, models presented in this thesis are based mainly on Bailey's paper, experimental data available in (Idelchik,

1986), and information published in monographs such as (Oosthuizen and Carscallen, 2003). As for nomenclature, "splitting manifold" and "distributor" will from now on denote the same element of a flow system. "Collecting manifold" and "collector" will be treated in a similar manner. Also, "manifold" will mean either a distributor or a collector while any conduit through which fluid is flowing will be called a "channel".

3.1 Common Problems

Aside from maldistribution, three possible flow-related issues – backflow, instabilities, and fouling – must be kept in mind when designing a parallel flow system, be it in a heat exchanger or in any process unit in general. These issues can occur even in very simple systems and complexity of the actual layout is therefore rather irrelevant. More importantly, each of them can lower efficiency, cause product degradation due to insufficient heating or overheating of the fluid, or even bring about malfunction of the system. In the following sections we will discuss the issues in a bit more detail.

3.1.1 Backflow

Let us consider a simple parallel flow system consisting of a distributor, several branches, and a collector with a fluid being fed into the distributor inlet (see Figure 3.1). Flow rate through an individual branch of such a system is governed by the pressure difference between its inlet in the distributor and its outlet in the collector, $\Delta p = p_{\text{out}} - p_{\text{in}}$. If $\Delta p < 0$, i.e., if pressure near the branch outlet in the collector is lower than pressure near the branch inlet in the distributor, then the fluid, indeed, flows in the expected direction from the distributor into the collector. If, however, $\Delta p > 0$, that is, if pressure near the branch outlet in the collector is higher than pressure near the branch inlet in the distributor, then the fluid flows in the opposite direction (see Figure 3.2). This behaviour is called "backflow" and is generally undesirable.

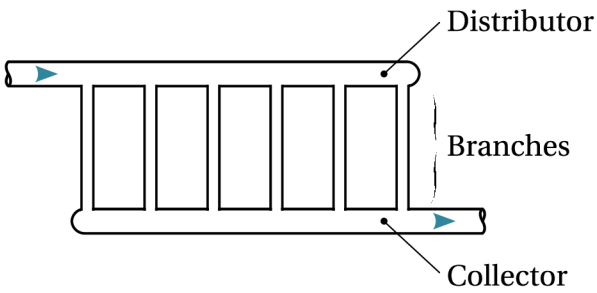

Figure 3.1. An sample parallel flow system

The usual way to remedy the situation is to change the flow system layout so that pressure differences are negative for all branches. Of course, we could artificially increase pressure drops in the respective branches e.g. by inserting orifices into the inlets, but this comes with an increased pumping cost and possible clogging (see Section 3.1.3). A technical-economic analysis of the available design modifications is thus necessary.

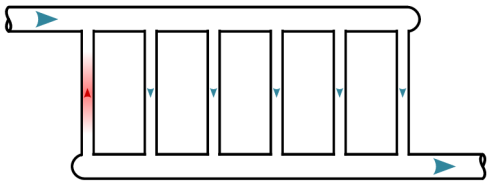

Figure 3.2. Backflow

3.1.2 Instabilities

Steady flow can, under certain conditions, become unsteady. As common examples, one might name creation of vortices when a fluid flows past an obstruction, buckling of a low-speed capillary jet approaching an obstacle, density stratification in a heated fluid, flickering of a flame, generation of surface waves by wind, etc. Generally speaking, any instability mechanism can be thought of as a selective frequency amplifier whose characteristics are given by flow parameters (Drazin, 2002). The energy required for amplification is then taken either from the mean flow or from externally supplied heat. In other words, any instability is caused by a random disturbance amplified by a positive feedback while its ultimate consequences are turbulence and random waves.

Detailed theoretical information related to flow instabilities can be found in (Sengupta and Poinsot, 2010). Additionally, instabilities specifically related to heat exchangers were studied by Houdek (2007). In this thesis, however, we will concern ourselves only with one of the effects of instabilities, namely unsteady flow distribution. As the name suggests, it means that flow rates through individual channels are not constant in time (see Figure 3.3). This is highly undesirable, especially in high-temperature applications (extraction of heat from flue gas etc.), since then channels are subjected to (non-periodic) variable loading due

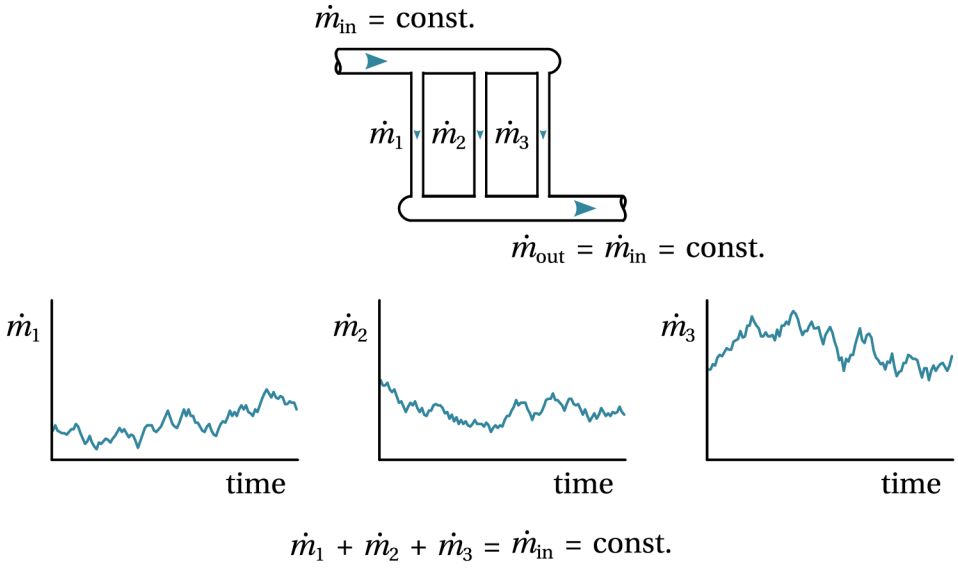

Figure 3.3. Unsteady flow distribution: even though the total flow rate is constant, flow rates through individual channels vary in time

to changes in their temperatures with a common end result being mechanical failures. We should therefore try to avoid any parallel flow system layout that exhibits such a behaviour.

3.1.3 Fouling

By fouling we mean any accumulation of unwanted material on surfaces of a process equipment that hinders the desired operation. This issue is particularly common in food industry, chemical industry, and energy industry (including waste-to-energy applications). According to Bott (1995), fouling layer can develop by one of the following mechanisms:

- precipitation: crystallization of solids from solutions;
- solidification: phase change from liquid to solid or de-sublimation;
- particle deposition;
- chemical reaction: typically on heat transfer areas;
- corrosion;
- biological fouling: e.g. growth of bacteria or algae;
- composite fouling: a combination of several of the above mechanisms.

Having a clean unit that we just started to operate, for a certain time period (called "induction period") it performs as designed and fouling rate is very low. Then, as the fouling layer starts to become more pronounced, surface roughness may increase thus increasing friction while overall heat transfer coefficient falls due to higher thermal resistance of the layer. Both these factors may further promote the fouling process. Moreover, with increasing thickness of a fouling layer on the inside wall of a narrow channel (e.g. a tube in a shell-and-tube heat exchanger) increases also the hydraulic resistance. Should this channel be a part of a parallel flow system, then – as explained in Section 3.1.1 – the respective flow rate falls due to increasing channel pressure drop. Lower flow velocity subsequently intensifies the deposition and can lead to clogging of the channel. Similarly, any build-up can induce formation of eddies which increase fouling rate as well (Blevins, 2003). What is more, lower value of the overall heat transfer coefficient implies lower heat exchanger efficiency which, in turn, generates huge economic losses. According to Walker et al. (2012), for example, costs arising from additional fuel requirements and production losses associated solely with condenser fouling were between 0.4 and 2.2 million USD in 2009. Another study by Mozdianfard and Behranvand (2012) reports that the extra cost of fuel required to compensate for the effect of fouling in a single Iranian oil refinery was estimated to be around 170 million USD per year (using the 2010 gas price of 5.0 USD per MMBtu), which translated to almost 1.175 billion USD per year for all refineries in Iran. For heat exchangers in general, Müller-Steinhagen et al. (2005) estimated the losses due to fouling to be about 0.25 % of gross domestic product in industrialized nations while Hewitt (1998) provided an estimate as large as 1.4 billion USD per year for plants in the United States. Many authors (see e.g. Polley et al., 2009) also stress that throughput losses due to the effects of fouling on hydraulic performance (for instance in crude oil preheat trains) play a major role as well.

From the above it is obvious that fouling must be taken into account when designing any process unit that is expected to work with a fluid having a high fouling propensity. We must

eliminate as many stagnation zones with swirling character of flow as possible or at least minimize formation of eddies. Plain surfaces and suitable materials should be used to further lower fouling rate. Additionally, units should be constructed in such a way that cleaning of heat transfer surfaces and other essential regions is easy.

3.2 Problem Mitigation Strategy

As outlined in the previous section, a thorough flow distribution analysis should be the core tool in the problem mitigation process. Considering backflow, steady analyses are sufficient. Obtained data can then be used as a basis for shape optimization of the relevant flow system parts – manifold profiles in general or even details such as shapes of channel inlets (see example optimization tools in Section 3.4).

In case of flow rate stability, on the other hand, transient analyses are necessary. Long enough time intervals must be simulated in order to be sure that flow rates will not become unsteady later on or that they will not settle in spite of an initial unsteady behaviour. Should any flow system geometry feature unsteady flow rates, we must weigh carefully whether such fluctuations could cause any additional problems, either by themselves alone or e.g. in combination with fouling. Again, shape optimization can be of tremendous help during flow rate stabilization.

As for fouling, we can minimize fouling propensity of the process fluid by employing additional filters or droplet separators provided that there is enough space for such equipment (this might prove rather problematic when dealing with retrofits). Furthermore, fouling can be significantly lessened by elimination – or at least decrease in the number and sizes – of stagnation zones. To obtain the necessary flow field characteristics, however, utilization of computational fluid dynamics is necessary (see Section 3.5.1 which explains this approach on an industrial example). Here, shape optimization is paramount.

With the importance of process equipment efficiency and reliability as well as possible operational cost reduction in mind, in the following sections we will focus on flow distribution analysis and shape optimization based on thus obtained data.

3.3 Methods for Flow Distribution Prediction

There are three main methods one can employ to predict flow rates and pressure profiles in individual branches of a flow system. Each of these methods provides a different level of accuracy and has different requirements considering time necessary for flow evaluation, cost and computing power. These methods are, in no particular order, experiment on a prototype, computational fluid dynamics, and successive branch-by-branch approach. Moreover, since CFD usually denotes numerical evaluation of 3D (or less commonly 2D) geometries, we will also add numerical evaluation of pseudo-1D geometry utilizing partial differential equations to the list of available methods.

3.3.1 Experiment on a Prototype

Building a flow system prototype and measuring flow rates and pressures (or any other quantity for that matter) as necessary will, obviously, provide high-quality data. However,

there is a shortcoming we must consider, i.e., prototypes sometimes do not allow us to fully imitate operating conditions of real equipment. In case of heat exchangers and especially those for high-temperature applications it means that we may not be able to heat up working fluid to as high a temperature as required. This, consequently, causes the obtained data to be inaccurate to a certain degree depending on properties of the working fluid (density and viscosity variation with temperature etc.).

3.3.2 Computational Fluid Dynamics

As mentioned in the previous section, an experiment on a prototype can, under certain circumstances, yield very precise data, but what if we need to investigate some hard-to-measure quantities or simulate hard-to-duplicate conditions? Then CFD modelling is the right method to employ, since we can evaluate not only temperatures, pressures, or mass flow rates, but also flow field variables (such as turbulent intensity, vorticity magnitude, velocity angle, etc.) anywhere within the investigated geometry. There are two major drawbacks to CFD, though. First, very high computational demand necessitates usage of clusters or grids[1] and even with these computation commonly takes many hours or days to complete. Second, accuracy of results is highly influenced by mesh quality and fineness, used models, solution methods, and other parameters. A coarse mesh results in larger numerical errors, yet using a fine mesh in the entire geometry may lead to unacceptable computational load. Thus the goal is to find a balance between accuracy and computing cost even though, ideally, mesh should be made gradually finer until there is an acceptable difference between obtained solutions. Moreover, mesh should not be of homogeneous density; rather it should be more refined in regions of large gradients.

To demonstrate this issue, let us briefly discuss the double U-tube exchanger module investigated in Section 3.4.3. This module, shown in Figure 3.4, consists of a distributor, two sets of U-tubes, and a collector. Working fluid – air – flows in through the distributor, then it is heated up in the inner and outer set of U-tubes, and finally the individual streams are combined again in the collector from which a single stream of hot air leaves the module. For the sake of simplicity, let us assume that both distributor and collector have constant rectangular cross-sections being e.g. 140 mm wide and 80 mm high. Also, let all U-tubes be mounted flush with manifold walls.

Considering problem formulation, the main parameters will be as follows:

- pressure-based solver with absolute velocity formulation, second order implicit transient formulation, and double precision;
- realizable k-ϵ model with standard wall functions and energy equation;
- SIMPLE pressure-velocity coupling;

[1] The main difference between a cluster and a grid is that cluster is tightly coupled (all nodes in a single location, identical or very similar hardware, single system image) and uses centralized job management and scheduling whereas grid is loosely coupled (nodes connected via LAN/WAN, diverse hardware and operating systems) and uses distributed job management and scheduling. In other words, a cluster operates as a single machine while a grid operates as a set of independent machines each of which processes a separate part of the entire job. Obviously, efficiency of clusters tends to be higher. Grids, on the other hand, are more scalable – it is not a problem to create a grid of 100 000 or more nodes connected via Internet and use their residual power to process CFD jobs. Creating a cluster of similar capacity, albeit with a much lower number of nodes, would be quite costly.

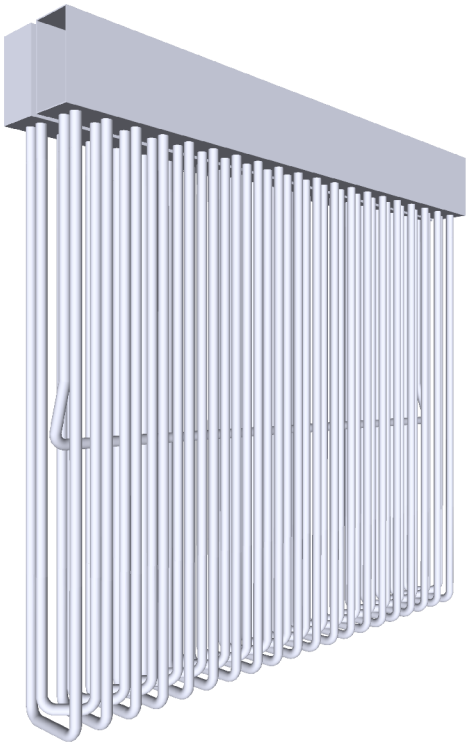

Figure 3.4. Double U-tube exchanger module

- Green-Gauss node based gradient calculation;
- spatial discretization: second order for pressure, second order upwind for density and momentum, and first order upwind for turbulent kinetic energy, turbulent dissipation rate, and energy;
- total air mass flow rate $\dot{m} = 1\ \mathrm{kg\,s^{-1}}$, air inlet temperature $t_{\mathrm{in}} = 30\ ^{\circ}\mathrm{C}$, and tube wall temperature $t_{\mathrm{w}} = 450\ ^{\circ}\mathrm{C}$.

We will evaluate two cases differing only in distributor and collector mesh fineness. Everything else will be left unchanged – including relatively fine mesh in U-tubes and Cooper meshing scheme. This meshing scheme was selected due to the fact that it employs hexahedral cells which are reported (Perić, 2004) to provide higher accuracy than tetrahedral cells at the same cell count.

Case 1: fine mesh – manifolds contain 327 704 cells in total. Mean cell volume is 126.3 mm^3, i.e., if every cell were a cube then their edges would have been 5.02 mm long.

Case 2: coarser mesh – manifolds contain 290 225 cells in total. Mean cell volume is 142.6 mm^3, i.e., if every cell were a cube then their edges would have been 5.22 mm long.

In both cases, smaller cells are generated near manifold walls with U-tube ends in them to increase accuracy.

Reported flow rates are shown in Figure 3.5 while relative differences (percentages of an ideal flow rate) can be found in Figure 3.6. The mean of absolute values of relative differences, or should we say the average difference in the obtained solutions, is 11.3 %. This is quite large

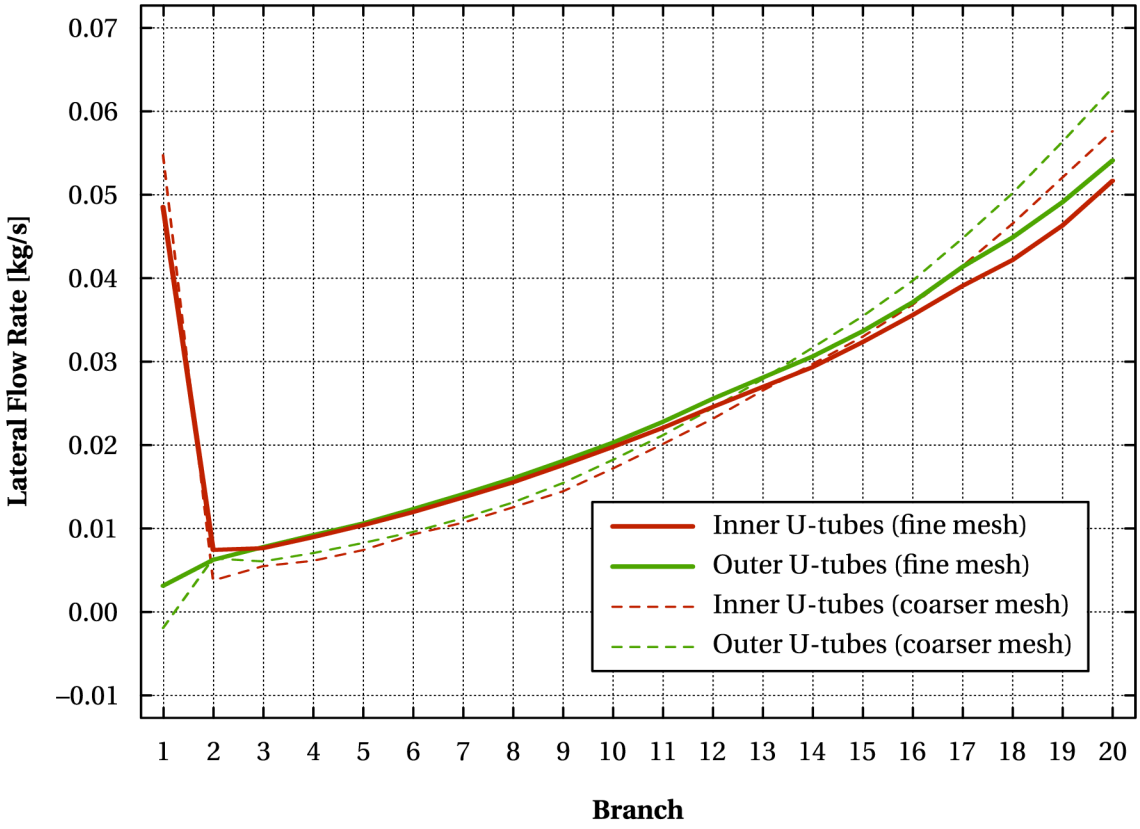

Figure 3.5. Flow rates obtained with the fine mesh and the coarser mesh

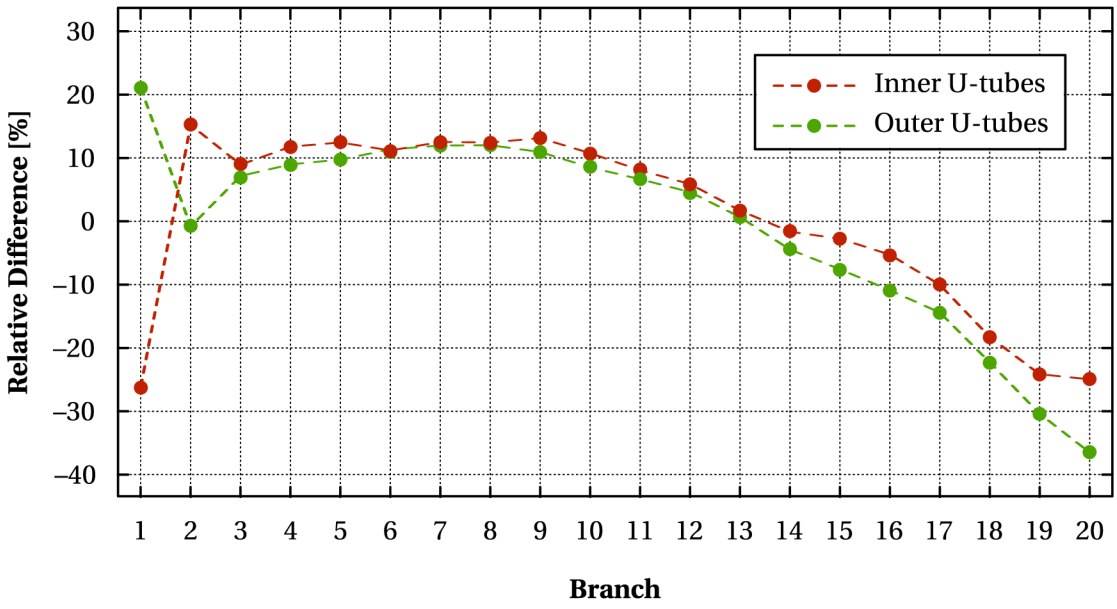

Figure 3.6. Relative differences (percentages of an ideal flow rate) in reported flow rates between the fine mesh and the coarser mesh

a value considering "mean cubic cell" edge length increased only by slightly less than 4 % (cell count decreased by 11.4 %[2]).

It should also be noted that in case of shape optimization of near-planar flow systems, i.e., systems with one dimension significantly smaller than the remaining two, we usually can afford to evaluate 2D geometries instead of detailed 3D ones. This approach lowers computational cost immensely, however, it is obvious that detailed 3D evaluation of the final configuration should be performed as well. A sample optimization problem illustrating the use of this technique is discussed in Section 3.5.1.

3.3.3 Pseudo-1D Discretization of a Flow System

Similarly as with 3D or 2D spatial discretization, we can apply the same principles to create a pseudo-1D mesh. The only difference is that now the mesh only contains nodes and edges – no faces or cells. Such an approach is advantageous for flow systems containing channels with small cross-sections compared to their lengths.

Construction of a pseudo-1D mesh is quite simple. Every channel is replaced by its axis which is then discretized with a chosen spatial step. This means that relative spatial disposition of individual channels is retained and, consequently, that changes in gravitational potential energy of fluid particles can be taken into account by any model we decide to use. A sample pseudo-1D mesh is shown in Figure 3.7.

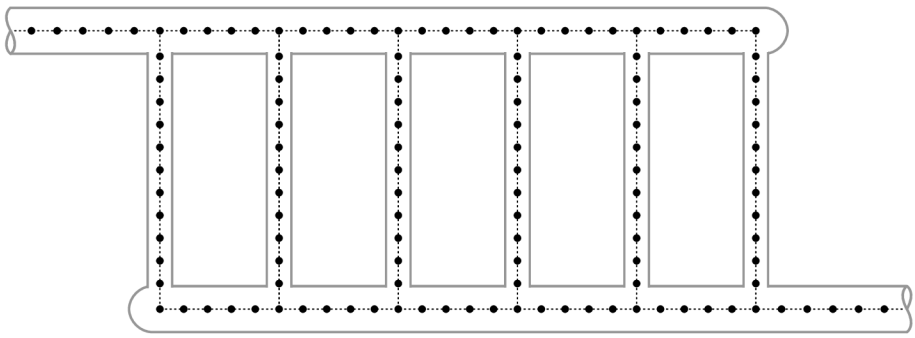

Figure 3.7. Pseudo-1D mesh of a simple flow system

This method, however, has a serious downside to it. Due to the very limited description of geometry, we must introduce additional equations governing many phenomena (such as minor losses – see Idelchik, 1986) into the model. Also, accuracy tends to be impaired and any model must be fine-tuned using experimental data or at least data from CFD simulations before we can proceed to production use.

3.3.4 Successive Branch-by-Branch Approach

Branch-by-branch approach is a special case of pseudo-1D discretization. It simplifies the problem even further by en bloc evaluation of each segment of a channel between two points where fluid is split or merged (so called wye joints or wyes). In other words, it examines a flow

[2]Although increased cell count implies to a certain degree increased accuracy, there is no indication of data variation being directly proportional to variation in cell count. Similarity of the two percentages is purely coincidental.

system sequentially using a very coarse pseudo-1D mesh and therefore suffers from similar problems as pseudo-1D discretization. Nonetheless, once a model is fine-tuned for a certain class of flow system geometries, its production use does not pose any significant risk.

This method is implemented in the majority of the models mentioned further due to the extremely fast evaluation and effortless modification of geometry characteristics. Section 3.4.3 demonstrates that it can be used even for relatively complex flow systems.

3.4 Simplified Mathematical Models

Simplified models are well worth the additional effort that must be devoted to fine-tuning them for a specific class of flow systems because then they need substantially less time to yield accurate enough data than other, more complex models. The following section therefore lists some of the tools that have been created by the author. These are all for single-phase flow and range from applications for simulation of plain distribution into a constant-pressure environment through distributor-collector systems with complex tube coils to a shape optimization tool for a specific double U-tube heat exchanger module.

3.4.1 Distribution from a Manifold Having Rectangular Cross-Section

Since successive branch-by-branch models for distribution from manifolds with constant circular cross-sections are readily available (Acrivos et al., 1959; Bailey, 1975), we will focus on manifolds with variable rectangular cross-sections and double lateral branches (see Figure 3.8). Such manifolds can perform much better than those with constant cross-sections while manufacturing them is still fairly simple. Please note that any segment of a manifold between two adjacent branches will be called “manifold section” – or simply “section” – from now on.

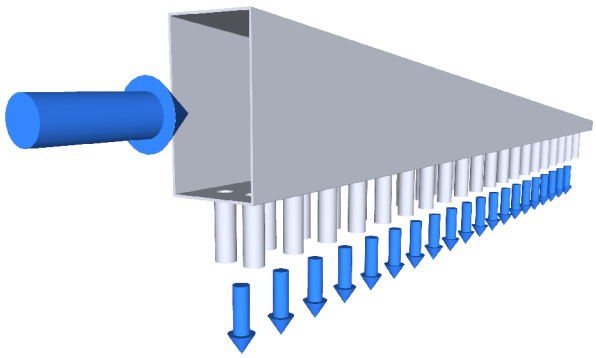

Figure 3.8. Distributor with variable rectangular cross-section and double lateral branches

We will assume uniform one-dimensional isothermal flow with fluid flowing as indicated by the velocities and cross-sectional areas of individual branches being small enough compared to internal areas of the nearby distributor sections. Should incompressible flow simulation be preferred then, obviously, fluid density would be constant throughout the entire distribution system.

To get a clear picture of what is happening in the manifold, let us now consider one branch and one subsequent section of the distributor. A portion of fluid is discharged through the branch due to surplus static pressure in the manifold while velocity of the remaining fluid inevitably decreases and thus its momentum changes. This consequently causes increase in pressure in the downstream direction. One way to incorporate this into our model is to use axial and lateral momentum correction factors as e.g. Bajura and Jones (1976) did. This approach, however, has a notable disadvantage, since it employs integral terms depending on an actual velocity profile near the tube entrance. Hence, we will introduce the coefficient of static regain C_r which Bailey (1975) defined as the ratio of the difference in static pressure between the flow upstream and downstream of the branch to the difference in dynamic pressure. Moreover, although it may seem so, discharging fluid does not generally lose all its original (axial) velocity and therefore the discharge angle θ (see further) is greater than zero.

Considering the law of conservation of mass, the amount of fluid discharging through the branch must correspond to the change in mass flow rate between the section upstream and the section downstream of the branch. However, since the joint of the distributor and the branch is usually made in such a way that it is impossible for the streamlines to suddenly bend along the edge of the entrance, the stream is contracted due to axial momentum of fluid particles. This means that we need to introduce one more correction factor – the discharge coefficient C_d.

In a manifold section, static pressure varies not only due to friction, but also because of changes in elevation above a reference plane (that is, changes in gravitational potential energy of particles) and changes in cross-sectional area. To include these factors into the model, we can simply use the Darcy-Weisbach equation (White, 1998, p. 340) without any additional corrections (per our requirement on branch cross-sectional areas) and the Bernoulli equation.

Governing Equations

Amounts of fluid discharging through individual branches are given by the variation of static pressure along the distributor and thus finding equations governing static pressure means we can predict the actual discharge flow rates. To do so, we will need four basic equations governing pressure changes due to outflow through branches, friction, changing distributor cross-section, and minor losses. Scheme of the investigated distributor is shown in Figure 3.9 in which superscript "U" denotes variables just upstream of a branch, "D" variables just downstream of a branch, and "M" variables related to the middle of a section.

We will first deal with pressure variations near branch entrances. Let us assume we already know pressure, velocity, and density just upstream of the ith branch – p_i^U, v_i^U, and ρ_i^U. Pressure change due to change in momentum of fluid particles near the branch is governed by the Bernoulli equation for adiabatic compressible flow (Clancy, 1975) modified as shown by Bailey (1975),

$$\left(\frac{\gamma}{\gamma-1}\right)\frac{p}{\rho}+gz+C_\mathrm{r}\frac{v^2}{2}=\text{const.}, \tag{3.1}$$

in which C_r denotes the coefficient of static regain, $\gamma=c_\mathrm{p}/c_\mathrm{v}$ heat capacity ratio, g the standard gravity, and z elevation above a reference plane. Thus, for our distributor we have

$$\left(\frac{\gamma}{\gamma-1}\right)\frac{p_i^\mathrm{U}}{\rho_i^\mathrm{U}}+C_{\mathrm{r},i}\frac{\left(v_i^\mathrm{U}\right)^2}{2}=\left(\frac{\gamma}{\gamma-1}\right)\frac{p_i^\mathrm{D}}{\rho_i^\mathrm{D}}+C_{\mathrm{r},i}\frac{\left(v_i^\mathrm{D}\right)^2}{2}. \tag{3.2}$$

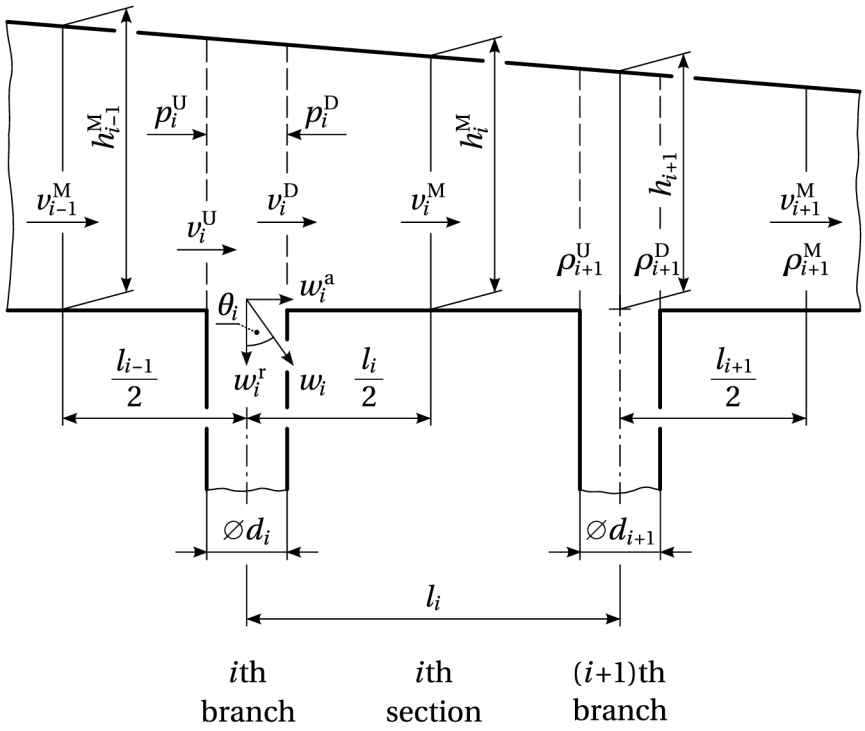

Figure 3.9. Scheme of the investigated distributor

Value of γ is constant throughout the entire system, because specific heats are temperature-dependent (Coulson and Richardson, 1999, vol. 1, p. 8) and the flow is – per our assumption – isothermal. Since Bailey (1975) successfully validated his model against a series of experiments and the geometries he investigated were relatively similar to our flow system, in this model we use the same formula for coefficient of static regain as he did, i.e.,

$$C_{\mathrm{r},i} = 0.780 + \left(0.284 + 0.098 \log_{10} \sqrt{\frac{\pi d_i^2}{2 b_i h_i}}\right) \log_{10} \frac{v_i^{\mathrm{U}}}{v_i^{\mathrm{U}} - v_i^{\mathrm{D}}} \tag{3.3}$$

where b_i is manifold cross-section width at the ith branch. Discharge through the ith branch, given by the excess static pressure, can then be calculated using

$$\dot{m}_i^{\mathrm{B}} = b_i h_i \left(\rho_i^{\mathrm{U}} v_i^{\mathrm{U}} - \rho_i^{\mathrm{D}} v_i^{\mathrm{D}}\right) = \frac{\pi d_i^2}{2} C_{\mathrm{d},i} \sqrt{\frac{\left(p_i^{\mathrm{U}} + p_i^{\mathrm{D}}\right)\left(\rho_i^{\mathrm{U}} + \rho_i^{\mathrm{D}}\right)}{2}}. \tag{3.4}$$

In the equation above, $C_{\mathrm{d},i}$ denotes discharge coefficient for the ith branch which, again, is taken from (Bailey, 1975):

$$C_{\mathrm{d},i} = 0.620 + 0.070\beta_i - 0.088\beta_i^2, \qquad \text{where } \beta = \log_{10}\left[\log_{10}\left(1 + \frac{p_i^{\mathrm{U}} + p_i^{\mathrm{D}}}{\left(v_i^{\mathrm{U}}\right)^2}\right)\right]. \tag{3.5}$$

To calculate mean fluid velocities in the branches, equal static pressures are assumed at tube exits:

$$p_i^{\mathrm{B}} = \frac{p_i^{\mathrm{U}} + p_i^{\mathrm{D}}}{2} - \zeta_i \frac{\rho_i^{\mathrm{U}} + \rho_i^{\mathrm{D}}}{2} \frac{w_i^2}{2} = p^{\mathrm{B}} = \text{const.} \qquad \forall i. \tag{3.6}$$

Coefficients of hydraulic resistance of branch entrances, ζ_i, depend not only on entrance geometry, but also on fluid velocities just upstream and in the branch (see Idelchik, 1986, Chapter 7). This dependence is not too complex, but it simplifies the subsequent computer implementation of the model a lot to estimate all the resistance coefficients by constants. Since flow system geometry is always known, we can calculate the necessary branch-to-manifold cross-sectional area ratios, s_i/S_i, and also make rough estimates of w_i/v_i^{D} to use these later as a basis for estimating ζ_i. For the sake of simplicity, let us consider $\zeta_i = 1\ \forall i$ here. Therefore, by making use of Equation 3.4 we have

$$p_i^{\mathrm{B}} = \frac{p_i^{\mathrm{U}} + p_i^{\mathrm{D}}}{2} - \frac{4\left(\dot{m}_i^{\mathrm{B}}\right)^2}{\pi^2 d_i^4 C_{\mathrm{d},i}^2 \left(\rho_i^{\mathrm{U}} + \rho_i^{\mathrm{D}}\right)} = p^{\mathrm{B}} = \text{const.} \qquad \forall i. \tag{3.7}$$

Now, let us focus on the subsequent distributor section. As mentioned above, pressure loss caused by friction can be modelled using the Darcy-Weisbach equation, i.e.,

$$\Delta p^{\mathrm{fr}} = -f \frac{l}{D_{\mathrm{h}}} \rho \frac{v^2}{2}, \tag{3.8}$$

where f denotes Darcy friction factor and D_{h} hydraulic diameter. Considering linear changes of cross-section width and height along the manifold length and the fact that such changes per one section are relatively small, we can approximate hydraulic diameter as well as fluid density and velocity without any significant loss of accuracy by values in the middle of the section. Equation 3.8 thus becomes

$$\Delta p_i^{\mathrm{fr}} = -\frac{1}{4} f_i l_i \frac{b_i^{\mathrm{M}} + h_i^{\mathrm{M}}}{b_i^{\mathrm{M}} h_i^{\mathrm{M}}} \rho_i^{\mathrm{M}} \left(v_i^{\mathrm{M}}\right)^2 \tag{3.9}$$

with b_i^{M} being width of distributor cross-section in the middle of the ith section. As for the Darcy friction factor, in laminar flow it depends solely on Reynolds number (White, 1998, p. 365) – e.g. for square cross-sections we have

$$f = \frac{57}{\mathrm{Re}}, \tag{3.10}$$

whereas in case of transitional and turbulent flow it also depends on absolute roughness of the inner surface of the manifold section, ϵ, and its hydraulic diameter. To get the value of the friction factor, one can either solve the implicit Colebrook-White equation (Colebrook, 1939)

$$\frac{1}{\sqrt{f}} = -2\log_{10}\left(\frac{\epsilon}{3.7 D_{\mathrm{h}}} + \frac{2.51}{\mathrm{Re}\sqrt{f}}\right) \tag{3.11}$$

or use an explicit approximation – e.g. the Churchill (1977), Chen (1979), Haaland (1983), Serghides (1984), Manadilli (1997), or Romeo et al. (2002) formula. In the present model, the Churchill approximation,

$$\begin{aligned} A &= \left[-2.457 \ln\left(\left(\frac{7}{\mathrm{Re}}\right)^{0.9} + \frac{0.27\epsilon}{D_{\mathrm{h}}}\right)\right]^{16} \\ B &= \left(\frac{37530}{\mathrm{Re}}\right)^{16} \\ f &= 8\left[\left(\frac{8}{\mathrm{Re}}\right)^{12} + \frac{1}{(A+B)^{1.5}}\right]^{\frac{1}{12}}, \end{aligned} \tag{3.12}$$

is used since it gives reasonably accurate values of the friction factor in both transitional and turbulent flow regimes (Salmasi et al., 2012; Schorle et al., 1980) while retaining computational simplicity. As for Reynolds number, it can, again, be approximated using values in the middle of the section, i.e.,

$$\mathrm{Re}_i = \frac{\rho_i^{\mathrm{M}} v_i^{\mathrm{M}} D_{\mathrm{h},i}^{\mathrm{M}}}{\mu} = 2\frac{\rho_i^{\mathrm{M}} v_i^{\mathrm{M}} b_i^{\mathrm{M}} h_i^{\mathrm{M}}}{\mu\left(b_i^{\mathrm{M}} + h_i^{\mathrm{M}}\right)}, \tag{3.13}$$

where μ denotes dynamic viscosity of the fluid. We can consider viscosity to be constant because under all but very high pressures in case of liquids it depends only on temperature (White, 1998, p. 24) which is constant throughout the entire system (we assume the flow is isothermal). If air flow was modelled, we could use e.g. the Sutherland equation (White, 1991),

$$\mu = \left(18.27 \cdot 10^{-6}\right) \frac{411.15}{120+T} \left(\frac{T}{291.15}\right)^{1.5}, \tag{3.14}$$

in which T denotes thermodynamic temperature. In case of water, Sutherland equation with adequate coefficients could, again, be employed, but the easier to evaluate Vogel equation (Dortmund Data Bank Software & Separation Technology GmbH, 2012),

$$\mu = e^{-3.7188 + \frac{578.919}{-137.546+T}}, \tag{3.15}$$

might be a better choice with respect to computational cost.

Pressure change caused by change in distributor cross-section is calculated using the original Bernoulli equation for adiabatic compressible flow,

$$\left(\frac{\gamma}{\gamma-1}\right)\frac{p}{\rho} + gz + \frac{v^2}{2} = \text{const.}, \tag{3.16}$$

and the continuity equation,

$$\rho S v = \text{const.}, \tag{3.17}$$

with S being cross-sectional area. Hence, for ith distributor section we have

$$\left(\frac{\gamma}{\gamma-1}\right)\frac{p_i^{\mathrm{D}}}{\rho_i^{\mathrm{D}}} + gz_i + \frac{\left(v_i^{\mathrm{D}}\right)^2}{2} = \left(\frac{\gamma}{\gamma-1}\right)\frac{p_{i+1}^{\mathrm{U}}}{\rho_{i+1}^{\mathrm{U}}} + gz_{i+1} + \frac{\left(v_{i+1}^{\mathrm{U}}\right)^2}{2} \tag{3.18}$$

and

$$\rho_i^{\mathrm{D}} b_i h_i v_i^{\mathrm{D}} = \rho_{i+1}^{\mathrm{U}} b_{i+1} h_{i+1} v_{i+1}^{\mathrm{U}}, \tag{3.19}$$

where b_i is width of distributor cross-section at the ith branch.

Should the system contain any elements causing minor losses (similarly as in case of branch entrances), we can calculate them in a manner analogous to Equation 3.6 with coefficients of hydraulic resistance taken for instance from (Idelchik, 1986).

The last equation that we need is an equation for fluid density which generally depends on pressure and temperature. For humid air, we could use

$$\rho = \frac{p_{\mathrm{da}}}{R_{\mathrm{da}} T} + \frac{p_{\mathrm{wv}}}{R_{\mathrm{wv}} T} \tag{3.20}$$

with p_{da} denoting partial pressure of dry air, $R_{da} = 287.058\,\mathrm{J/(kgK)}$ specific gas constant for dry air, p_{wv} partial pressure of water vapour, and $R_{wv} = 461.505\,\mathrm{J/(kgK)}$ specific gas constant for water vapour. Knowing mole fraction of water vapour in the air, x_{wv}, we could write

$$\rho = \frac{p(1-x_{wv})}{R_{da}T} + \frac{px_{wv}}{R_{wv}T} = \frac{p(1-x_{wv})}{287.058T} + \frac{px_{wv}}{461.505T}. \tag{3.21}$$

In case of water being fed into the distributor, for example the DIPPR105 equation (Design Institute for Physical Property Research/AIChE, 2012b),

$$\rho = \frac{0.14395}{0.0112^{1+\left(1-\frac{T}{649.727}\right)^{0.05107}}}. \tag{3.22}$$

could be employed to calculate density.

Considering computer implementation itself, it is clear that – as far as compressible flow is concerned – we will either need to solve several relatively complex implicit equations or create a custom iterative mechanism. With respect to the fact that solving implicit equations numerically can be quite troublesome and, moreover, we might want to be able to use different formulae for physical properties of the modelled fluid, it is far better to implement the latter approach. Let us suppose that p^{D}_{i-1}, ρ^{D}_{i-1}, and v^{D}_{i-1} are known. Then the algorithm might be for example as follows:

(1) Estimate density just upstream of the ith branch, e.g. $\rho^{\mathrm{U}}_i := \rho^{\mathrm{D}}_{i-1}$.

(2) Solve Equation 3.19 for v^{U}_i.

(3) Solve Equation 3.18 for p^{U}_i, thus obtaining a zero-friction pressure estimate just upstream of the ith branch, $\widetilde{p}^{\mathrm{U}}_i$.

(4) Calculate $\Delta p^{\mathrm{fr}}_{i-1}$ using Equation 3.9. This will require estimates $\rho^{\mathrm{M}}_{i-1} := (\rho^{\mathrm{D}}_{i-1} + \rho(\widetilde{p}^{\mathrm{U}}_i))/2$, v^{M}_{i-1} (calculated using slightly modified Equation 3.19), Re_i (see Equation 3.13), and subsequently an estimate of Darcy friction factor for the $(i-1)$th section, f_{i-1}, which can be calculated e.g. with Equation 3.12.

(5) Calculate $p^{\mathrm{U}}_i := \widetilde{p}^{\mathrm{U}}_i + \Delta p^{\mathrm{fr}}_{i-1}$ and the corresponding density, $\rho^{\mathrm{U}}_i := \rho(p^{\mathrm{U}}_i, T)$, using an equation of your choice (e.g. Equation 3.21).

(6) Is ρ^{U}_i close enough to the previous estimate? If so, calculate the final value of v^{U}_i using Equation 3.18 and continue to Step 7, otherwise return to Step 2.

(7) Estimate density and pressure just downstream of the ith branch, e.g. $\rho^{\mathrm{D}}_i := \rho^{\mathrm{U}}_i$ and $p^{\mathrm{D}}_i := p^{\mathrm{U}}_i$.

(8) If $i = 1$ then go to Step 9, otherwise go to Step 12.

(9) If this is the first iteration over the entire flow system then go to Step 10, otherwise go to Step 11.

(10) Estimate $\dot{m}^{\mathrm{B}}_1 := \dot{m}_{\mathrm{tot}}/n$ ($\dot{m}_{\mathrm{tot}}$ is the amount of fluid fed into the distributor and n the total number of branches).

(11) Calculate the external pressure p^{B} using Equation 3.7 and continue to Step 13.

(12) Estimate $\dot{m}_i^{\mathrm{B}}$ using Equation 3.7.

(13) Solve Equation 3.4 for v_i^{D}.

(14) Calculate $C_{\mathrm{r},i}$ (see Equation 3.3), solve Equation 3.2 for p_i^{D}, and find the corresponding density, $\rho_i^{\mathrm{D}} := \rho(p_i^{\mathrm{D}}, T)$, using an equation of your choice (e.g. Equation 3.21).

(15) Is ρ_i^{D} close enough to the previous estimate? If so, continue to Step 16, otherwise return to Step 8.

(16) If $i < n$ then $i := i+1$ and return to Step 1, otherwise normalize flow rates, check for convergence and iterate through the entire system again if necessary.

Having obtained the mass flow rates through individual branches, their non-uniformity is used to assess suitability of a given distributor geometry. Since pure distribution commonly means delivering fluid into a significantly lower pressure environment, we do not expect backflow in any of the branches and therefore the percentage

$$\delta = 100 \cdot \left(1 - \frac{\min\limits_i \left\{ \dot{m}_i^{\mathrm{B}} \right\}}{\max\limits_i \left\{ \dot{m}_i^{\mathrm{B}} \right\}} \right) \tag{3.23}$$

can be employed. The closer the value of δ to zero, the more uniform the distribution and hence the more suitable the geometry.

Now, let us discuss the model of incompressible flow. The equations it uses are a bit simpler than those employed in the model of compressible flow described above. However, fluid density is constant here and therefore computer implementation requires comparably less effort. Since for low Mach number flows, i.e., for flows with velocities much lower than the speed of sound, the incompressible approximation is valid even for fluids like air (Acheson, 1990, p. 58), such a simplification may bring substantial shortening of evaluation time.

Near branch entrances, instead of Equation 3.1 we must use the modified Bernoulli equation for incompressible flow,

$$\frac{p}{\rho} + gz + C_{\mathrm{r}} \frac{v^2}{2} = \text{const.}, \tag{3.24}$$

and hence Equation 3.2 becomes

$$\frac{p_i^{\mathrm{U}}}{\rho} + C_{\mathrm{r},i} \frac{\left(v_i^{\mathrm{U}}\right)^2}{2} = \frac{p_i^{\mathrm{D}}}{\rho} + C_{\mathrm{r},i} \frac{\left(v_i^{\mathrm{D}}\right)^2}{2}. \tag{3.25}$$

Equation 3.3 necessary to calculate the coefficient of static regain remains the same, but Equation 3.4 governing discharge through the ith branch changes to

$$\dot{m}_i^{\mathrm{B}} = \rho b_i h_i \left(v_i^{\mathrm{U}} - v_i^{\mathrm{D}} \right) = \frac{\pi d_i^2}{2} C_{\mathrm{d},i} \sqrt{\rho \left(p_i^{\mathrm{U}} + p_i^{\mathrm{D}} \right)}. \tag{3.26}$$

Discharge coefficient $C_{\mathrm{d},i}$ is, again, calculated in the same manner as in case of compressible flow, thus we can use Equation 3.5 without any modifications. Furthermore, the original condition of equal external static pressures (Equation 3.6) is replaced by

$$p_i^{\mathrm{B}} = \frac{p_i^{\mathrm{U}} + p_i^{\mathrm{D}}}{2} - \zeta_i \rho \frac{w_i^2}{2} = p^{\mathrm{B}} = \text{const.} \qquad \forall i \tag{3.27}$$

which, combined with Equation 3.26, becomes

$$p_i^{\mathrm{B}} = \frac{p_i^{\mathrm{U}} + p_i^{\mathrm{D}}}{2} - \frac{2\left(\dot{m}_i^{\mathrm{B}}\right)^2}{\pi^2 d_i^4 C_{\mathrm{d},i}^2 \rho} = p^{\mathrm{B}} = \text{const.} \qquad \forall i \tag{3.28}$$

for $\zeta_i = 1\ \forall i$ similarly as we assumed before.

Considering pressure changes in distributor sections caused by friction, Equations 3.9 and 3.13 must be substituted by

$$\Delta p_i^{\mathrm{fr}} = -\frac{1}{4} f_i l_i \frac{b_i^{\mathrm{M}} + h_i^{\mathrm{M}}}{b_i^{\mathrm{M}} h_i^{\mathrm{M}}} \rho \left(v_i^{\mathrm{M}}\right)^2 \tag{3.29}$$

and

$$\mathrm{Re}_i = \frac{\rho v_i^{\mathrm{M}} D_{\mathrm{h},i}^{\mathrm{M}}}{\mu} = 2\frac{\rho v_i^{\mathrm{M}} b_i^{\mathrm{M}} h_i^{\mathrm{M}}}{\mu\left(b_i^{\mathrm{M}} + h_i^{\mathrm{M}}\right)}. \tag{3.30}$$

Pressure changes due to variation in manifold cross-section are, again, governed by the continuity equation (Equation 3.17) and a variant of the Bernoulli equation. Here, however, we must use the common Bernoulli equation for incompressible flow,

$$\frac{p}{\rho} + gz + \frac{v^2}{2} = \text{const.}, \tag{3.31}$$

instead of Equation 3.16. Hence, for the ith section of our distributor we have

$$\frac{p_i^{\mathrm{D}}}{\rho} + gz_i + \frac{\left(v_i^{\mathrm{D}}\right)^2}{2} = \frac{p_{i+1}^{\mathrm{U}}}{\rho} + gz_{i+1} + \frac{\left(v_{i+1}^{\mathrm{U}}\right)^2}{2} \tag{3.32}$$

and

$$b_i h_i v_i^{\mathrm{D}} = b_{i+1} h_{i+1} v_{i+1}^{\mathrm{U}}. \tag{3.33}$$

Equations 3.29 and 3.32 can be combined to obtain a new equation for pressure just upstream of the $(i+1)$th branch which includes the effect of both friction and change of manifold cross-section:

$$p_{i+1}^{\mathrm{U}} = p_i^{\mathrm{D}} + \rho\left[g(z_i - z_{i+1}) + \frac{\left(v_i^{\mathrm{D}}\right)^2 - \left(v_{i+1}^{\mathrm{U}}\right)^2}{2} - \frac{1}{4} f_i l_i \frac{b_i^{\mathrm{M}} + h_i^{\mathrm{M}}}{b_i^{\mathrm{M}} h_i^{\mathrm{M}}} \left(v_i^{\mathrm{M}}\right)^2\right]. \tag{3.34}$$

Other equations describing physical properties of fluids, Darcy friction factor, as well as Equation 3.23 for calculating non-uniformity of mass flow rates through individual branches remain the same.

Computer implementation of the model of incompressible flow is relatively straightforward. Nevertheless, we still have to use a custom iterative mechanism or solve an implicit equation when dealing with pressures near branch entrance, because we have set a boundary condition for branch outlets (equal external static pressure). Let us suppose that we know p_{i-1}^{D} and v_{i-1}^{D}. Also, $\rho := \rho(p_{\mathrm{in}}, T)$, where p_{in} is the pressure at distributor inlet. Then:

(1) Solve Equation 3.33 for velocities v_{i-1}^{M} and v_i^{U} and calculate Reynolds number Re_{i-1} (see Equation 3.30); then find Darcy friction factor f_{i-1} using equation of your choice (for instance Equation 3.12).

(2) Calculate p_i^{U} using Equation 3.34.

(3) Estimate pressure just downstream of the ith branch, e.g. $p_i^{\mathrm{D}} := p_i^{\mathrm{U}}$.

(4) Calculate $C_{\mathrm{d},i}$ using Equation 3.5.

(5) If $i = 1$ then go to Step 6, otherwise go to Step 9.

(6) If this is the first iteration over the entire flow system then go to Step 7, otherwise go to Step 8.

(7) Estimate $\dot{m}_1^{\mathrm{B}} := \dot{m}_{\mathrm{tot}}/n$ ($\dot{m}_{\mathrm{tot}}$ is the amount of fluid fed into the distributor and n the total number of branches).

(8) Calculate the external pressure p^{B} using Equation 3.28 and continue to Step 10.

(9) Estimate $\dot{m}_i^{\mathrm{B}}$ using Equation 3.28.

(10) Solve Equation 3.26 for v_i^{D}.

(11) Calculate $C_{\mathrm{r},i}$ (see Equation 3.3) and solve Equation 3.25 for p_i^{D}.

(12) Is p_i^{D} close enough to the previous estimate? If so, continue to Step 13, otherwise return to Step 5.

(13) If $i < n$ then $i := i + 1$ and return to Step 1, otherwise normalize flow rates, check for convergence and iterate through the entire system again if necessary.

Simulation Tool: Multi-Platform Java Application

Both variants – compressible and incompressible – of the model above have been implemented in Java[3] so that one can easily evaluate distributors of the described class. The application models, however, are a little less general:

- the entire distribution system is in a single gravitational potential energy level and
- distributor width is kept constant.

The other difference is that in the application implicit equations are solved whenever possible instead of using custom iterative algorithms.

The tool can also be used for distributor shape optimization. Even though the brute-force approach is employed to search given optimization spaces (i.e., all possible distributor shapes within the given boundary dimensions are evaluated), optimum is usually obtained within a couple of seconds due to the simplicity of the model.

[3]Although implementation in Java requires Java Runtime Environment to be installed on the target machines, it allows us to use the tool right away in virtually any modern operating system without porting the code to a different programming language.

Screenshot of the application is shown in Figure 3.10. As can be seen, every parameter is fully customizable. Results of geometry evaluations or shape optimization processes are saved to disk to a specified folder (in plain text format) either as a brief report or as a full one based on user preference. Any such file has a timestamp in its name so that results of different optimization processes can be easily distinguished.

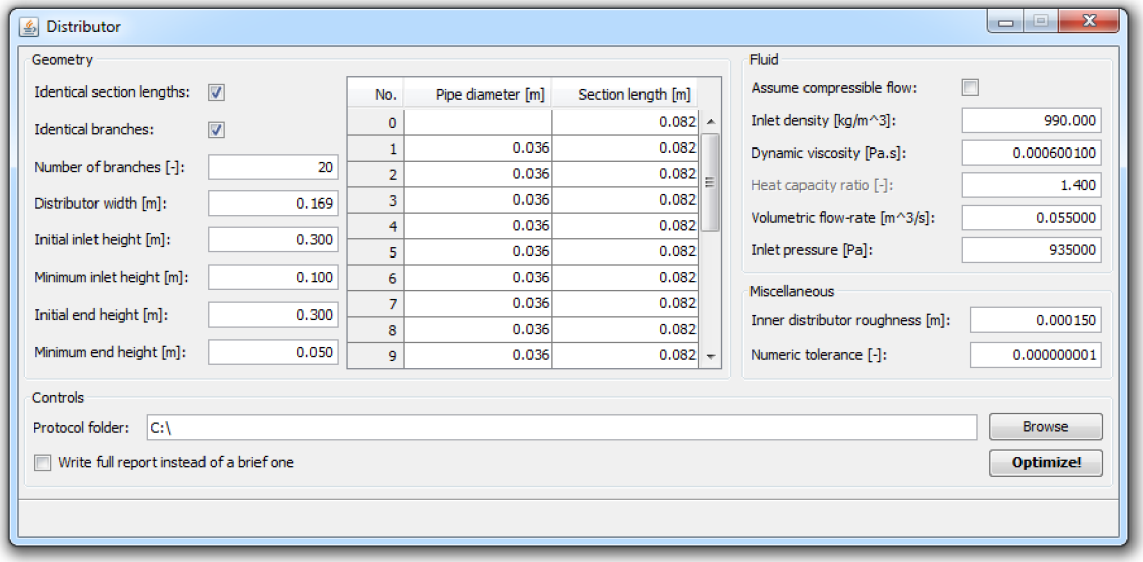

Figure 3.10. Screenshot of the multi-platform Java application

Considering report types, a full report contains results for every evaluated geometry whereas a brief report contains data related to a specific evaluated geometry only if this geometry performs better than the best geometry found so far. The best geometry is therefore mentioned once more at the end of a full report while the last geometry present in a brief report is also automatically the best one. Moreover, a comma-separated values (.CSV) file, which can be opened in any spreadsheet application, is saved along with the report for easier solution data post-processing. Any .CSV data file has the same timestamp in its name as the related report.

Pure distribution, however, is not as common as complete distributor-collector flow systems present in virtually any heat exchanger. This is why we will deal only with such configurations from now on.

3.4.2 Distributor-Collector System with Circular Manifolds

Now we will describe a pseudo-1D model of a relatively simple distributor-collector system. Such parallel flow systems, as they are sometimes called, often contain manifolds with constant circular cross-sections and are commonly used in heat exchange units with single inlet, single outlet, and a tube bundle connecting these two elements. Employing pseudo-1D discretization is beneficial here, because the model remains uncomplicated due to cross-section invariability. Therefore, it can be easily built with a certain level of automation using available integrated technical computing environments such as MathWorks MATLAB (MathWorks, Inc., 2012), Maplesoft Maple (Maplesoft, 2012), or Wolfram Mathematica (Wolfram Research, Inc., 2010).

As before, fluid enters the system through the distributor where it is split into individual tubes of the tube bundle. Then it is heated up or cooled down as required and subsequently it enters the collector to be merged again into a single stream. We distinguish between three main layouts – "U" (Figure 3.11a), "Z" (Figure 3.11b), and "T" (Figure 3.11c).

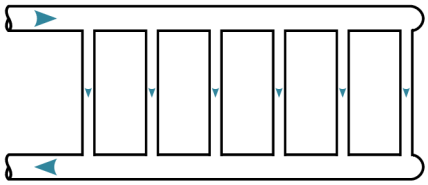

(a) "U" arrangement

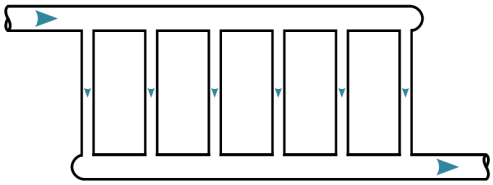

(b) "Z" arrangement

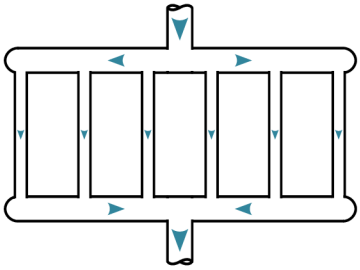

(c) "T" arrangement

Figure 3.11. Flow system arrangements

The model described below is based on the model proposed by Ngoma and Godard (2005), but features the following modifications:

- quantities are evaluated along the manifolds instead of considering those to be mass points;
- mixing of fluid streams of different temperatures is supported at tube entrances and exits in both manifolds due to the possibility of backflow;
- geometry of each tube in a bundle can be defined arbitrarily as a function instead of being specified only by a number of equidistant passes;
- heat flux into each tube can, again, be defined as a function instead of being constant throughout the entire tube bundle; and
- three types of tube ends can be simulated – exserted, conical, and circular bellmouth (see Figure 3.12) – instead of the tubes being just flush with manifold walls.

The former two improvements should provide a noticeable increase in accuracy while the latter three improvements make the new model easily applicable to a wider range of process units. Figure 3.13 shows a sample parallel flow system with moderately complex tube bundle that is easily evaluable using the discussed pseudo-1D model.

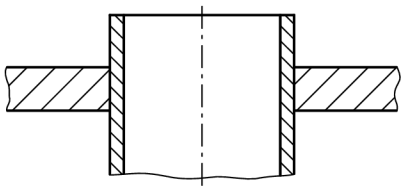

(a) exserted tube end

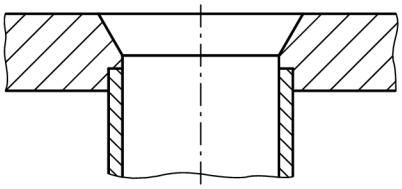

(b) conical tube end

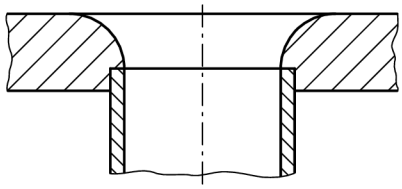

(c) circular bellmouth tube end

Figure 3.12. Tube end types

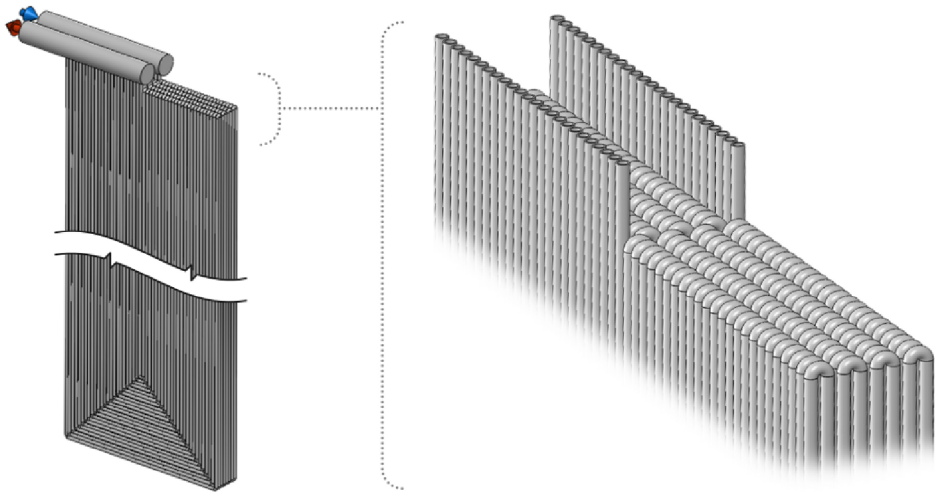

Figure 3.13. Example parallel flow system

Governing Equations

For a one-dimensional steady single-phase flow in a channel having constant cross-section, conservation laws can be written as follows (Ngoma and Godard, 2005):

$$\text{mass}: \quad \frac{\partial(\rho v)}{\partial x} = 0, \tag{3.35}$$

$$\text{momentum}: \quad \frac{\partial(\rho v^2)}{\partial x} + \rho g \sin\beta + \frac{\partial p}{\partial x} + \left.\frac{\partial p}{\partial x}\right|_{\text{friction}} = 0, \quad \text{and} \tag{3.36}$$

$$\text{energy}: \quad \frac{\partial}{\partial x}\left[\rho v\left(H + \frac{v^2}{2} + g x \sin\beta\right)\right] = \dot{q}\frac{U}{S}, \tag{3.37}$$

where x denotes position along a manifold or a tube, β angle of inclination, H enthalpy, $\dot{q}$ heat flux density, U channel circumference, and S cross-sectional area. Density and enthalpy depend on pressure and temperature, hence

$$\frac{\partial \rho}{\partial x} = \frac{\partial \rho}{\partial p}\frac{\partial p}{\partial x} + \frac{\partial \rho}{\partial T}\frac{\partial T}{\partial x} \quad \text{and} \tag{3.38}$$

$$\frac{\partial H}{\partial x} = \frac{\partial H}{\partial p}\frac{\partial p}{\partial x} + \frac{\partial H}{\partial T}\frac{\partial T}{\partial x}. \tag{3.39}$$

Other quantities depend only on position along the channel.

Analogously to Equation 3.8, the friction term in Equation 3.36 can be written as

$$\left.\frac{\partial p}{\partial x}\right|_{\text{friction}} = f\frac{\rho v^2}{2D_\text{h}}. \tag{3.40}$$

As for minor losses between nodes due to flow through an entrance, exit, or a bend, we can incorporate them into Equation 3.36 by adding the standard equation,

$$\left.\frac{\partial p}{\partial x}\right|_{\text{minor loss}} = \zeta\rho\frac{v^2}{2}, \tag{3.41}$$

with coefficients of hydraulic resistance, ζ, taken from (Idelchik, 1986). Implementation-wise, this can be easily done by employing an automatically generated indicator function (see e.g. Doob, 1994, p. 1) on the set of pseudo-1D mesh nodes for each minor loss type (more than one such function is necessary because coefficients of hydraulic resistance are calculated differently for wyes, bends, etc.).

Considering control volumes enclosing entrances and exits of lateral tubes through which fluid flows in or out of the manifolds, the equation system cannot be the same, because inflow or outflow causes momentum changes as well. To factor in the subsequent pressure changes, the present model uses the simplified approach involving coefficient of static regain (see Section 3.4.1). The other thing we must take into account is that now streams of different temperatures can mix near each tube end. For the sake of simplicity, we will assume perfect mixing. Since there always are three channels and the amount of fluid flowing into the control volume must inevitably flow out, we can calculate the temperature of outbound streams using

$$T_\text{out} = \sum_{\substack{j=1\\ \dot{m}_j>0}}^{3} \dot{m}_j c_\text{p}\left(T_j\right) T_j \Bigg/ \sum_{\substack{j=1\\ \dot{m}_j>0}}^{3} \dot{m}_j c_\text{p}\left(\widetilde{T}\right), \quad \text{where} \quad \widetilde{T} = \sum_{\substack{j=1\\ \dot{m}_j>0}}^{3} \dot{m}_j T_j \Bigg/ \sum_{\substack{j=1\\ \dot{m}_j>0}}^{3} \dot{m}_j. \tag{3.42}$$

In case of air, specific heat capacity at constant pressure necessary in the equation above can be calculated using

$$c_\text{p} = \frac{c_\text{p,da}(1-x_\text{wv})}{m_\text{da}} + \frac{c_\text{p,wv}\,x_\text{wv}}{m_\text{wv}} \tag{3.43}$$

with specific heat capacity of dry air being computed for example via the DIPPR107 equation (Design Institute for Physical Property Research/AIChE, 2012a),

$$c_\text{p,da} = 28958 + 9390\left(\frac{\frac{3012}{T}}{\sinh\frac{3012}{T}}\right)^2 + 7580\left(\frac{\frac{1484}{T}}{\cosh\frac{1484}{T}}\right)^2, \tag{3.44}$$

and specific heat capacity of water vapour via the same equation with different coefficients (Design Institute for Physical Property Research/AIChE, 2012b),

$$c_{\mathrm{p,wv}} = 33363 + 26790 \left(\frac{\frac{2610.5}{T}}{\sinh \frac{2610.5}{T}} \right)^2 + 8896 \left(\frac{\frac{1169}{T}}{\cosh \frac{1169}{T}} \right)^2. \tag{3.45}$$

Molar masses of dry air and water vapour are $m_{\mathrm{da}} = 28.966\,\mathrm{kg/kmol}$ and $m_{\mathrm{wv}} = 18.016\,\mathrm{kg/kmol}$, respectively. If necessary, specific heat capacity at constant volume would then be easy to obtain using the Mayer's relation,

$$c_{\mathrm{v}} = c_{\mathrm{p}} - R = c_{\mathrm{p}} - \frac{\bar{R}}{(1 - x_{\mathrm{wv}})\, m_{\mathrm{da}} + x_{\mathrm{wv}} m_{\mathrm{wv}}}, \tag{3.46}$$

in which R denotes the specific gas constant and $\bar{R} = 8314.472\,\mathrm{J/(kmol\,K)}$ the universal gas constant. As for water, we might employ the DIPPR100 equation (Design Institute for Physical Property Research/AIChE, 2012b),

$$c_{\mathrm{p}} = 276370 - 2090.1T + 8.125T^2 - 1.412 \cdot 10^{-2} T^3 + 9.370 \cdot 10^{-6} T^4, \tag{3.47}$$

for calculation of both c_{p} and c_{v}, since in case of liquid water their differences are negligible (Smith, 1965).

Spatial Discretization of the Flow System

Although splitting manifold, combining manifold, and tubes in the tube bundle can be discretized separately, it is beneficial to do it in such a way that key nodes are shared between these subsystems. This means that the inlet node of each tube is identical to a corresponding node in the splitting manifold and, similarly, the outlet node of each tube is identical to a corresponding node in the combining manifold. For numerical reasons, it may also be advantageous to keep spatial step constant if possible, although sharing of key nodes usually does not permit equidistant spacing in the areas around entrances and exits in the splitting and combining manifold.

Approximation of Partial Derivatives and Non-Linear Terms

Partial derivatives can be approximated for example using the forward finite difference method (Ames, 1992, p. 16), i.e., in case of pressure we would have

$$\frac{\partial p}{\partial x} \approx \frac{\Delta p}{\Delta x} = \frac{p(x + \Delta x) - p(x)}{\Delta x} \tag{3.48}$$

while in general for kth partial derivative we can write

$$\frac{\partial^k p}{\partial x^k} \approx \frac{1}{\Delta x^k} \sum_{i=0}^{k} (-1)^i \binom{k}{i} p(x + (k - i)\Delta x) \tag{3.49}$$

where Δx denotes spatial step. Approximating partial derivatives of other quantities can be done in an analogous manner.

Should any equation contain non-linear terms, we can either completely rely on an internal solver incorporated in the technical computing environment of our choice or approximate

such non-linearities e.g. by their first order Taylor expansions[4] (Patankar, 1980, p. 49). For a function $f(x)$ approximated near $x = x_0$, Taylor expansion can generally be written as a power series

$$\begin{aligned} \mathrm{T}_f(x_0) &= f(x_0) + \frac{f'(x_0)}{1!}(x - x_0) + \frac{f''(x_0)}{2!}(x - x_0)^2 + \frac{f^{(3)}(x_0)}{3!}(x - x_0)^3 + \cdots = \\ &= \sum_{k=0}^{\infty} \frac{f^{(k)}(x_0)}{k!}(x - x_0)^k. \end{aligned} \tag{3.50}$$

Obviously, the function f must be infinitely differentiable for the above series to exist, however, since we only need the first order Taylor expansion,

$$f(x) \approx f(x_0) + f'(x_0)(x - x_0), \tag{3.51}$$

existence of first derivative is sufficient (virtually any reasonable function used in models of physical problems satisfies this condition). In any case, once a non-linear term appears in any of the equations, we are forced to use iterative solution methods instead of much faster methods for systems of linear equations.

Comparison with Other Models

The only models of single-phase flow validated with experimental data that the author was able to find were those assuming adiabatic flow systems. Figure 3.14 compares data obtained using the present model with predictions of models by Wang and Yu (1989) and Ablanque et al. (2010) (for flow system geometry etc. please refer to either of these two papers). It can be seen that agreement among the models is good, especially between the present model and the one by Ablanque et al. (2010).

Simulation Tool: Maple Worksheet

Maplesoft Maple was chosen for computer implementation of the pseudo-1D model for its symbolic computation capabilities. Nonetheless, the worksheet is built with maximum automation in mind and thus only the input data, i.e.,

- characteristic dimensions of the flow system and function describing geometry of tubes in the tube bundle,
- pressure and temperature at inlet and functions for fluid properties calculation,
- function describing heat flux into individual tubes, and
- general data such as spatial step or numerical tolerance,

must be entered by the user. Spatial discretization of the flow system is performed by an internal algorithm. Due to the fact that no elements other than wyes and bends causing minor losses are assumed to be present, such losses can, too, be calculated without user interaction. In case of bends, channel curvature around the current node is estimated using

[4] We can still use the solver to deal with the resulting set of equations, but in some computing environments such a pre-processing might mean the difference between getting a solution and getting an error message.

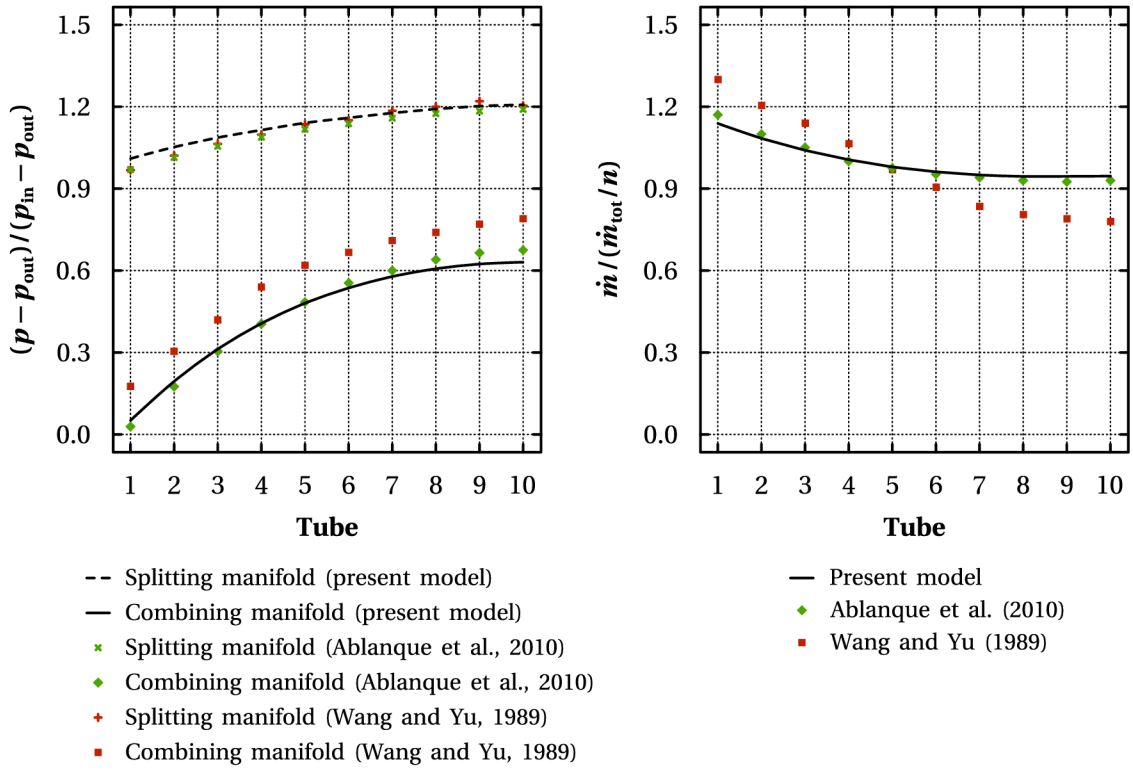

Figure 3.14. Comparison of results yielded by three different models. Flow system inlet and outlet pressures are denoted p_{in} and p_{out}.

the provided function describing tube geometry and the obtained value is then taken as a basis for estimation of the respective coefficient of hydraulic resistance (see Idelchik, 1986, Chapter 6). Minor losses due to flow through wyes are calculated similarly as in the model of pure distribution (the set of key nodes indicating wye positions is generated during spatial discretization).

The worksheet can also be used to optimize distributor and collector diameters. The brute-force approach is employed, but the model is computationally simple enough to swiftly search the optimization space and find the optimum manifold diameter. Flow rates through individual tubes and pressure and temperature profiles in the manifolds obtained during evaluation of each geometry configuration are then presented in graphs along with pressure and temperature at collector outlet, overall pressure drop, and relative standard deviation from uniform flow distribution[5],

$$\delta = \frac{100}{\dot{m}_{id}} \sqrt{\frac{1}{n} \sum_{i=1}^{n} (\dot{m}_i - \dot{m}_{id})^2}, \tag{3.52}$$

with $\dot{m}_{id}$ denoting mass flow rate through one tube corresponding to a uniform flow distribution, n number of tubes in the tube bundle, and $\dot{m}_i$ mass flow rate thought the ith tube.

As an example, let us consider optimization of manifold diameters in a parallel flow system with the 24-tube bundle shown in Figure 3.13. This flow system is a part of an economizer

[5]We cannot utilize Equation 3.23 mentioned before, because backflow can occur in the present model.

preheating high-pressure (10 MPa) water from temperature $T_{\text{in}} = 188.8$ °C to $T_{\text{out}} \approx 275$ °C at the total mass flow rate of $\dot{m}_{\text{tot}} = 6.028$ m^3/s. For simplicity's sake, heat flux density will be considered constant for the entire tube bundle, even though we could easily define it as a function of position along each separate tube if we needed to. We will discretize the manifolds using the spatial step $\Delta x_{\text{M}} = 0.005$ m while the tubes will be discretized with $\Delta x_{\text{T}} = 0.02$ m because of their rather large lengths. Also, we will allow the algorithm to use adaptive step size to speed up evaluation of long straight tube segments. For the diameter range of $[0.01,\ 0.35]$ m the worksheet provides the optimum diameter $D_{\text{opt}} = 0.05$ m in roughly 62 s using the Intel Core i5-2500K processor[6]. Approximately one half of this time is spent on spatial discretization and subsequent grid analysis necessary for estimation of minor losses since the respective algorithms use cycles which Maple, as of yet, is not able to process as efficiently as (pre-)compiled codes are. If we used larger spatial steps then the optimization time would have been significantly shorter.

Considering performance of the optimum geometry, relative standard deviation from uniform flow distribution is 1.96 % with pressure drop being close to 19.5 kPa. Flow rates and pressure and temperature profiles are shown in Figure 3.15. From the flow rates being positive and also from the fact that temperature remains constant throughout the entire distributor we can see that no backflow occurs in the system.

If, however, the best flow distribution obtainable with manifolds having constant cross-sections was still too non-uniform for our needs, we would have to use distributor and collector with variable cross-sectional areas along their lengths similarly as we did in case of pure distribution (see Section 3.4.1; we could opt for manifolds with gradually varied circular cross-sections or for step manifolds consisting of constant-diameter segments connected by transition pieces, but these tend to be harder to manufacture compared to the previously described "rectangular" manifolds). The following text thus presents a model of a more complex parallel flow system containing a distributor and a collector with rectangular cross-sections.

3.4.3 Double U-Tube Heat Exchanger Module

The double U-tube heat exchanger module, shown in Figure 3.16, is a part of the heat exchanger for high temperature gas–gas applications briefly presented in Section 2.3. Commonly, such an exchanger is used to preheat fluidizing and combustion air and contains several identical modules stacked horizontally in a vertical hexahedral shell (see Figure 3.17). Each of the modules then consists of two stepless manifolds and two sets of U-tubes connecting them. The manifolds are, in principle, identical to the distributor discussed in Section 3.4.1 and the mathematical model is very similar as well. This time, however, we must take into consideration the fact that pressure drops in individual U-tubes are different from each other and that the U-tube outlet pressures must correspond to pressures at branching points in the collector.

To increase the accuracy of predictions, here we derived the formula for coefficient of static regain my means of approximating data obtained by evaluation of many configurations of such distribution systems using the fluid flow modelling software ANSYS FLUENT (Fluent, Inc., 2006). Fine meshes were always generated to ensure data from CFD were accurate enough. Moreover, steady-state calculations were performed before transient ones in which

[6] Please note that to be able to take full advantage of multi-core processors at least version 16 of Maple is necessary.

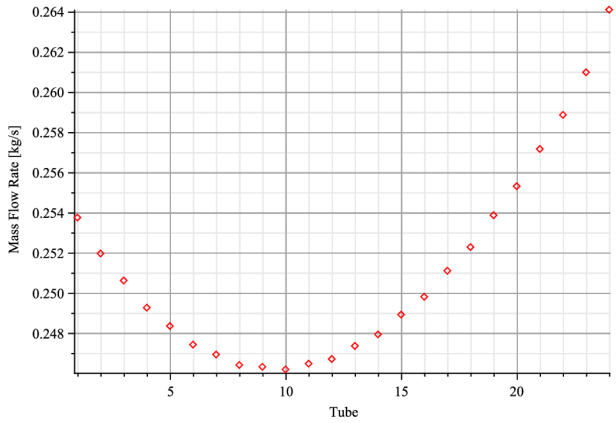

(a) flow rates through individual tubes

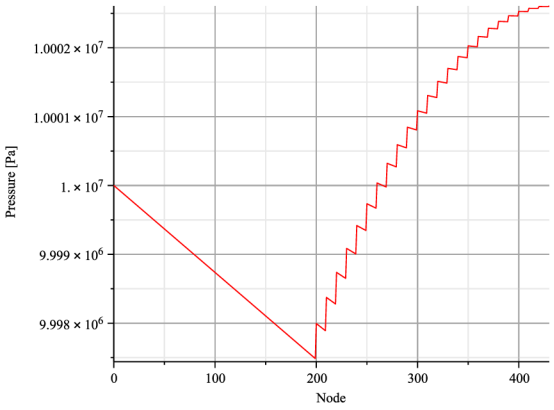

(b) distributor: pressure profile

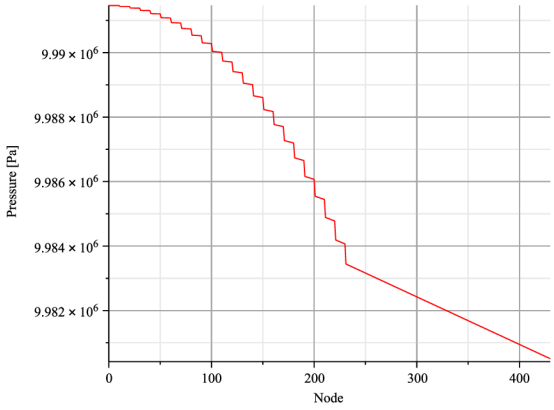

(c) collector: pressure profile

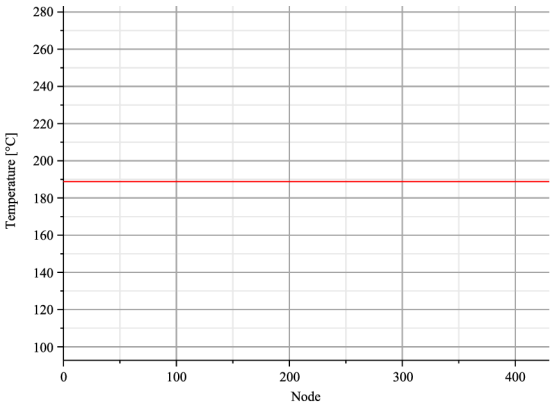

(d) distributor: temperature profile

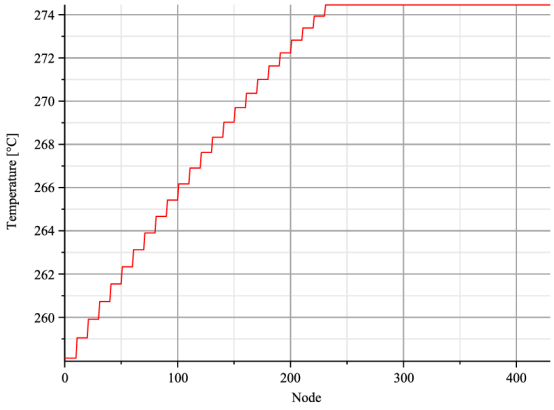

(e) collector: temperature profile

Figure 3.15. Graphs of flow rates and pressure and temperature profiles for the optimum manifold diameter $D_{\text{opt}} = 0.05$ m as presented in the Maple worksheet

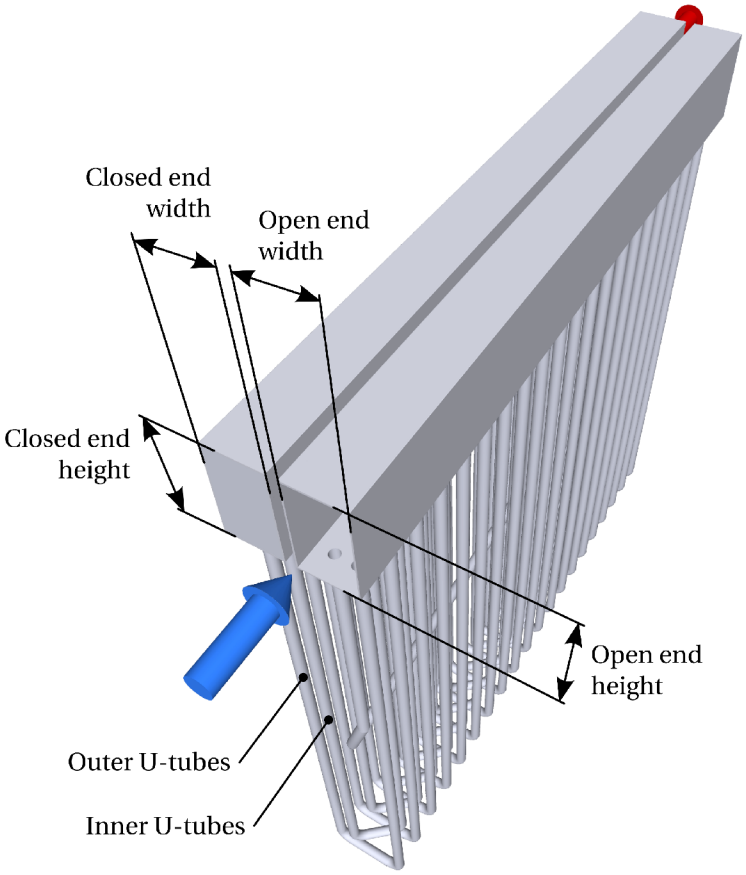

Figure 3.16. Double U-tube heat exchanger module

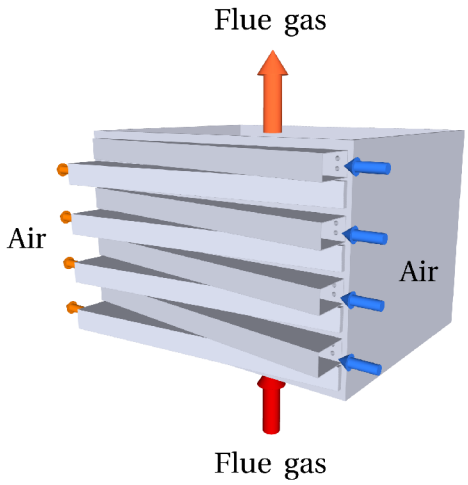

Figure 3.17. Hexahedral shell containing four modules with linearly tapered manifolds

time step was always set to 0.005 s with simulated time periods being chosen ad hoc according to the behaviour of mass flow rates. Data from calculations for which flow rates fluctuated significantly (i.e., when standard deviation of flow rates was greater than 10 % of a flow rate through one U-tube in case of a uniform flow distribution) even after 200 s of simulated time were not considered. Graph of a typical flow rate behaviour is shown in Figure 3.18.

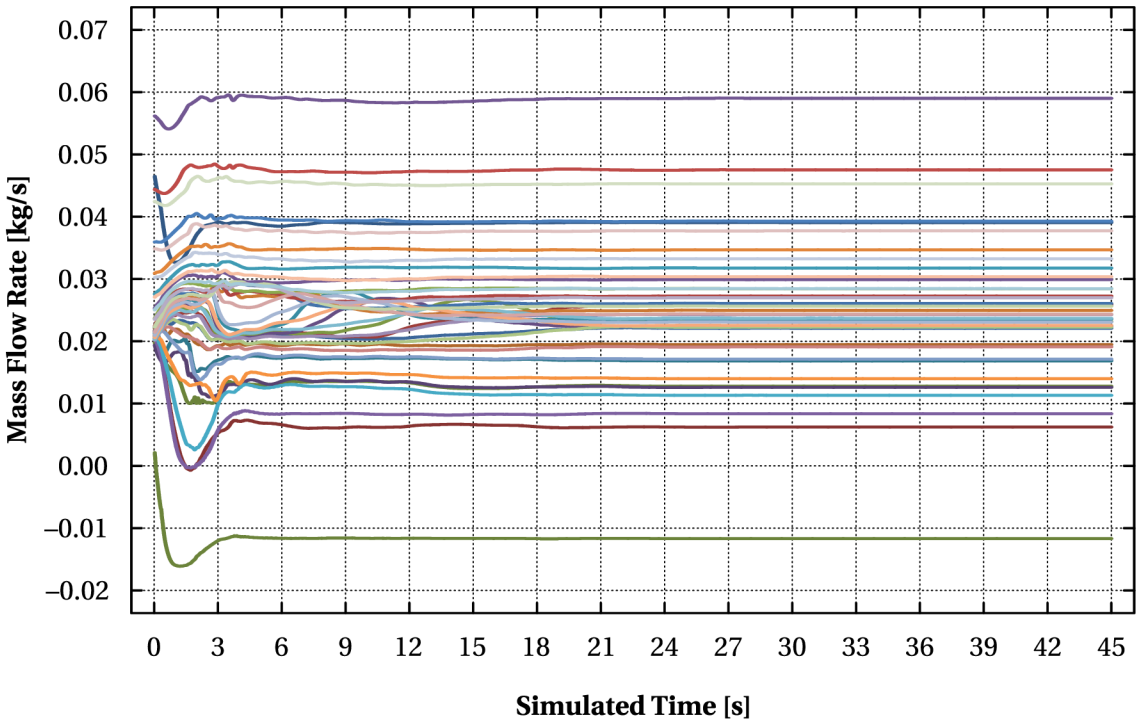

Figure 3.18. Typical flow rate behaviour for a system in which air is preheated from 30 °C to 350 °C at the rate of 1 kg/s (each curve represents one U-tube). It can be seen that flow rates remain constant after the 32 s time mark and also that backflow occurs in one of the U-tubes. In this case normalized mean flow rates for simulated time $\hat{t} \geq 32$ s were used for finding the formula for C_r.

Coefficient of Static Regain

One can predict flow distribution without ever using estimates of coefficients of static regain (see Bajura and Jones, 1976) or, alternatively, calculate their values exactly (see Wang et al., 2001). Nevertheless, the former scenario requires us to solve non-linear partial differential equations with a detailed knowledge of the actual velocity profiles in the ducts being necessary. Similarly, the latter scenario demands solving non-linear ordinary differential equations and then using the calculated coefficients in the usual manner. In both cases it is quite difficult a task even for a geometrically very simple system. On the other hand, Bailey (1975) demonstrated that it is possible to estimate values of the coefficients with sufficient accuracy using a function of hole-to-duct area ratio and velocity ratio,

$$C_r = 0.78 + \left(0.284 + 0.098 \log_{10} \frac{d}{D}\right) \log_{10} \frac{v_U}{v_U - v_D}, \tag{3.53}$$

where d denotes discharge port diameter, D manifold diameter, v_{U} fluid velocity in the manifold upstream of the discharge port, and v_{D} fluid velocity in the manifold downstream of the discharge port. However, this formula might not perform optimally in the studied family of parallel distribution systems. A comprehensive set of various geometries was therefore evaluated in ANSYS FLUENT to acquire relevant data. The new coefficient was then assumed to be a sum of several sub-terms each of which would account for a different distribution system characteristic. Please note that to make matters easier, nomenclature will generally remain the same as in the pure distribution model (see the schematic in Figure 3.9).

A baseline coefficient for constant cross-section manifolds and sharp tube ends mounted flush with manifold walls was evaluated first. For this, data obtained using 61 different manifold geometries ranging from 140 × 50 mm (cross-section width × height) to 185 × 500 mm[7] were analysed in Minitab (Minitab, Inc., 2006). Denoting a common logarithm of velocity ratio $\log_{10}\frac{v}{\Delta v}$, duct-to-hole area ratio $\frac{S}{s}$, and manifold cross-section height-to-width ratio $\frac{h}{b}$, C_{r} was assumed to be a function of $\log_{10}\frac{v}{\Delta v}$ along with one of the following six separate predictors or three pairs of predictors:

$\frac{S}{s}$	$\sqrt{\frac{S}{s}}$	$\log_{10}\sqrt{\frac{S}{s}}$
$\frac{h}{b}\frac{S}{s}$	$\frac{h}{b}\sqrt{\frac{S}{s}}$	$\frac{h}{b}\log_{10}\sqrt{\frac{S}{s}}$
$\frac{S}{s}$ and $\frac{h}{b}$	$\sqrt{\frac{S}{s}}$ and $\frac{h}{b}$	$\log_{10}\sqrt{\frac{S}{s}}$ and $\frac{h}{b}$

The best fit was then obtained with $C_{\mathrm{r}} = C_{\mathrm{r}}\left(\log_{10}\frac{v}{\Delta v}, \frac{S}{s}, \frac{h}{b}\right)$ and the main constant term from Equation 3.53 being slightly decreased from 0.78 to 0.75. Thus, for the ith branch the formula for coefficient of static regain was

$$C_{\mathrm{r},i} = 0.750 + \left(0.437 - 0.00470\frac{S_i}{s_i} + 0.338\frac{h_i}{b_i}\right)\log_{10}\frac{v_i^{\mathrm{U}}}{v_i^{\mathrm{U}} - v_i^{\mathrm{D}}} = \tau_i^{\mathrm{const},0}. \tag{3.54}$$

The Greek letter τ used in the above equation represents sub-terms while in the superscript it is specified for which type of manifold feature the corresponding sub-term accounts for. Namely, the superscript states information about manifold cross-section variability and U-tube exsertion variability, respectively. Symbol $\tau_i^{\mathrm{const},0}$ therefore denotes the sub-term related to the ith branch of a constant cross-section manifold with zero exsertion of U-tube ends (i.e., U-tubes are mounted flush with manifold walls). Detailed results of the regression analysis provided by Minitab were as follows:

```
Regression Analysis: COEF versus S/s; h/b

The regression equation is
COEF = 0.437 - 0.00470 S/s + 0.338 h/b

Predictor       Coef   SE Coef      T      P    VIF
Constant     0.43685   0.01078  40.53  0.000
S/s        -0.004697  0.001392  -3.38  0.001  7.936
```

[7]The minimum as well as the maximum cross-section width (140 mm and 180 mm, respectively) are given by the U-tube bundle geometry.

```
h/b          0.33789   0.01860  18.16  0.000  7.936

S = 0.0444655   R-Sq = 96.9%   R-Sq(adj) = 96.8%
PRESS = 0.131845   R-Sq(pred) = 96.41%

Analysis of Variance
Source          DF      SS      MS       F      P
Regression       2  3.5558  1.7779  899.20  0.000
Residual Error  58  0.1147  0.0020
Total           60  3.6705

Source  DF  Seq SS
S/s      1  2.9036
h/b      1  0.6522

Unusual Observations
Obs   S/s     COEF      Fit   SE Fit  Residual  St Resid
 10  34.4  1.40000  1.45842  0.02274  -0.05842     -1.46 X
 30  39.3  1.40000  1.29511  0.01337   0.10489      2.38 R
 48  25.0  0.75000  0.86366  0.00822  -0.11366     -2.51 R
 58  27.3  0.75000  0.85484  0.01072  -0.10484     -2.34 R
 60  44.5  1.10000  1.12088  0.01846  -0.02088     -0.50 X
 61  45.4  1.20000  1.13488  0.01891   0.06512      1.55 X

R denotes an observation with a large standardized residual.
X denotes an observation whose X value gives it large leverage.

No evidence of lack of fit (P >= 0.1).
```

It can be seen from the p-value (0.000) in the Analysis of Variance section that the obtained model is statistically significant at the α-level of 0.05. The same holds for all three coefficients, since their p-values are also well below 0.05. The model explains 96.90 % (R^2) of the variance in C_r, i.e., it fits the data very well. The predicted R^2 (96.41 %) is quite close to R^2 which means that the model is not overfit and has adequate predictive ability. Moreover, Minitab did not find any evidence of lack of fit. Observations 10, 30, 48, 58, 60, and 61 were marked as unusual thus indicating they may be outliers, however, histogram (see Figure 3.19) fits probability density function of a normal distribution nicely and does not contain any outlying column. Also, all residuals are within 95 % confidence interval (see the normal probability plot in Figure 3.20).

Both histogram and normal probability plot of residuals visually confirm that the first requirement for regression analysis is met – residuals are consistent with a normal distribution having zero mean. Statistically, this is warranted by the p-value (see the box beside normal probability plot) being well over the α-level of 0.05 and by the low value of the Anderson-Darling statistic (denoted as "AD" in the box; see Meloun and Militký, 2004, p. 130). For a large number of observations N and $\alpha = 0.05$, its critical value can be estimated (Meloun and Militký, 2004, p. 131) by

$$D_{1-\alpha} = D_{0.95} \approx 1.0348 \left(1 - \frac{1.013}{N} - \frac{0.93}{N^2}\right) \tag{3.55}$$

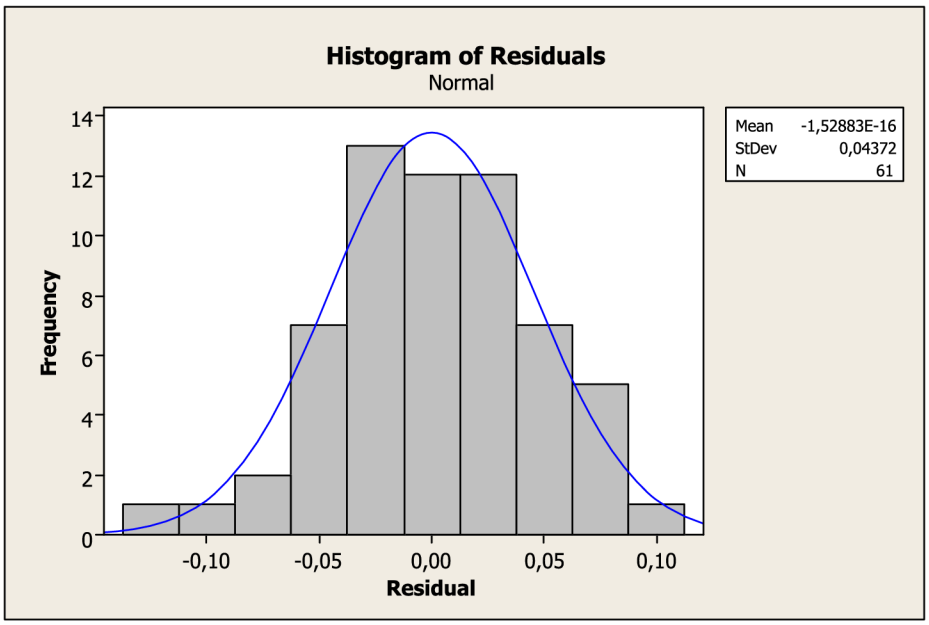

Figure 3.19. Histogram of residuals with a normal distribution fit

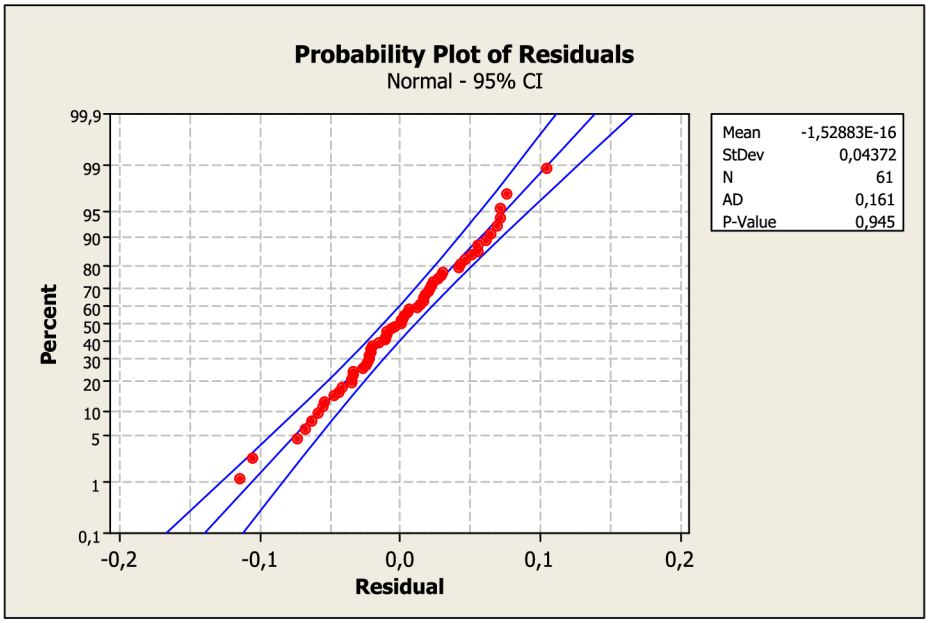

Figure 3.20. Normal probability plot of residuals with 95% confidence interval

and for AD $< D_{0.95}$ we do not reject the hypothesis that the residuals follow a normal distribution. In this case $D_{0.95} = 1.0348\left(1 - \frac{1.013}{61} - \frac{0.93}{61^2}\right) = 1.017 > 0.161$ and therefore the hypothesis was, indeed, not rejected. The second assumption made when performing least-squares regression modelling is that the residuals have approximately constant variance. This is visually confirmed by Residuals vs. Fits and Residuals vs. Predictors scatterplots in Figures 3.21 through 3.23.

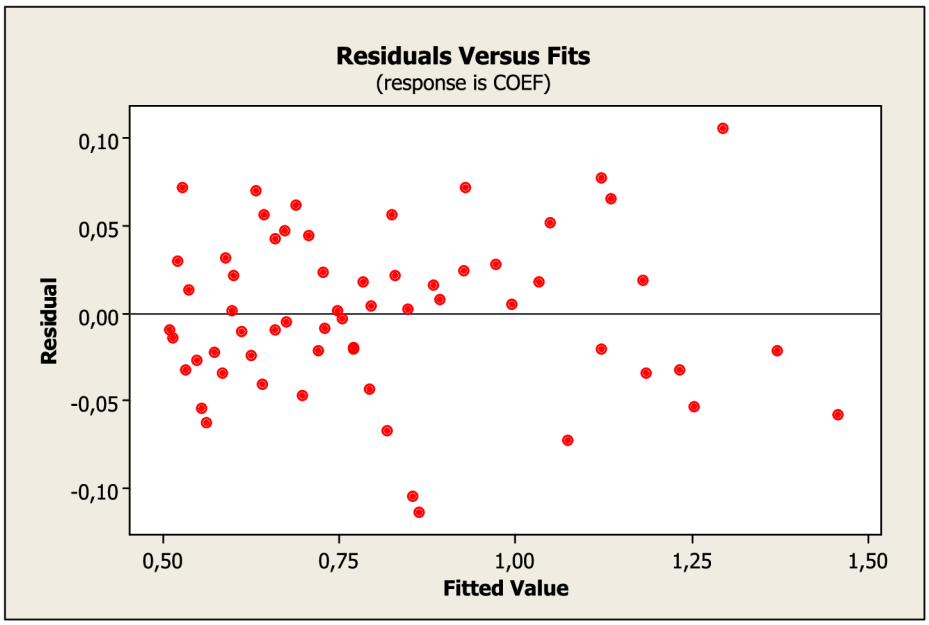

Figure 3.21. Scatterplot showing Residuals vs. Fits

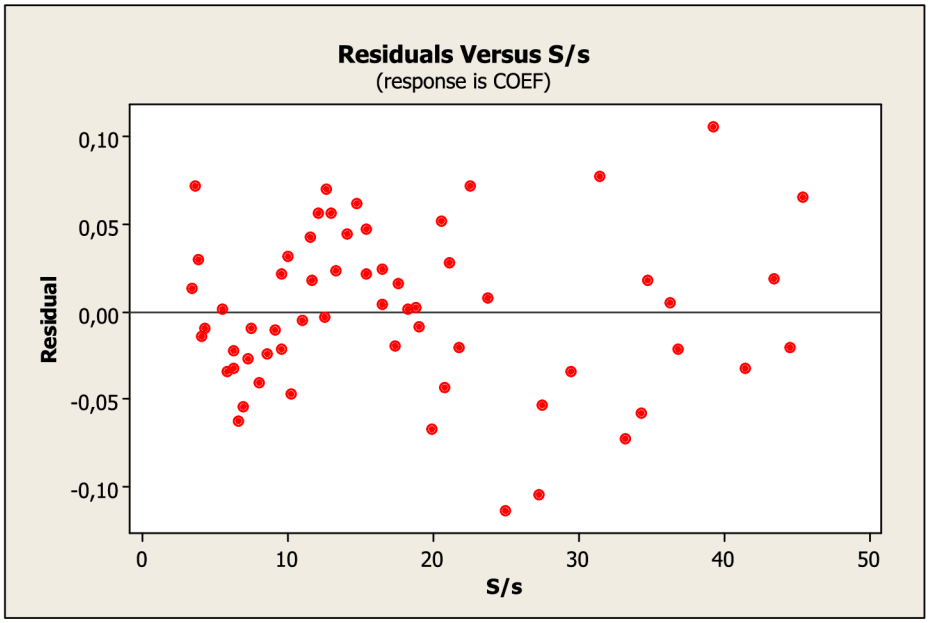

Figure 3.22. Scatterplot showing Residuals vs. $\frac{S}{s}$

Although the remaining sub-terms of the formula for coefficient of static regain are in some cases fairly complex, it is necessary so that no other decision logic is required and that accuracy is not lost. In any case, before we proceed to the actual sub-terms we must define several auxiliary variables:

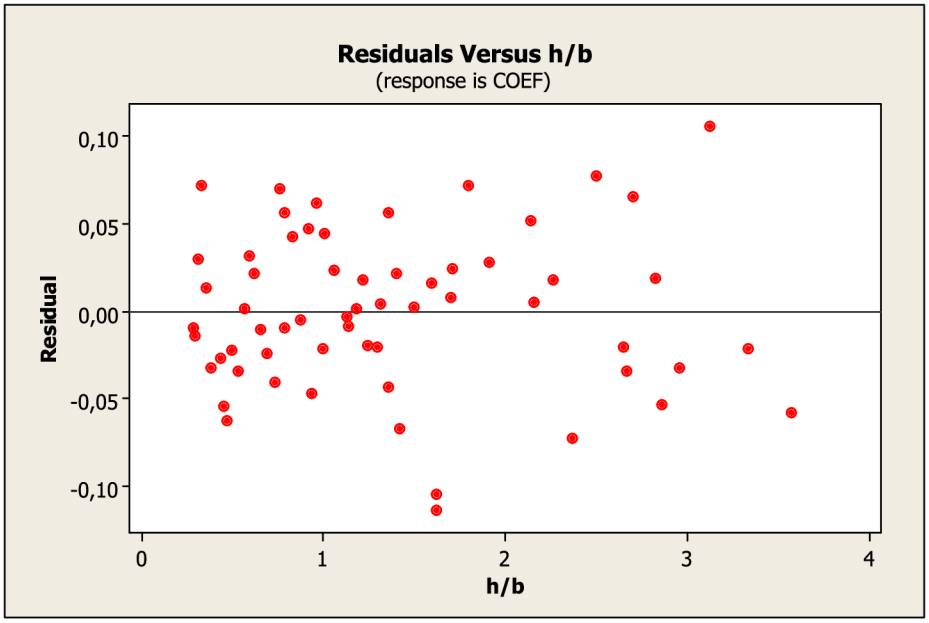

Figure 3.23. Scatterplot showing Residuals vs. $\frac{h}{b}$

- manifold multiplier

$$\kappa_{\text{man}} = \begin{cases} 1 & \text{for splitting manifold} \\ -1 & \text{for collecting manifold;} \end{cases} \tag{3.56}$$

- corrected overall change in hydraulic diameter

$$\Delta D_{\text{h}}^{\text{ovr}} = \kappa_{\text{man}} \left(\frac{2 b_n^{\text{M}} h_n^{\text{M}}}{b_n^{\text{M}} + h_n^{\text{M}}} - \frac{2 b_0^{\text{M}} h_0^{\text{M}}}{b_0^{\text{M}} + h_0^{\text{M}}} \right); \tag{3.57}$$

- hydraulic diameter ratio in the section just upstream of the ith manifold branch

$$D_{\text{h},i}^{\text{rat}} = \begin{cases} \dfrac{D_{\text{h},i}}{D_{\text{h},i-1}} = \dfrac{2 b_i h_i}{b_i + h_i} \Big/ \dfrac{2 b_{i-1} h_{i-1}}{b_{i-1} + h_{i-1}} & \text{if } D_{\text{h},i-1} > 0 \\ 1 & \text{otherwise;} \end{cases} \tag{3.58}$$

- closed to open end cross-sectional area ratio

$$S_{\text{CO}}^{\text{rat}} = \left(\frac{b_n^{\text{M}} h_n^{\text{M}}}{b_0^{\text{M}} h_0^{\text{M}}} \right)^{\kappa_{\text{man}}}; \tag{3.59}$$

- absolute value of the overall change in cross-sectional area

$$\Delta S_{\text{abs}}^{\text{ovr}} = \left| b_n^{\text{M}} h_n^{\text{M}} - b_0^{\text{M}} h_0^{\text{M}} \right|; \tag{3.60}$$

- area multiplier for the ith branch

$$\kappa_{S,i} = \begin{cases} \dfrac{b_i h_i - b_1 h_1}{b_n h_n - b_1 h_1} - \dfrac{1}{2}\left(1 + \kappa_{\text{man}} \dfrac{\Delta S_i}{|\Delta S^{\text{avg}}|}\right) & \text{if } |\Delta S^{\text{avg}}| > 0 \\ 1 & \text{otherwise,} \end{cases} \tag{3.61}$$

  where ΔS_i denotes cross-sectional area change in the section just upstream of the ith branch and $\Delta S^{\text{avg}} = \frac{b_n h_n - b_1 h_1}{n-1}$ average cross-sectional area change per one non-inlet/outlet manifold section;

- cross-section height multiplier for the ith branch

$$\kappa_{h,i} = \begin{cases} \left|\dfrac{h_i - h_1}{h_n - h_1}\right| & \text{if } h_n - h_1 < 0 \\ 0 & \text{otherwise;} \end{cases} \tag{3.62}$$

- exserted U-tube end area to manifold cross-sectional area ratio for the ith branch

$$S_i^{\text{rat}} = \frac{2 d_i E_i}{b_i h_i}, \tag{3.63}$$

  where E_i is the exsertion length of the ith U-tube end;

- average exsertion of U-tube ends

$$E^{\text{avg}} = \frac{1}{n} \sum_{i=1}^{n} E_i; \tag{3.64}$$

- difference from the average U-tube exsertion

$$E_i^{\text{diff}} = E_i - E^{\text{avg}}; \tag{3.65}$$

- corrected average U-tube exsertion to cross-section height ratio

$$E_i^{\text{rat}} = \kappa_{\text{man}} \text{sgn}(E_n - E_1) \frac{E^{\text{avg}}}{h_i}. \tag{3.66}$$

All the sub-terms listed in the following paragraphs, i.e., sub-terms accounting for

- linearly variable cross-section width and height and U-tubes mounted flush with manifold walls,
- constant cross-section dimensions with constant exsertion of U-tube ends,
- linearly variable cross-section width and height and constant exsertion of U-tube ends, and
- variable exsertion of U-tube ends,

were obtained using Minitab via the procedure described earlier while it was made sure that the regression models were statistically sound and that they fit the data well. If linear regression proved to be inadequate by having a low coefficient of determination (R^2), a more complex regression model was proposed based on actual behaviour of the mathematical model of the exchanger module. Such a regression model was built successively using partial sub-terms and then it was manually analysed en bloc in Minitab. Even though this statistical software can only perform linear regression, once we had the full model we could easily find residuals

$$r_i = y_i - \hat{f}_i \qquad i = 1, \ldots, k \tag{3.67}$$

where y_i were observed data, $\hat{f}_i$ values obtained with the regression model, and k the number of data points; total sum of squares

$$\mathrm{SS}_{\mathrm{tot}} = \sum_{i=1}^{k} \left(y_i - \bar{y}\right)^2 \tag{3.68}$$

in which $\bar{y} = \frac{1}{k}\sum_{i=1}^{k} y_i$ denotes the estimate of the mean of the observed data; residual sum of squares

$$\mathrm{SS}_{\mathrm{res}} = \sum_{i=1}^{k} r_i^2 = \sum_{i=1}^{k} \left(y_i - \hat{f}_i\right)^2; \tag{3.69}$$

coefficient of determination

$$R^2 = 1 - \frac{\mathrm{SS}_{\mathrm{res}}}{\mathrm{SS}_{\mathrm{tot}}}; \tag{3.70}$$

or any other related statistic that might be of interest.

To obtain the sub-term accounting for linear variation in cross-section widths and heights while sharp U-tube ends are mounted flush with manifold walls, 51 additional geometries were evaluated. As before, the data were used to find corresponding regression coefficients using the model with preliminary formula for C_{r} containing

$$\widetilde{\tau}_i^{\mathrm{var},0} = D_{\mathrm{h},i}^{\mathrm{rat}} \left(A + B\left(1 - \kappa_{S,i}\right)^4\right) \tag{3.71}$$

in addition to $\tau_i^{\mathrm{const},0}$. Coefficients A and B were then analysed in Minitab which for the ith branch ultimately yielded

$$\begin{aligned} \tau_i^{\mathrm{var},0} = D_{\mathrm{h},i}^{\mathrm{rat}} \Big(& -4.807\Delta D_{\mathrm{h}}^{\mathrm{ovr}} - 11.451\left(\Delta D_{\mathrm{h}}^{\mathrm{ovr}}\right)^2 - 14.001\left(\Delta D_{\mathrm{h}}^{\mathrm{ovr}}\right)^3 + \\ & + \kappa^{\mathrm{var},0}\left(1 - \kappa_{S,i}\right)^4 \Big) \end{aligned} \tag{3.72}$$

where

$$\kappa^{\mathrm{var},0} = \begin{cases} -0.2 & \text{if } \Delta D_{\mathrm{h}}^{\mathrm{ovr}} > 0.28 \\ 1 - e^{-4.302\cdot 10^2\left(\Delta D_{\mathrm{h}}^{\mathrm{ovr}}\right)^2} & \text{if } \Delta D_{\mathrm{h}}^{\mathrm{ovr}} \leq 0 \\ -7.710\left(\Delta D_{\mathrm{h}}^{\mathrm{ovr}}\right)^2 + 18.425\left(\Delta D_{\mathrm{h}}^{\mathrm{ovr}}\right)^3 & \text{otherwise.} \end{cases} \tag{3.73}$$

The overall coefficient of determination (R^2) of the sub-term $\tau_i^{\text{var},0}$ is 99.8 % and therefore the model fits the data extremely well.

Next, let us focus on the sub-term that deals with constant non-zero exsertion of U-tube ends in a constant cross-section manifold. This sub-term was obtained using data from evaluation of 48 additional geometries and is as follows:

$$\tau_i^{\text{const,const}} = \frac{S_i^{\text{rat}}}{0.518\,S_i^{\text{rat}} + 3.310\cdot 10^{-2}}. \tag{3.74}$$

In this case, the overall coefficient of determination was 99.5 % which, again, means that the model is more than adequate.

Now we will consider manifolds having variable rectangular cross-sections in which exserted U-tube ends are of a constant non-zero length. Here, 74 additional geometries were evaluated and the result was a bit more complex term, namely

$$\begin{aligned}\tau_i^{\text{var,const}} = {} & \kappa_{S,i} S_i^{\text{rat}} D_{\text{h},i}^{\text{rat}} \frac{-2.174\cdot 10^2 \Delta S_{\text{abs}}^{\text{ovr}}}{\left(1 + 1.952\cdot 10^2 E_i + 2.166\cdot 10^3 E_i^2\right)\left(6.131\cdot 10^{-2} + \Delta S_{\text{abs}}^{\text{ovr}}\right)} + \\ & + \kappa_{\text{A}}^{\text{var,const}} \left(\kappa_{h,i}\right)^{\kappa_{\text{B}}^{\text{var,const}}\left(6.272 - 5.272 e^{-1.071\cdot 10^2 E_i}\right)}\end{aligned} \tag{3.75}$$

where

$$\kappa_{\text{A}}^{\text{var,const}} = -3.027 + \frac{3.070}{1 + e^{-40.761\Delta D_{\text{h}}^{\text{ovr}} - 4.293}} \tag{3.76}$$

and

$$\kappa_{\text{B}}^{\text{var,const}} = \begin{cases} 0 & \text{if } S_{\text{CO}}^{\text{rat}} \geq 1 \\ 14.438 e^{-2.667 S_{\text{CO}}^{\text{rat}}} & \text{otherwise.} \end{cases} \tag{3.77}$$

Similarly as before, the overall coefficient of determination was very close to unity ($R^2 = 99.7$ %).

The last sub-term corrects value of the coefficient of static regain so that it reflects variable U-tube exsertion in manifolds with either constant or linearly variable cross-section widths and heights. This sub-term was found by analysing data from evaluations of 48 additional geometries and can be written as

$$\tau_i^{\text{any,var}} = \begin{cases} 0 & \text{if } E_1 = E_2 = \cdots = E_n \\ 70\,\kappa_{\text{A},i}^{\text{any,var}} \operatorname{sgn}\left(E_i^{\text{diff}}\right)\left|E_i^{\text{diff}}\right|^{0.8} + \kappa_{\text{B},i}^{\text{any,var}} & \text{otherwise,} \end{cases} \tag{3.78}$$

in which

$$\kappa_{\text{A},i}^{\text{any,var}} = \left(\frac{1}{2} - \operatorname{sgn}(E_i - E_1)\left(\frac{E_i}{\max_i\{E_i\}} - \frac{1}{2}\right)\right)^4 \tag{3.79}$$

and

$$\begin{aligned} \kappa_{b,i}^{\text{A}} &= \max\{0,\ -5.172 b_i + 0.874\} \\ \kappa_{b,i}^{\text{B}} &= \min\{0,\ 8.621 b_i - 1.457\} \\ \kappa_{\text{B},i}^{\text{any,var}} &= \begin{cases} \kappa_{b,i}^{\text{B}} & \text{if } E_i^{\text{rat}} \leq 0.056 + \kappa_{b,i}^{\text{A}} \\ \kappa_{b,i}^{\text{B}} - 0.671 - 0.537 \log_{10}\left(E_i^{\text{rat}} - \kappa_{b,i}^{\text{A}}\right) & \text{otherwise.} \end{cases} \end{aligned} \tag{3.80}$$

For this sub-term the overall coefficient of determination was $R^2 = 99.9$ %.

In total, 282 exchanger module configurations were evaluated with several different total mass flow rates. As mentioned before, coefficient of static regain was assumed to be a sum of the above sub-terms. Thus for manifolds with constant or linearly variable cross-section widths and heights and zero, constant, or variable length of exserted U-tube ends we can write

$$C_{\mathrm{r},i} = \tau_i^{\mathrm{const},0} + \tau_i^{\mathrm{var},0} + \tau_i^{\mathrm{const,const}} + \tau_i^{\mathrm{var,const}} + \tau_i^{\mathrm{any,var}}. \tag{3.81}$$

Below are three graphs with example results obtained using this coefficient, specifically:

Example 1: Mass flow rates through individual U-tubes in a module containing manifolds with linear changes of cross-section widths and heights, open end dimensions 185×500 mm, closed end dimensions 140×50 mm, and all U-tube ends being exserted 5 mm into the manifolds (Figure 3.24).

Example 2: Mass flow rates through individual U-tubes in a module containing manifolds with linear changes of cross-section widths and heights, open end dimensions 140×110 mm, closed end dimensions 185×500 mm, and all U-tube ends being exserted 12 mm into the manifolds (Figure 3.25).

Example 3: Mass flow rates through individual U-tubes in a module containing manifolds with constant 169×80 mm cross-sections and U-tube exsertions ranging from 30 mm at open ends to 2 mm at closed ends (Figure 3.26).

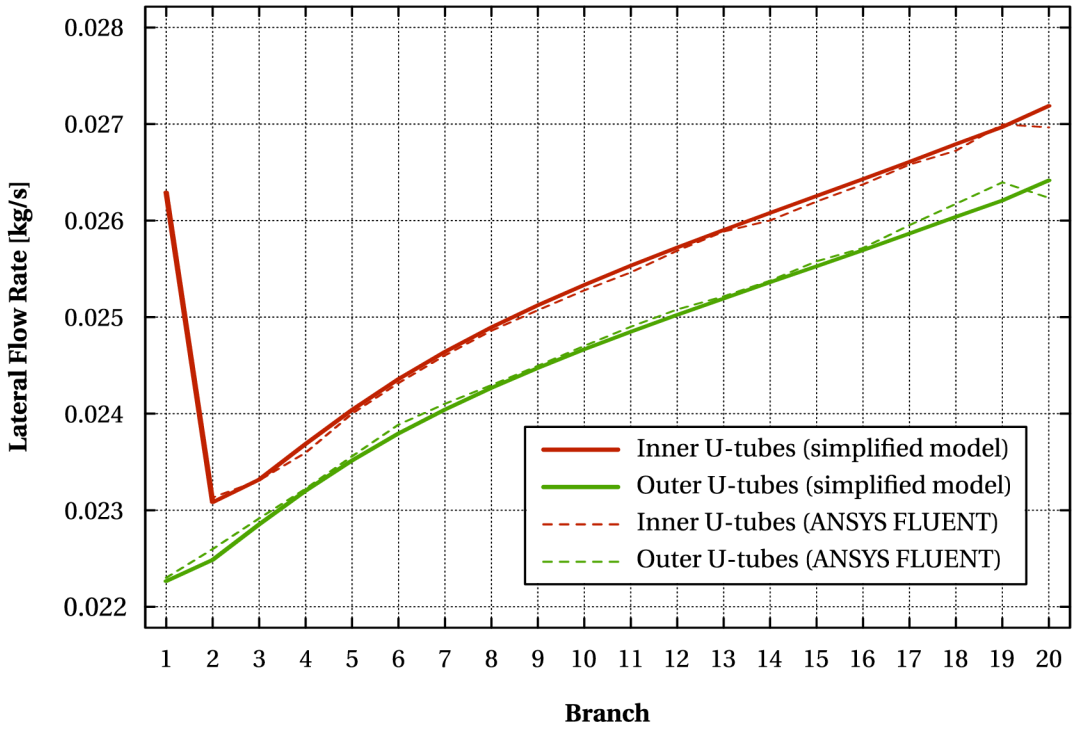

Figure 3.24. Example 1: 185×500 mm → 140×50 mm, 5 mm exsertion

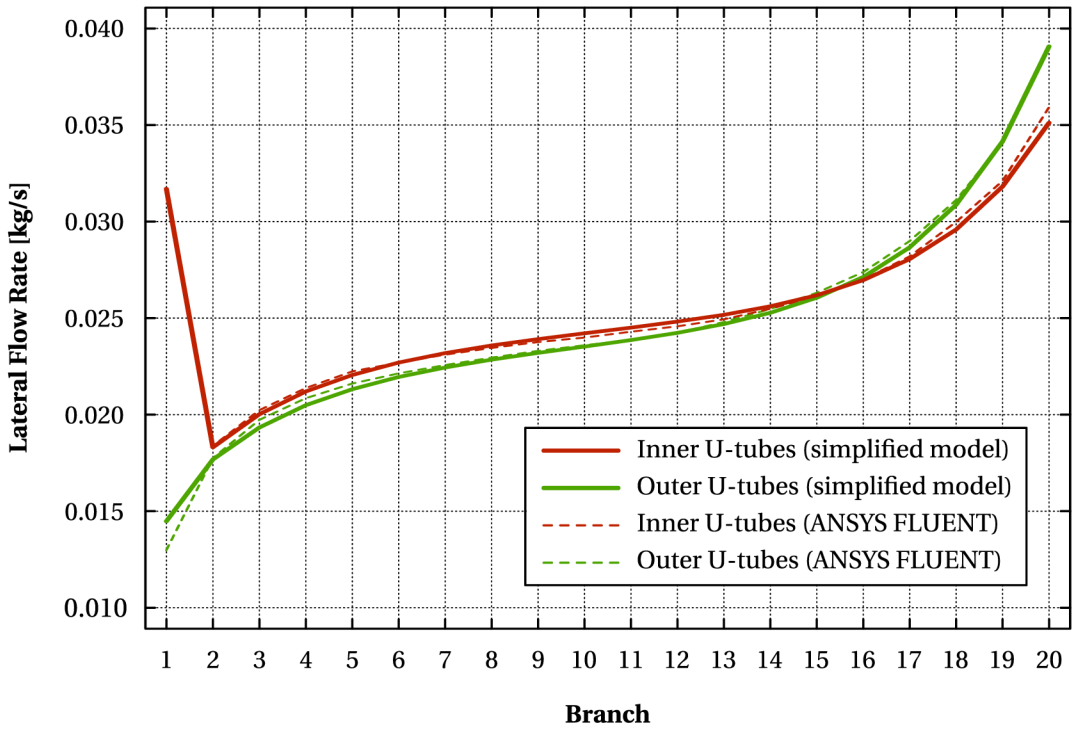

Figure 3.25. Example 2: 140 × 110 mm → 185 × 500 mm, 12 mm exsertion

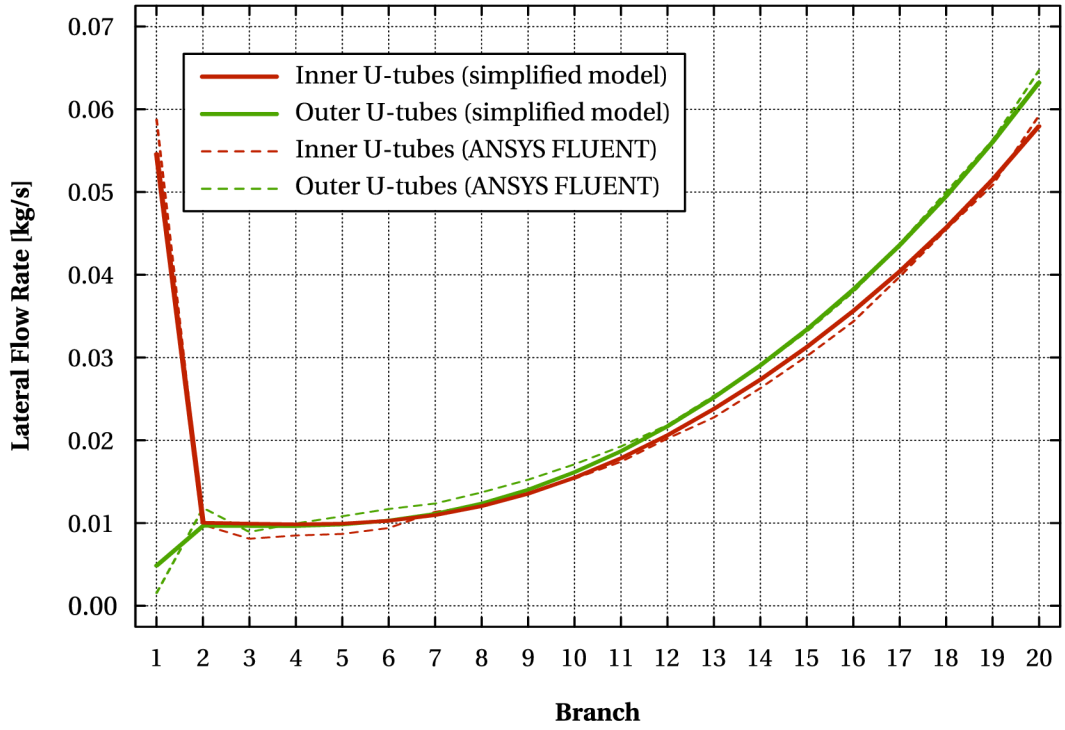

Figure 3.26. Example 3: 169 × 80 mm, 30 mm → 2 mm exsertion

In all three cases the total mass flow rate of air was 1 kg/s. If, however, we wanted to use this coefficient to predict flow distribution in a heat exchanger module with manifold cross-section widths or heights variable in a different manner (e.g. if in plan view manifold side walls were shaped as circular arcs), the formula would not have been accurate enough. This can be demonstrated for example with a module containing manifolds having circularly variable cross-section widths and heights with open end dimensions 169×287 mm, closed end dimensions 140×95 mm, and U-tube ends being mounted flush with manifold walls (the total mass flow rate of air through the exchanger module remains 1 kg/s). Flow rates yielded by the model using C_r from Equation 3.81 are shown in Figure 3.27 alongside flow rates obtained with ANSYS FLUENT. To remedy the situation, we might add another correction term to the current coefficient of static regain. Unfortunately, so far the author of this thesis was only able to find a rather artificial one based solely on the required flow rate adjustments,

$$\tau_i^{\mathrm{circ}} = \frac{0.4 \operatorname{sgn}\left(\Delta D_\mathrm{h}^{\mathrm{ovr}}\right)}{1 + 3.696 \cdot 10^7 e^{-2.953 \cdot 10^2 \left|\Delta D_\mathrm{h}^{\mathrm{ovr}}\right|}} \sin\frac{5i\pi}{2n} + \left(\frac{1}{R_\mathrm{H}} + \frac{1}{R_\mathrm{W}}\right)\left(-50E_i + \kappa_i^{\mathrm{circ}}\right), \tag{3.82}$$

where R_H denotes radius of curvature of the top manifold wall, R_W radius of curvature of the side manifold walls, and

$$\kappa_i^{\mathrm{circ}} = \begin{cases} 0 & \text{if } \Delta D_\mathrm{h}^{\mathrm{ovr}} \leq 0 \\ 60\kappa_{h,i}\Delta D_\mathrm{h}^{\mathrm{ovr}} & \text{otherwise.} \end{cases} \tag{3.83}$$

The correction term performs nicely in case of manifolds with circular cross-section dimensions variability – relative error was less than 5 % for all 24 tested geometries (see sample

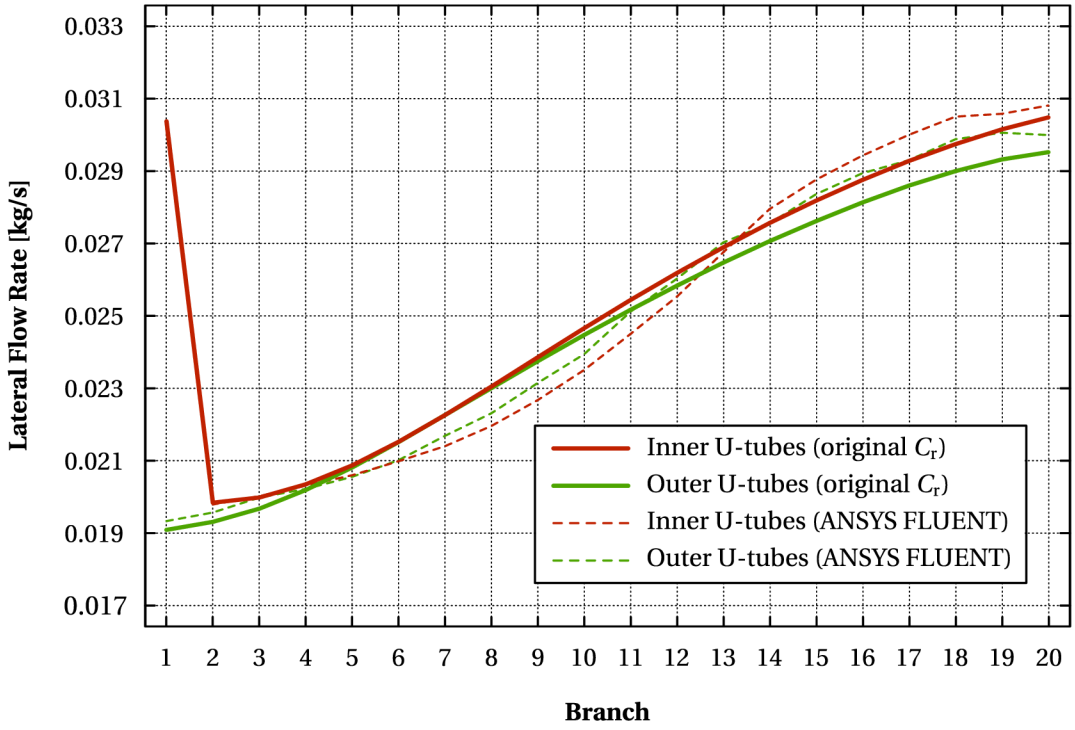

Figure 3.27. 169×287 mm → 140×95 mm (circularly variable cross-section dimensions), U-tube ends flush with manifold walls; flow rates yielded by the model using the original C_r from Equation 3.81

results shown in Figure 3.28). Considering U-arranged modules, other than exserted U-tube ends, or fluids with densities far from the density of air, the current coefficient (see Equation 3.81) lacks accuracy as well. Moreover, for manifolds with small cross-sectional areas in which the baffle effect is significant (other phenomena may too be of greater influence), predicted pressure profiles should be considered estimates rather than accurate data. All these inaccuracies will be a part of a continued research.

Simulation Tool: Multi-Platform Java Application

Computer implementation of the above model for both compressible and incompressible fluids was, again, done in Java to ensure the resulting application can be run on a wide variety of operating systems. Screenshot of the main window is shown in Figure 3.29. As in part discussed in the previous text, however, some of the functionalities are still experimental – namely:

- manifold cross-section width larger than 185 mm (i.e., the maximum possible width with the current geometry of U-tubes);
- manifold cross-section height larger than 500 mm;
- non-linear manifold width and height profiles;
- 'U' (opposite inlet and outlet flow direction) module arrangement;

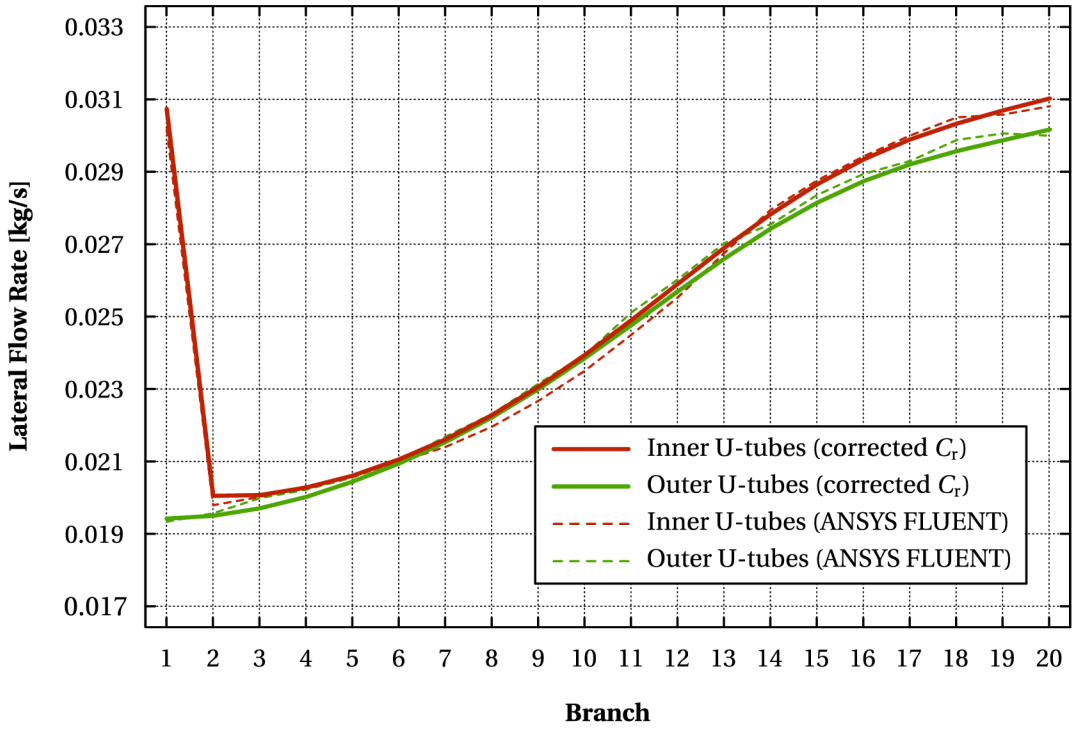

Figure 3.28. 169 × 287 mm → 140 × 95 mm (circularly variable cross-section dimensions), U-tube ends flush with manifold walls; flow rates yielded by the model using the artificially corrected C_r (see Equation 3.82)

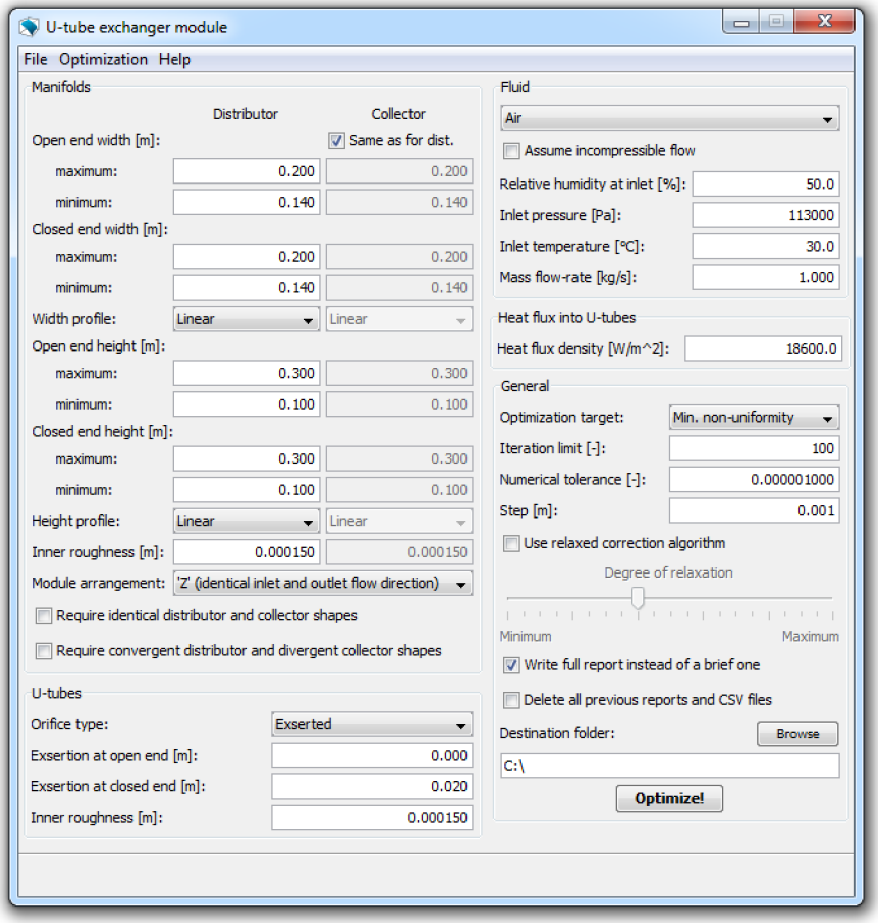

Figure 3.29. Main window of the application for analysis of flow in the double U-tube heat exchanger module

- circular bellmouth and conical U-tube ends; and
- simulation of flow of water (also, in the application's internal fluid database there is no fluid other than air and water at the moment).

The implemented model does not take gravity into account as its effect is negligible no matter how dense a working fluid flows through the module or how it is oriented with respect to the Earth's gravitational field. Figures 3.30 and 3.31, obtained using ANSYS FLUENT for an upright mounted module with constant 169×287 mm cross-section manifolds and 12 mm U-tube exsertion lengths, show mass flow rates of air and water, respectively, with and without gravity being taken into account. From these it is obvious that even for a relatively dense fluid like water introducing gravitational terms into the equations would result in unnecessary increase of computational workload and, consequently, longer evaluation times.

Although the tool has been designed primarily for shape optimization of splitting and collecting manifolds, it can also be used to analyse flow in a module of a specific configuration by simply constraining optimization space to a single geometry. Results of any optimization process are always saved to disk to a user-specified location and, additionally, graphs of flow rates through individual U-tubes as well as of pressure profiles for the best geometry are

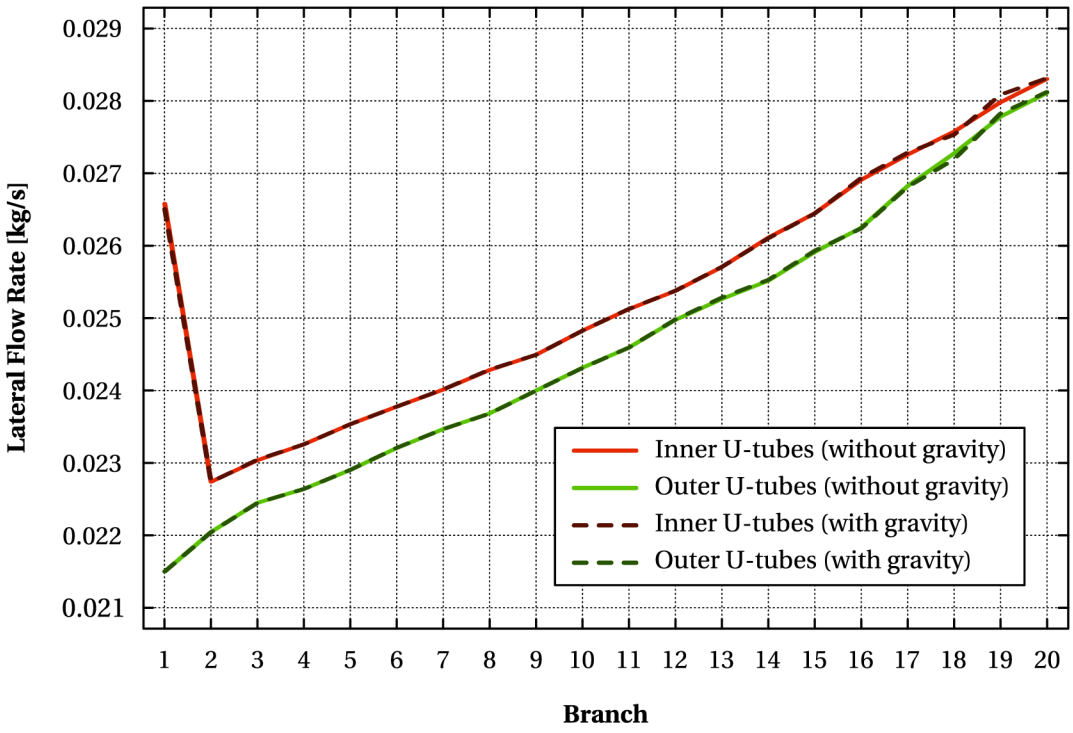

Figure 3.30. Mass flow rates of air with and without gravity being taken into account (total mass flow rate was 1 kg/s)

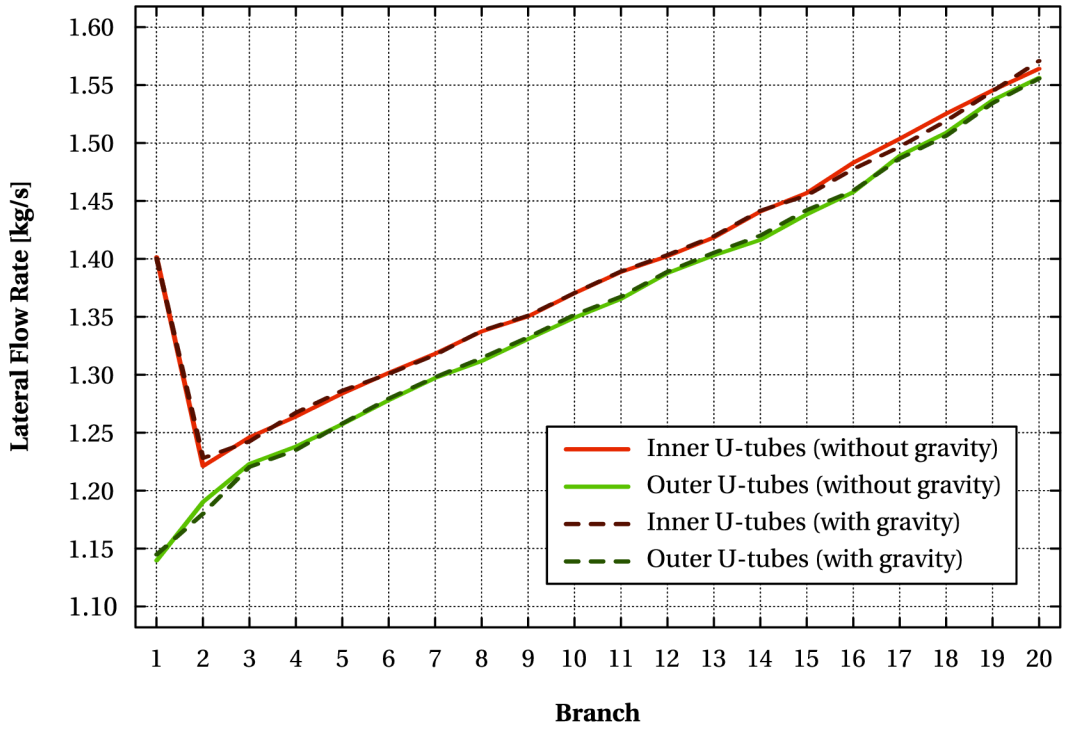

Figure 3.31. Mass flow rates of water with and without gravity being taken into account (total mass flow rate was 55 kg/s)

shown in a separate window along with a short summary and a complete optimization report. Full description of all the functionalities can be found in the application Quick start guide.

Optimization algorithm employed in this application is a bit more complex compared to the brute force approach implemented in case of pure distribution (see Section 3.4.1) where only one optimization variable (i.e., manifold height) was present. Now we have eight optimization variables – open and closed end widths and heights for both manifolds. Direct search methods must be used because calculating or approximating gradients and derivatives would be virtually impossible. Hence, the Hooke and Jeeves method (Ravindran et al., 2006, pp. 92–97) with two additional modifications (see further) and the Golden section method (Ravindran et al., 2006, pp. 51–53) are implemented to speed up optimization processes. Although a more robust 2D optimization method could be used, for example the Nelder and Mead method, modified Hooke and Jeeves algorithm was chosen due to its ease of implementation and generally shorter evaluation times (Wetter and Wright, 2004). A higher-dimensional implementation was avoided because then local optima may possibly exist which apparently would be undesirable. This problem, however, must be researched further in order to determine whether the objective function is smooth and monotone in higher-dimensional spaces. If so, then such an approach would bring a substantial decrease in optimization time.

The original Hooke and Jeeves method is comprised of two basic sub-routines – an exploration step about a pivot point and a pattern step by which a new pivot point is selected. The two modifications introduced into the optimization algorithm are intelligent selection of an initial estimate and adaptive length of pattern steps. What we thus do, essentially, is that at the beginning we find objective values in all four "corners" and in the centroid of the 2D optimization space and choose the best point of these five as the initial estimate, that is, as the initial pivot point. Then we perform an exploration step about this pivot point which, if successful, results in a pattern step in the favourable direction. Should other steps in the same direction – now with gradually longer and longer pattern steps – be successful, we move the pivot point for as long as possible. As soon as this procedure yields worse objective value or is not feasible, we return to exploration about the current pivot point and thus generate a new pattern step direction. In case this exploration provides no feasible direction, the explored neighbourhood is reduced and a new exploration is performed. Optimization process ends once size of the explored neighbourhood decreases below a pre-defined tolerance.

The Golden section method used for 1D optimization, on the other hand, is fairly simple yet still very efficient. It divides an entire optimization space, that is, an interval $[A, B]$ in which the optimization variable must lie, by two points – say P_1 and P_2 – located in accordance with the Golden ratio $\varphi = 1 : \frac{1+\sqrt{5}}{2}$. Thus we have three sub-intervals $[A, P_1]$, $[P_1, P_2]$, and $[P_2, B]$ satisfying $[A, P_1] \cup [P_1, P_2] \cup [P_2, B] = [A, B]$, $[A, P_1] \cap [P_1, P_2] = \{P_1\}$, $[P_1, P_2] \cap [P_2, B] = \{P_2\}$, and $\|P_1B\| : \|AB\| = \|AP_2\| : \|AB\| = \|AP_1\| : \|P_1B\| = \|P_2B\| : \|AP_2\| = \varphi$. Should objective value be more favourable in P_1 than in P_2, the optimization space is reduced to $[A, P_2]$, otherwise $[P_1, B]$ is chosen. Due to the properties of the Golden ratio interval division, only one inside point and the related objective value must be calculated now – the other can be taken from the previous iteration. This process is repeated for as long as the length of the reduced optimization space is greater than a pre-defined tolerance.

Considering these two methods, the following hybrid optimization algorithm was implemented:

(1) Find the number of steps necessary to span the entire feasible range of each optimization variable x_i, $i = 1, \ldots, 8$, with the user-defined optimization step.

(2) Sort all optimization variables in descending order according to the number of necessary steps thus obtaining a rearranged vector of optimization variables $\widetilde{\mathbf{x}} = \left(x_{j_1}, \ldots, x_{j_8}\right)$ in which the first element is the optimization variable with the largest feasible value range and the last element is the optimization variable with the smallest feasible value range.

(3) The third (x_{j_3}) through eighth (x_{j_8}) variables in the rearranged vector $\widetilde{\mathbf{x}}$ are fixed with values being assigned using the brute force approach.

(4) If step counts necessary to span feasible ranges of variables x_{j_1} and x_{j_2} are both non-zero, the modified Hooke and Jeeves method is used to find optimum values of both these variables at once. Otherwise, if step count is greater than zero only for x_{j_1}, value of x_{j_2} is fixed as well (it can attain only one value anyway; this also means that all other variables must be in zero-length ranges, since we have sorted the vector according to step counts) and the Golden section method is employed to find the optimum value of x_{j_1}. If both x_{j_1} and x_{j_2} lie in zero-length feasible ranges, we simply fix both of them and perform a single evaluation (in this case the entire optimization space contains only one feasible geometry).

(5) The above process is repeated until all of the six shortest ranges are spanned via the brute force approach.

Of course, if we required both manifolds to be of an identical shape, then the number of optimization variables would be four instead of eight.

At first glance it might seem that this algorithm would not shorten evaluation time much, because six out of eight variables are still optimized via the brute force approach. This, however, is not the case, since two variables with largest feasible ranges are optimized using substantially faster methods. As an example, let us consider shape optimization of a module with manifold open and closed end widths in [140, 169] mm, open end heights in [100, 287] mm, closed end heights in [0, 287] mm, and both manifolds being the same. Also, we will require the optimization step, that is, the tolerance to be 1 mm. As far as brute force approach is concerned, this gives us $\left(\frac{169-140}{1}+1\right)^2 \cdot \left(\frac{287-100}{1}+1\right) \cdot \left(\frac{287-0}{1}+1\right) = 48\,729\,600$ different geometries that should be evaluated. It is obvious that this would take a very long time even on a very fast machine. In contrast, the hybrid algorithm found optimum after evaluating 10 804 geometries and the entire optimization process took 817 s on a machine with Intel Core i5-2500K CPU. It should be stated here that relaxation was necessary due to the fact that manifolds with small cross-sectional areas had to be evaluated. This, apparently, increased the necessary number of iterations per one geometry and thus also the evaluation time. Moreover, if the application was able to utilize parallel processing then the evaluation time would be much shorter.

It is clear that some geometries may be evaluated more than once because of the exploration steps performed by the Hooke and Jeeves method. We might try to maintain a database of evaluated geometries, but with its increasing size it would represent a significant increase of workload (we would need to perform at least a partial search of this database before every evaluation). To put this into perspective, with an unsorted database the above optimization process needed 4119 s to complete while with a sorted database and partial searches being performed it took 2573 s to find the optimum. Both these values are far larger than the original 817 s necessary when no database was maintained at all.

3.5 Application of Computational Fluid Dynamics

Simplified models described in the previous sections can provide excellent results in very short time frames. Yet, when geometry of a flow system is too complex or when we need detailed information regarding flow field variables, these models are inadequate. Then computational fluid dynamics is the right tool for the purpose. The following text discusses two industrial examples in which CFD was employed to improve flow distribution and lower fouling rate.

3.5.1 Example I: Shape Optimization of Inlet Transition Piece of a Preheater

The first example concerns a process waste gas (PWG) preheater (see Figure 3.32) in a liquid and gaseous wastes incineration unit. PWG enters the heat exchanger through the inlet transition piece and then it is split into roughly 1100 U-tubes in which it is preheated by high-temperature flue gas. There are two major problems though. First, the PWG stream contains a relatively large amount of sticky liquid droplets that we are not able to extract because there is no room for an additional droplet separator in the unit. As a consequence, the inlet tube sheet gets clogged up very rapidly by jelly-like deposits and therefore the preheater's efficiency drops significantly. This also leads to non-uniform thermal expansion of individual tubes in the tube bank. Since there are U-tube support plates in the tube bank with very small diametral clearances, rigid connections are formed between tubes and plates thus causing the displacements to be carried across from excessively heated tubes to lower-temperature ones. Eventually, it results in mechanical failures – the respective cooler tubes fracture just below the inlet tube sheet and let PWG leak into the flue gas stream. Hence, increasing distribution uniformity is crucial. Moreover, vortical character of flow in inlet regions of individual U-tubes (see Figures 3.34 through 3.36 later in the text) aggravates the issue even further. Due to this fact, reduction in quantity and sizes of stagnation zones is desirable as well.

During shape optimization, the entire tube-side subsystem (inlet duct – inlet transition piece – U-tubes – outlet transition piece) was evaluated using ANSYS FLUENT for every considered geometry. In most cases, however, simplified 2D models were employed to speed

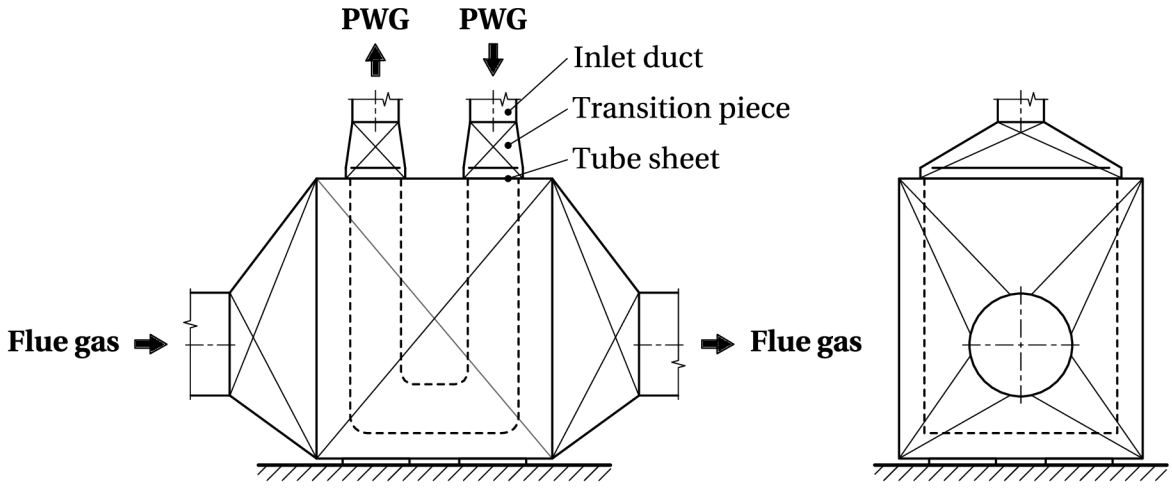

Figure 3.32. Scheme of the process waste gas preheater

up the optimization process and only a few key geometries were then verified using detailed 3D models. Naturally, a question arises whether this approach is acceptable. The baseline geometry was therefore evaluated using both types of models and the results were then compared. Figure 3.33 shows mass flow rates[8] obtained with these models and, clearly, after a transformation data from a simplified 2D model can be very similar to data yielded by a detailed 3D model. The linear transformation employed in this particular case was found ad hoc using the least squares method so that the difference between the 3D and 2D data is as low as possible.

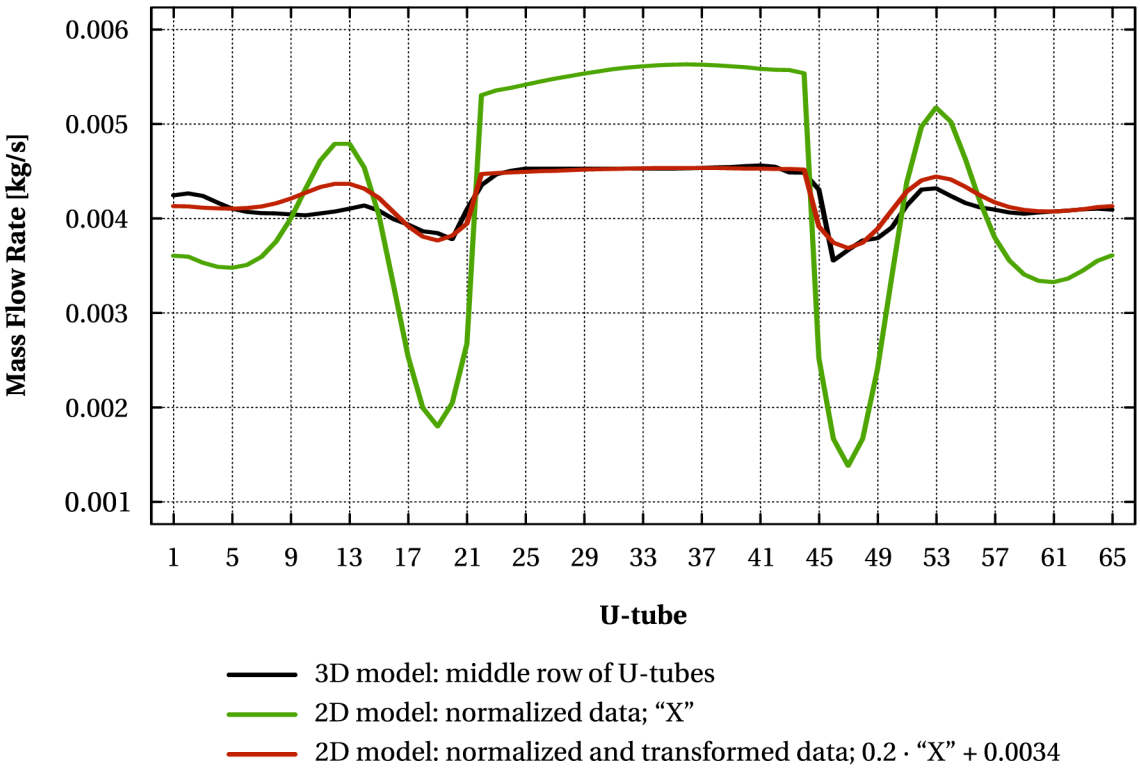

Figure 3.33. Comparison of mass flow rates obtained for the baseline geometry using 3D and 2D models (from the 3D model only flow rates through the middle row of U-tubes are shown)

All models were transient with simulated time periods being at least 500 s (usually more than 1000 s). These periods were, too, chosen ad hoc according to the behaviour of flow rates (steady state must be reached otherwise U-tubes would be subjected to variable/cyclic loading due to changes in their temperature). Simulated time period was at least 3000 s when flow rates oscillated to be sure that these will not reach a steady state after an initial oscillation and that the respective geometry should therefore not be used.

[8] Please note that "spatial" quantities (mass flow rate etc.) are used also in 2D models since these are, in fact, pseudo-3D models created internally by the CFD software. Such quantities cannot be directly compared to their true-3D counterparts, however, 2D results can be normalized to the actual total mass flow rate and a transformation can be applied to them for a rough comparison of 2D and 3D data (constant velocity boundary condition was set on the entrance to the inlet duct and thus the total mass flow rates in 2D and 3D models were different).

To compare individual geometries during shape optimization, two performance indices were used. The first was the vorticity index,

$$\Omega = \sum_{i=1}^{n} \int_{\mathrm{T}_i} \omega \mathrm{d}V, \tag{3.84}$$

that is, sum of volume integrals of vorticity magnitude over inlet parts of U-tubes (denoted as T_i). Simply speaking, vorticity is the tendency of fluid particles to swirl. In the mathematical sense, it is a vector field defined as the curl of the velocity field,

$$\vec{\omega} = \vec{\nabla} \times \vec{v}. \tag{3.85}$$

Obviously, a vector quantity was of little use and therefore vorticity magnitudes ("lengths" of the vectors in the field; ω) in individual cells of the mesh were employed. These could then be easily summed up over any selected sub-volume. The other, uniformity index was calculated similarly as in the earlier sections as relative standard deviation from uniform flow distribution (see Equation 3.52). In both cases it holds that the lower the value of the index, the better.

Vorticity magnitude above the inlet tube sheet as well as a photograph of the actual fouled tube sheet are shown in Figure 3.34. It is obvious that fouling pattern matches vorticity pattern just above the tube sheet quite nicely.

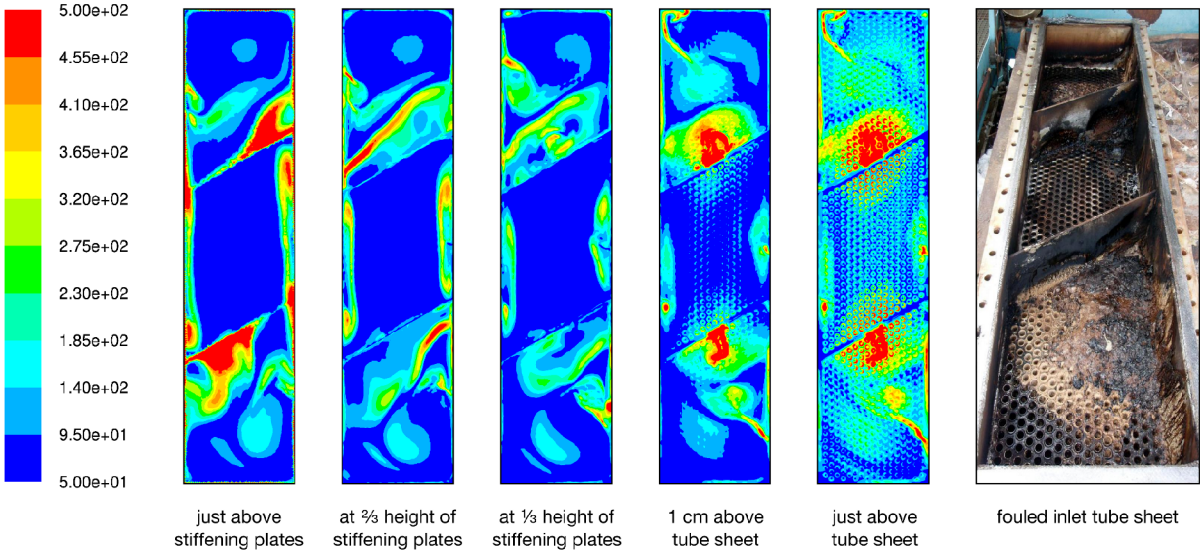

Figure 3.34. Vorticity magnitude (1/s) in several layers above the inlet tube sheet (left) and a photograph of the actual tube sheet (far right)

Pathlines yielded by the simplified 2D model can be found in Figure 3.35. The large empty areas are stagnation zones, which is visually confirmed by the graph of vorticity magnitude in Figure 3.36. Here we can also see that PWG swirls considerably in the inlet parts of U-tubes. As for the values of performance indices, 2D model gave us $\delta = 29.14$ % and $\Omega = 141.3$ m^3/s while the detailed 3D model reported $\delta = 6.62$ % and $\Omega = 135.2$ m^3/s.

As mentioned above, the goal was to lower vorticity and increase flow distribution uniformity. To do so, it was necessary to widen the PWG stream to the entire width of the inlet

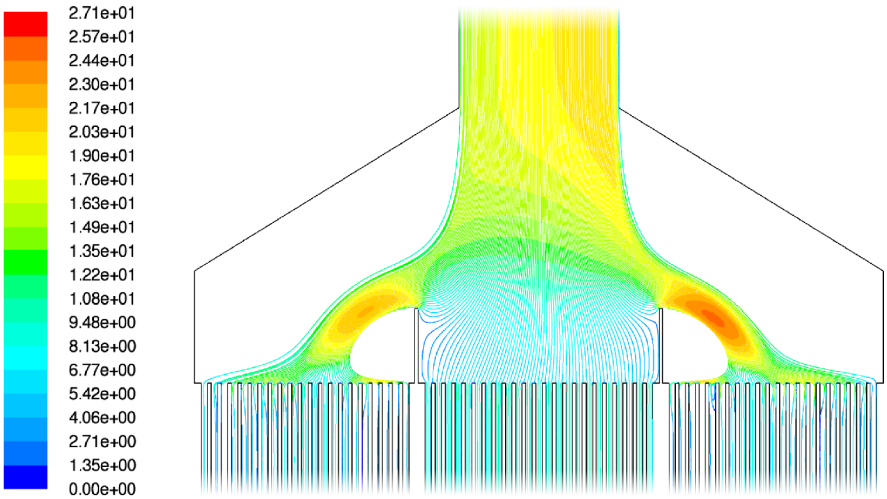

Figure 3.35. Pathlines coloured by velocity magnitude (m/s) in the simplified 2D model of the existing inlet region; empty areas are stagnation zones

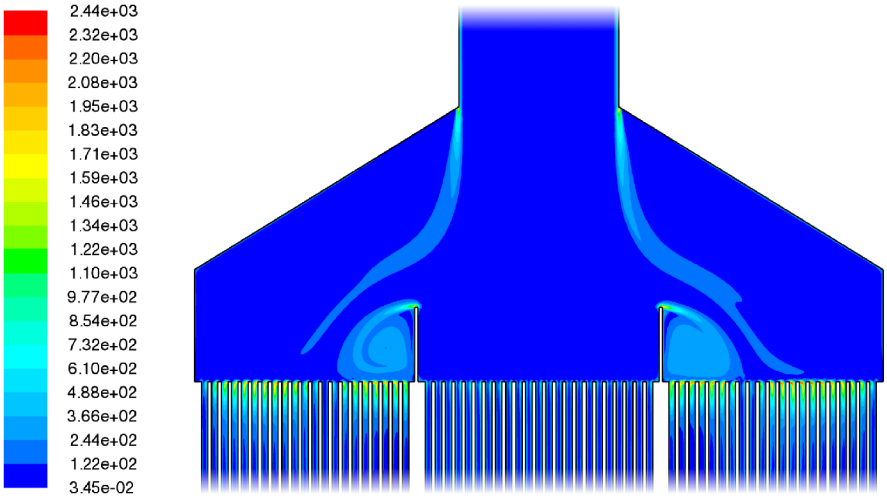

Figure 3.36. Vorticity magnitude (1/s) in the simplified 2D model of the existing inlet region

tube sheet. Ideally, one could add a flow homogenizer into the current inlet transition piece, but with regard to the fouling capability of the fluid this was not possible. The only other option was to use guiding vanes, however, with the current transition piece being too short the number of required guiding vanes was prohibitively large (their spacing would be too small to keep the gaps unclogged). The shortest transition piece satisfying our conditions on spacing of guiding vanes was 2.5 times higher than the baseline geometry and contained five top and ten bottom guiding vanes (see Figures 3.37 and 3.38). The top guiding vanes were perpendicular to the longer tube sheet edge while bottom ones were mounted parallel to the two stiffening transverse partition plates.

Both 2D performance indices were now much lower, specifically $\delta = 7.64$ % and $\Omega = 94.8$ m^3/s. Comparison of volume integrals of vorticity magnitude in inlet parts of

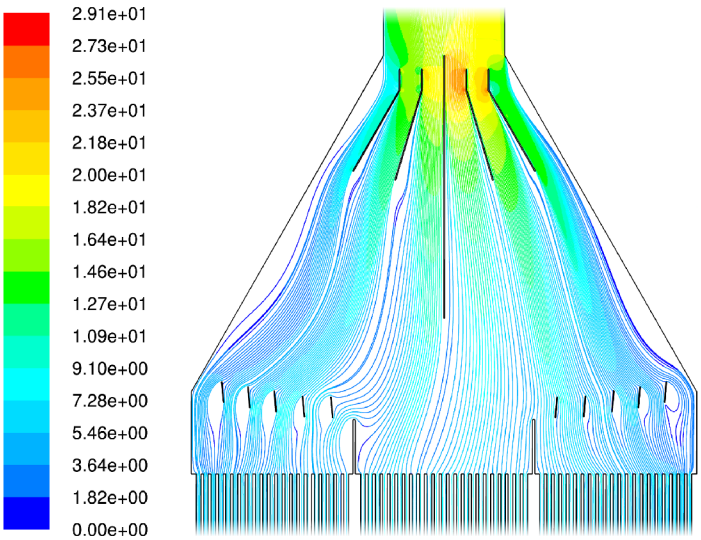

Figure 3.37. Pathlines coloured by velocity magnitude (m/s) in the simplified 2D model of the optimum inlet region

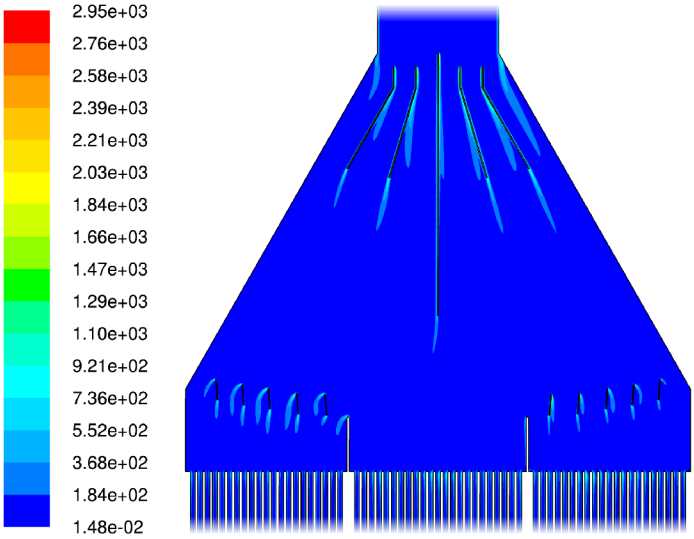

Figure 3.38. Vorticity magnitude (1/s) in the simplified 2D model of the optimum inlet region

individual U-tubes is shown in Figure 3.39 while flow rates are compared in Figure 3.40. As for the detailed 3D model of the optimum geometry, mass flow rates through the middle row of U-tubes are matched to the data obtained using the simplified 2D model in Figure 3.41 (the transformation used here is the same as the one we employed for the baseline flow rates). Additionally, vorticity magnitude above the inlet tube sheet, now significantly decreased, can be found in Figure 3.42. Performance indices yielded by the 3D model were, too, lower, namely $\delta = 4.08$ % and $\Omega = 81.0$ m^3/s.

Therefore, by making the inlet transition piece higher and installing guiding vanes into it we obtained a geometry that performs much better vorticity-wise as well as in terms of flow

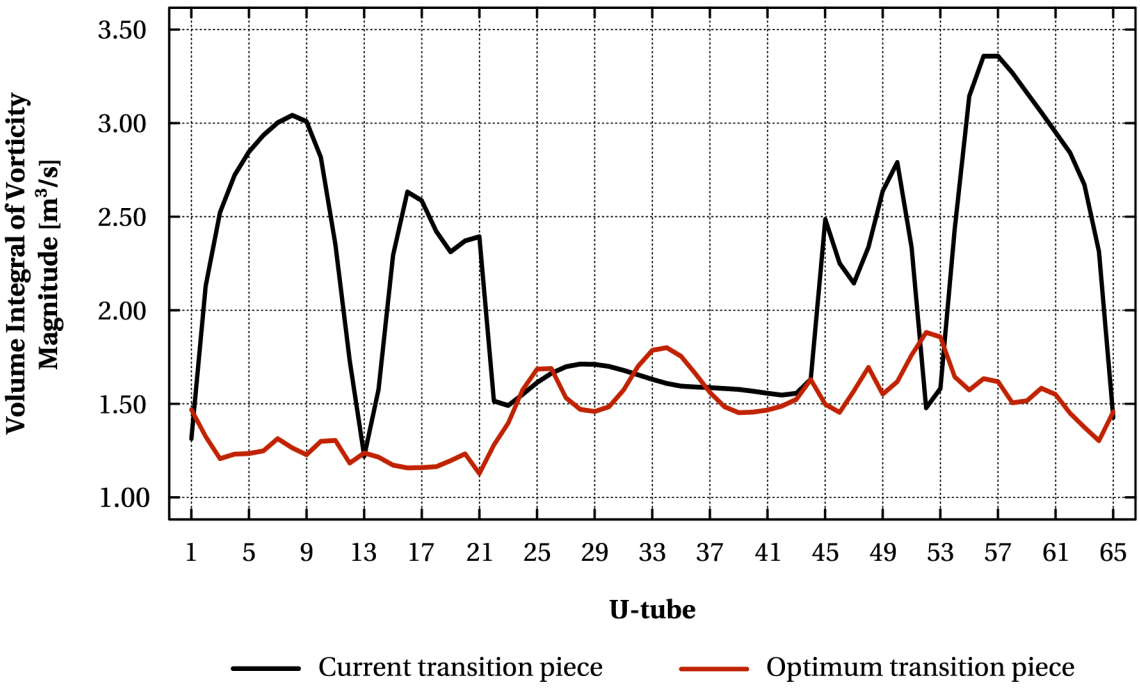

Figure 3.39. Baseline vs. optimum geometry: volume integrals of vorticity magnitude in inlet parts of individual U-tubes

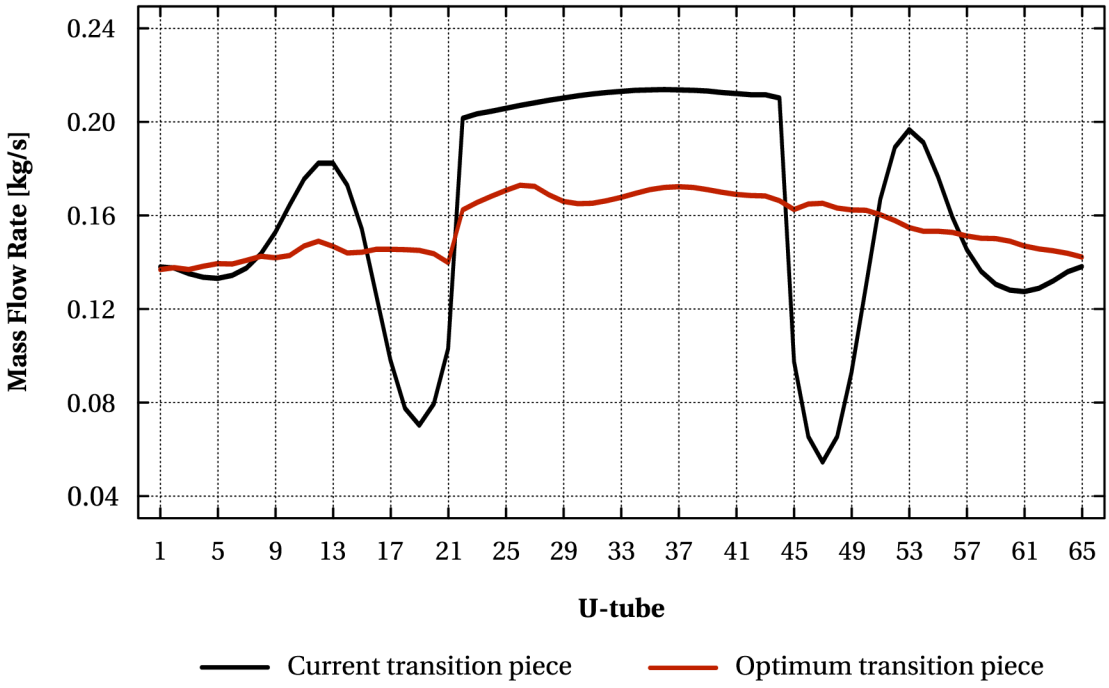

Figure 3.40. Baseline vs. optimum geometry: mass flow rates obtained using the simplified 2D model

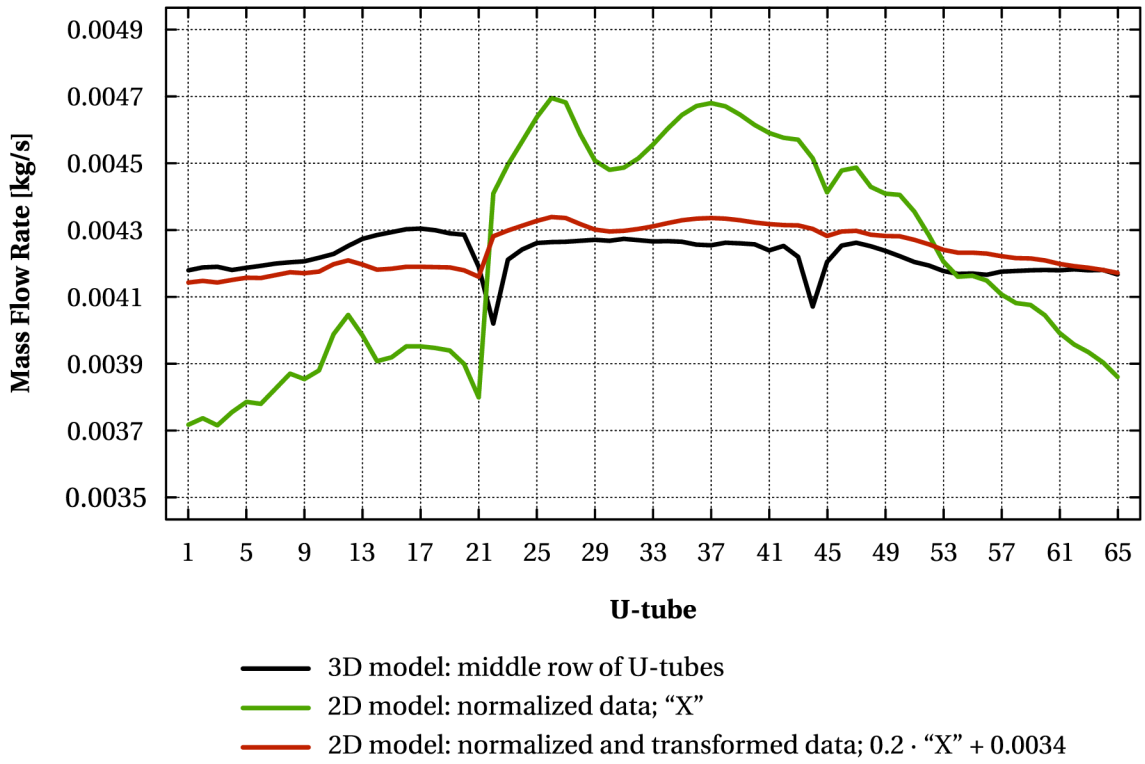

Figure 3.41. Optimum geometry: comparison of data from 3D and 2D models (from the 3D model only flow rates through the middle row of U-tubes are shown)

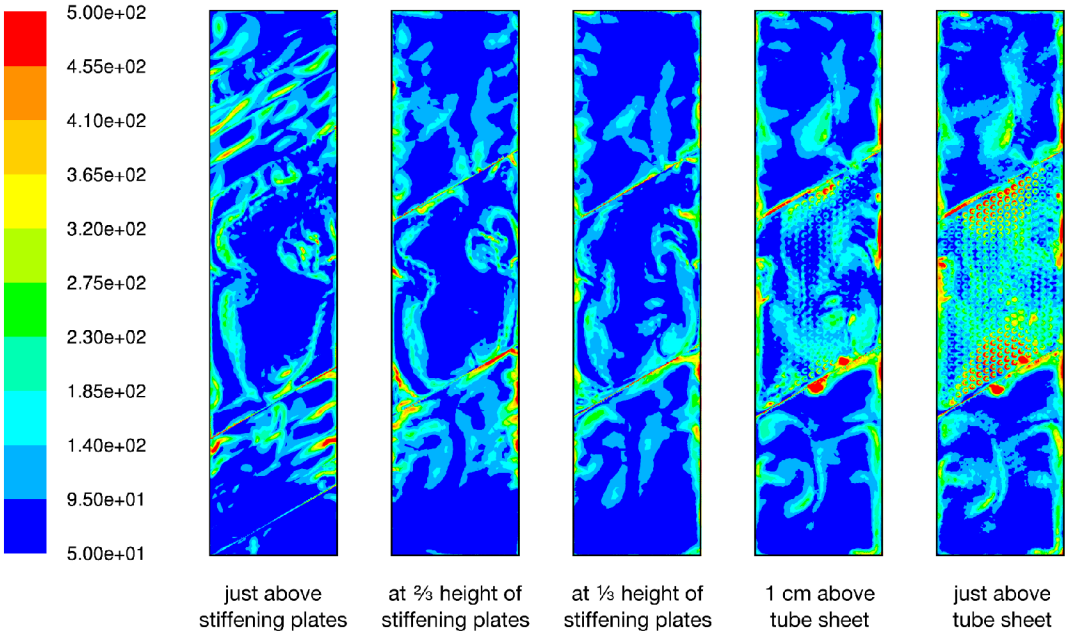

Figure 3.42. Optimum geometry: vorticity magnitude (1/s) in several layers above the inlet tube sheet

distribution uniformity. The graphs presented here also suggest that if only a quantitative comparison of relatively complex but similar near-planar geometries is needed – for example during shape optimization –, simplified 2D models of considerably lower computational costs can be used instead of detailed 3D models. To estimate performance of an actual 3D geometry via a 2D approximation, however, we still need data from a baseline 3D model.

3.5.2 Example II: Shape Optimization of $NaHCO_3$ Distribution Manifold

The second example demonstrates that improving flow distribution is important in a far wider a range of industrial applications than just heat exchange. Here we will discuss the dry flue gas desulfurization ($DeSO_x$) technology that is based on injection of a dry sorption agent, namely sodium bicarbonate ($NaHCO_3$), into a flue gas stream. This can be done simply by inserting several perforated manifolds into the flue gas duct – typically just downstream of the secondary combustion chamber – and feeding an $NaHCO_3$ aerosol into the manifolds at the required flow rate. Sodium bicarbonate then reacts with acidic compounds present in the flue gas stream which produces sodium fluoride (NaF), sodium chloride (NaCl), and sodium sulfate (Na_2SO_4) with by-products being water (H_2O) and carbon dioxide (CO_2). Consequently, the salts are separated from the stream in a bag filter, ceramic filter, or via an electrostatic precipitator. The problem is, though, that residence time of the sodium bicarbonate particles in the flue gas stream is relatively short and thus we have to ensure that these two compounds are well mixed. In other words, even though the flue gas flow is highly turbulent, we need to disperse the $NaHCO_3$ particles as evenly as possible, that is, have as much a uniform distribution of the aerosol as possible.

From previous industrial experiments performed by the manifold manufacturer it was known that in this particular case the best results can be obtained with triangular exit ports (see Figure 3.43). With a constant manifold diameter and one size of exit ports, however, flow velocity is relatively low near the last two ports and these often get clogged by sodium bicarbonate particles building up from the closed end towards the inlet of the manifold. The goal therefore was to find a manifold design that would provide sufficient aerosol velocities and, if possible, also better flow distribution. The minimum acceptable velocity, obtained from the above mentioned experiments, was 7 m/s.

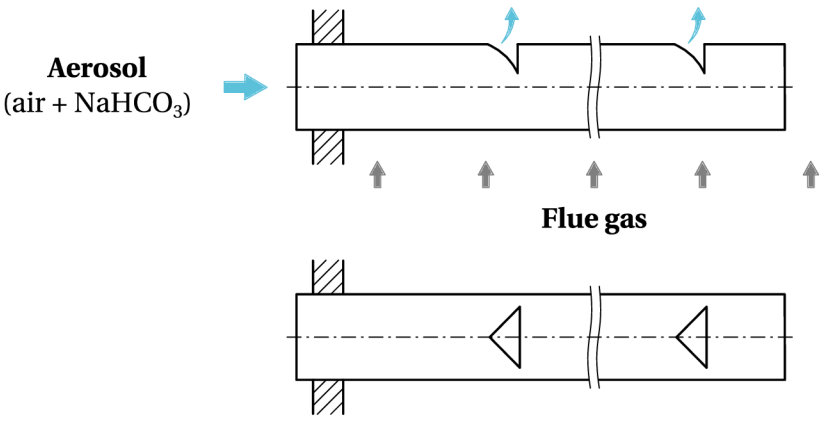

Figure 3.43. Scheme of a manifold for distribution of $NaHCO_3$ aerosol into flue gas stream

A series of simulations performed using ANSYS FLUENT confirmed that to get reasonable results it would be best to design the manifolds not only as step ones with segments of different diameters being connected by tapered transition pieces, but also with several sets of differently sized exit ports. It was also found that to improve mixing of flue gas with the aerosol it would be beneficial to stagger the exit ports with a 45° angle difference (see Figure 3.44). Additionally, the number of exit ports was limited to six since otherwise flow velocity dropped below the feasible threshold near the closed end of the manifold.

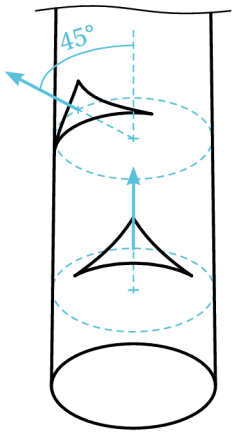

Figure 3.44. Staggered exit ports

Considering all the above facts as well as manufacturing cost, the optimum layout comprised four manifolds each of which consisted of two segments (DN100 and DN80) connected with a tapered transition piece and two sets of staggered exit ports (five smaller and one larger port; see Figure 3.45). Although relative standard deviation from uniform flow distribution was slightly greater than in case of the baseline constant-diameter geometry with only one size of exit ports (7.3 % compared to 6.4 %), flow velocities were considerably higher (see Figure 3.46) thus warranting manifolds without significant particle build-up.

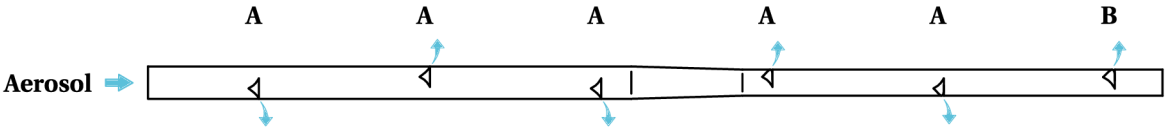

Figure 3.45. One of the four manifolds used in the final $NaHCO_3$ aerosol dispenser; letters A and B denote exit port sizes (A ... smaller port, B ... larger port)

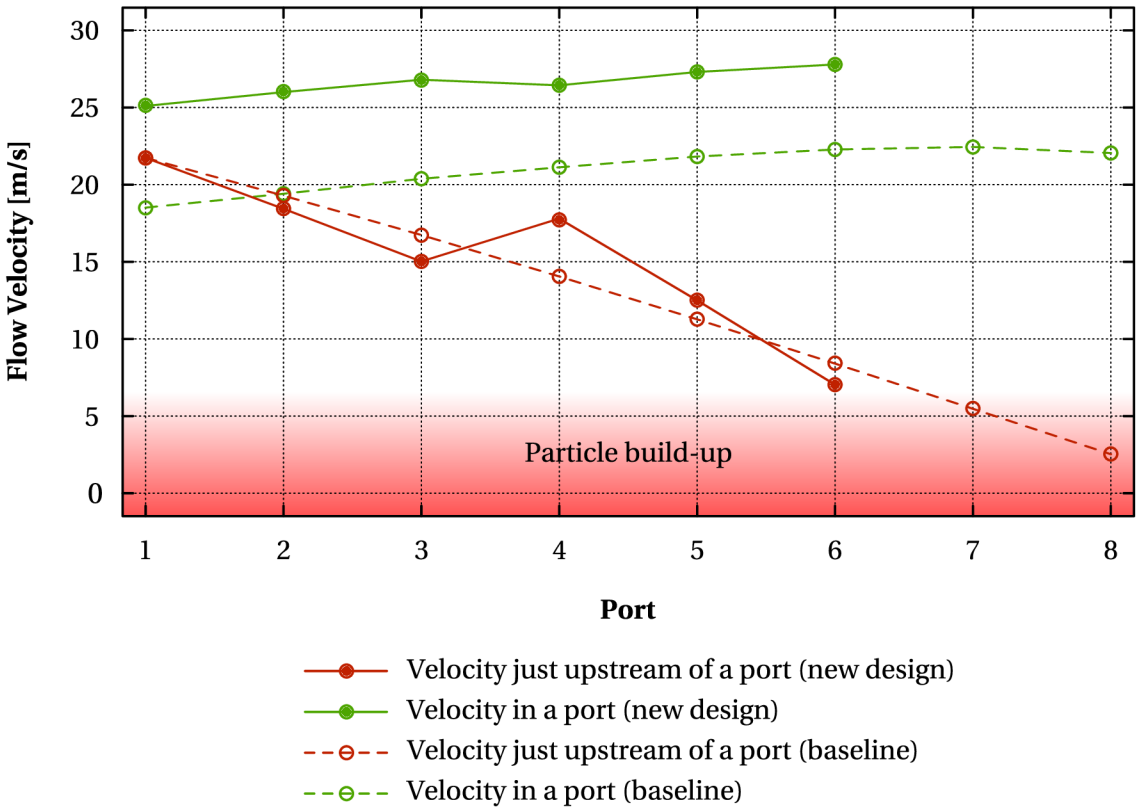

Figure 3.46. Baseline vs. optimum design: comparison of flow velocities in the manifolds just upstream of exit ports and in the actual exit ports

4

Future Work

The presented simplified mathematical models of flow systems are fairly complex and cover all of the common situations except for change of phase and two-phase flow. This is one of the main topics the author would like to continue working on since in heat exchangers phase-changes are fairly common. However, it will require a full-scale revision of the existing models as well as of their computer implementations and the supporting libraries dealing with physical properties of fluids.

Considering the single-phase versions of applications for shape optimization, it must still be verified that they provide sufficiently accurate results even for parameters outside of the current input data ranges, i.e., manifold cross-section width larger than 185 mm, manifold cross-section height larger than 500 mm, circular bellmouth and conical U-tube ends, and 'U' (opposite inlet and outlet flow direction) module arrangement. The existing formula for coefficient of static regain will also need to be modified for it to satisfactorily predict pressure changes in manifolds with non-linear width and height profiles and when water flows through the system.

The author would further like to implement multi-threaded computation and an intelligent algorithm for automatic detection of situations when relaxation is necessary coupled with subsequent selection of an appropriate relaxation degree. Additionally, it would be beneficial to investigate behaviour of the discussed class of parallel flow systems so that a higher-degree optimization algorithm can be employed if possible. All these modifications would result in immensely faster optimization.

As for graphical user interface of the "U-tube exchanger module" application, interactive solution browser would considerably enhance user experience. Furthermore, as of now U-tube bundle geometry is hard-coded. Form controls for specifying the key bundle dimensions would thus improve usability because no programming skills would be necessary to alter the respective input data.

Finally, the author would like to devote some time to investigation of the actual influence of flow field characteristics on fouling rate using data from existing equipment. This might provide a reasonable basis for estimation of intensity of particle deposition solely on the grounds of information easily obtainable with computational fluid dynamics.

5

Summary

In this thesis we focused on shape optimization of flow systems in heat exchange units since we can significantly increase heat transfer efficiency via improvement of flow distribution and abatement of fouling. As flow analysis is necessary in the process, three simplified mathematical models were presented. Two variants of each of them exist so that both compressible and incompressible flows can be analysed. The models were built with their use in optimization algorithms in mind, that is, they were made as simple and easy to evaluate as possible while retaining reasonable accuracy of the provided data and applicability to a wide range of flow system geometries.

The first model is based on the simplified branch-by-branch approach and describes pure distribution from a manifold with variable rectangular cross-section into a constant-pressure environment. The respective application software can then be run in virtually any modern operating system due to its implementation in Java and allows the user to modify all the input parameters directly in the graphical user interface. Although the brute-force optimization algorithm is employed, results are provided within seconds given the simplicity of the mathematical model.

The second model was built using partial differential equations and works with a pseudo-1D mesh of a parallel flow system (distributor – tube bundle – collector). Only circular manifolds with constant cross-sections are supported with respect to the differential nature of the model, since otherwise its complexity would prohibit utilizing it as a core of an optimization algorithm. The advantages, however, are fully automated generation of the mesh and possibility to specify shapes and thermal loads of each of the tubes in the bundle as functions thus rendering the model to be capable of evaluating even relatively complex flow systems. This model has been implemented in Maplesoft Maple and, again, employs the brute-force optimization algorithm. In spite of this, no significant increase in optimization time should be noticeable as only one optimization variable, i.e., manifold diameter, is present.

The last mathematical model describes a parallel flow system consisting of manifolds with variable rectangular cross-sections and a double U-tube bundle. Similarly as in case of pure distribution, the simplified branch-by-branch approach is applied, but here a relatively complex hybrid optimization algorithm is used to shorten optimization times as much as possible because now we search for the optimum in an eight-dimensional space. Considering

the fact that general behaviour of the objective function hyperplane in this space has not yet been investigated except for 1D and 2D sub-spaces, only one- and two-dimensional direct optimization methods are employed as necessary to ensure global optima are always found. In order to increase accuracy of the results that the model provides, formula for coefficient of static regain was derived using data obtained by evaluation of 282 geometries, which belonged to the respective class of flow systems, in ANSYS FLUENT. As for computer implementation, the corresponding optimization package has been written in Java so that users can benefit from its functionalities without being limited in their choice of operating system or hardware platform.

Additionally, through two industrial examples we discussed the effect of flow field characteristics upon fouling rate. Nonetheless, the proposed approach to fouling analysis needs to be researched further before it is ready for production use.

Bibliography

Ablanque N., Oliet C., Rigola J., Pérez-Segarra C. and Oliva A. (2010) Two-phase flow distribution in multiple parallel tubes, *International Journal of Thermal Sciences* **49**(6), 909–921.

Acheson D. (1990) *Elementary Fluid Dynamics*, Oxford University Press USA, New York, NY, USA, 3rd edn.

Acrivos A., Babcock B. and Pigford R. (1959) Flow distribution in manifolds, *Chemical Engineering Science* **10**(1), 112–124.

Ahmed M., Shuaib N., Yusoff M. and Al-Falahi A. (2011) Numerical investigations of flow and heat transfer enhancement in a corrugated channel using nanofluid, *International Communications in Heat and Mass Transfer* **38**(10), 1368–1375.

Amador C., Gavriilidis A. and Angeli P. (2004) Flow distribution in different microreactor scale-out geometries and the effect of manufacturing tolerances and channel blockage, *Chemical Engineering Journal* **101**(1–3), 379–390.

Ames W. (1992) *Numerical methods for partial differential equations*, Academic Press, Inc., San Diego, CA, USA, 3rd edn.

Arsenyeva O., Tovazhnyansky L., Kapustenko P., Perevertaylenko O. and Khavin G. (2011) Investigation of the new corrugation pattern for low pressure plate condensers, *Applied Thermal Engineering* **31**(13), 2146–2152.

Bailey B. (1975) Fluid flow in perforated pipes, *Journal of Mechanical Engineering Science* **17**(6), 338–347.

Bajura R. and Jones E. (1976) Flow distribution manifolds, *Journal of Fluids Engineering* **98**(4), 654–666.

Bas H. and Ozceyhan V. (2012) Heat transfer enhancement in a tube with twisted tape inserts placed separately from the tube wall, *Experimental Thermal and Fluid Science* **41**, 51–58.

Bazmi M., Hashemabadi S. and Bayat M. (2012) CFD simulation and experimental study of liquid flow mal-distribution through the randomly trickle bed reactors, *International Communications in Heat and Mass Transfer* **39**(5), 736–743.

Bébar L., Martinák P., Hájek J., Stehlík P., Hajný Z. and Oral J. (2002) Waste to energy in the field of thermal processing of waste, *Applied Thermal Engineering* **22**(8), 897–906.

BHUIYA M., AHAMED J., CHOWDHURY M., SARKAR M., SALAM B., SAIDUR R., MASJUKI H. and KALAM M. (2012) Heat transfer enhancement and development of correlation for turbulent flow through a tube with triple helical tape inserts, *International Communications in Heat and Mass Transfer* **39**(1), 94–101.

BI H., SAURIOL P. and STUMPER J. (2010) Two-phase flow distributors for fuel cell flow channels, *Particuology* **8**(6), 582–587.

BLEVINS R. (2003) *Applied Fluid Dynamics Handbook*, Krieger Publishing Company, Malabar, FL, USA, reprinted ed. with corrections edn.

BOTT T. (1995) *Fouling of Heat Exchangers*, Elsevier Science, Amsterdam, Netherlands.

BYUN H. and KIM N. (2011) Refrigerant distribution in a parallel flow heat exchanger having vertical headers and heated horizontal tubes, *Experimental Thermal and Fluid Science* **35**(6), 920–932.

CASTELLÕES F., QUARESMA J. and COTTA R. (2010) Convective heat transfer enhancement in low reynolds number flows with wavy walls, *International Journal of Heat and Mass Transfer* **53**(9–10), 2022–2034.

CB&I LUMMUS TECHNOLOGY (2012) Helixchanger Heat Exchanger (online), `http://www.lummusonline.com/global/tools/helixchanger/helixchanger_index.htm`, accessed: 17 August 2012.

CHANDRAKER D., MAHESHWARI N., SAHA D. and VENKAT RAJ V. (2002) Experimental and analytical investigations on core flow distribution and pressure distribution in the outlet header of a PHWR, *Experimental Thermal and Fluid Science* **27**(1), 11–24.

CHEN C., JUNG S. and YEN S. (2007) Flow distribution in the manifold of PEM fuel cell stack, *Journal of Power Sources* **173**(1), 249–263.

CHEN N. (1979) An explicit equation for friction factor in pipe, *Industrial & Engineering Chemistry Fundamentals* **18**(3), 196–297.

CHENG L., LUAN T., DU W. and XU M. (2009) Heat transfer enhancement by flow-induced vibration in heat exchangers, *International Journal of Heat and Mass Transfer* **52**(3–4), 1053–1057.

CHENG Z., HE Y. and CUI F. (2012) Numerical study of heat transfer enhancement by unilateral longitudinal vortex generators inside parabolic trough solar receivers, *International Journal of Heat and Mass Transfer* **55**(21–22), 5631–5641.

CHOI S., SHIN S. and CHO Y. (1993a) The effect of area ratio on the flow distribution in liquid cooling module manifolds for electronic packaging, *International Communications in Heat and Mass Transfer* **20**(2), 221–234.

CHOI S., SHIN S. and CHO Y. (1993b) The effects of the Reynolds number and width ratio on the flow distribution in manifolds of liquid cooling modules for electronic packaging, *International Communications in Heat and Mass Transfer* **20**(5), 607–617.

Churchill S. (1977) Friction-factor equation spans all fluid and flow regimes, *Chemical Engineering* **84**(24), 91–92.

Clancy L. (1975) *Aerodynamics*, John Wiley & Sons, Inc., Hoboken, NJ, USA.

Colebrook C. (1939) Turbulent flows in pipes, with particular reference to the transition region between the smooth and rough pipe laws, *Journal of the Institution of Civil Engineers* **11**, 133–156.

Commenge J., Falk L., Corriou J. and Matlosz M. (2002) Optimal design for flow uniformity in microchannel reactors, *AIChE Journal* **48**(2), 345–358.

Coulson J. and Richardson J. (1999) *Chemical Engineering*, Butterworth-Heinemann Ltd., Oxford, UK, 6th edn.

Datta A. and Majumdar A. (1980) Flow distribution in parallel and reverse flow manifolds, *International Journal of Heat and Fluid Flow* **2**(4), 253–262.

Design Institute for Physical Property Research/AIChE (2012a) DIPPR Project 801: Properties of air (online), `http://www.knovel.com/web/portal/browse/display?_EXT_KNOVEL_DISPLAY_bookid=1187`, accessed: 14 August 2012.

Design Institute for Physical Property Research/AIChE (2012b) DIPPR Project 801: Properties of water (online), `http://www.knovel.com/web/portal/browse/display?_EXT_KNOVEL_DISPLAY_bookid=1187`, accessed: 14 August 2012.

Doob J. (1994) *Measure Theory*, Springer-Verlag, Inc., New York, NY, USA.

Dortmund Data Bank Software & Separation Technology GmbH (2012) Liquid dynamic viscosity (online), `http://ddbonline.ddbst.de/VogelCalculation/VogelCalculationCGI.exe`, accessed: 14 August 2012.

Drazin P. (2002) *Introduction to Hydrodynamic Stability*, Cambridge University Press, Cambridge, UK.

Du X., Feng L., Yang Y. and Yang L. (2013) Experimental study on heat transfer enhancement of wavy finned flat tube with longitudinal vortex generators, *Applied Thermal Engineering* **50**(1), 55–62.

Dyga R. and Płaczek M. (2010) Efficiency of heat transfer in heat exchangers with wire mesh packing, *International Journal of Heat and Mass Transfer* **53**(23–24), 5499–5508.

Eiamsa-ard S., Thianpong C. and Eiamsa-ard P. (2010a) Turbulent heat transfer enhancement by counter/co-swirling flow in a tube fitted with twin twisted tapes, *Experimental Thermal and Fluid Science* **34**(1), 53–62.

Eiamsa-ard S., Wongcharee K., Eiamsa-ard P. and Thianpong C. (2010b) Heat transfer enhancement in a tube using delta-winglet twisted tape inserts, *Applied Thermal Engineering* **30**(4), 310–318.

El Achkar G., Lavieille P., Lluc J. and Miscevic M. (2011) Heat transfer and flow distribution in a multichannel microcondenser working at low mass fluxes, *International Journal of Heat and Mass Transfer* **54**(11–12), 2319–2325.

ESCHER W., MICHEL B. and POULIKAKOS D. (2009) Efficiency of optimized bifurcating tree-like and parallel microchannel networks in the cooling of electronics, *International Journal of Heat and Mass Transfer* **52**(5–6), 1421–1430.

FERNÁNDEZ-SEARA J., DIZ R. and UHÍA F. (2012) Pressure drop and heat transfer characteristics of a titanium brazed plate-fin heat exchanger with offset strip fins, *Applied Thermal Engineering*, **in press**, DOI: 10.1016/j.applthermaleng.2012.08.066.

FLUENT, INC. (2006) *FLUENT 6.3 User's Guide*, Fluent, Inc., Lebanon, NH, USA.

FU H., WATKINS A. and YIANNESKIS M. (1994) The effects of flow split ratio and flow rate in manifolds, *International Journal for Numerical Methods in Fluids* **18**(9), 871–886.

GANDHI M., GANGULI A., JOSHI J. and VIJAYAN P. (2012) CFD simulation for steam distribution in header and tube assemblies, *Chemical Engineering Research and Design* **90**(4), 487–506.

GARCÍA A., SOLANO J., VICENTE P. and VIEDMA A. (2012) The influence of artificial roughness shape on heat transfer enhancement: Corrugated tubes, dimpled tubes and wire coils, *Applied Thermal Engineering* **35**, 196–201.

GHANI F., DUKE M. and CARSON J. (2012) Effect of flow distribution on the photovoltaic performance of a building integrated photovoltaic/thermal (BIPV/T) collector, *Solar Energy* **86**(5), 1518–1530.

GUNES S., OZCEYHAN V. and BUYUKALACA O. (2010) Heat transfer enhancement in a tube with equilateral triangle cross sectioned coiled wire inserts, *Experimental Thermal and Fluid Science* **34**(6), 684–691.

GUZMÁN A., CÁRDENAS M., URZÚA F. and ARAYA P. (2009) Heat transfer enhancement by flow bifurcations in asymmetric wavy wall channels, *International Journal of Heat and Mass Transfer* **52**(15–16), 3778–3789.

HAALAND S. (1983) Simple and explicit formulas for the friction factor in turbulent pipe flow, *Journal of Fluids Engineering* **105**(1), 89–90.

HABIB M., BEN-MANSOUR R., SAID S., AL-QAHTANI M., AL-BAGAWI J. and AL-MANSOUR K. (2009) Evaluation of flow maldistribution in air-cooled heat exchangers, *Computers & Fluids* **38**(3), 677–690.

HASAN M., SAHA S. and SAHA S. (2012) Effects of corrugation frequency and aspect ratio on natural convection within an enclosure having sinusoidal corrugation over a heated top surface, *International Communications in Heat and Mass Transfer* **39**(3), 368–377.

HE Y., HAN H., TAO W. and ZHANG Y. (2012) Numerical study of heat-transfer enhancement by punched winglet-type vortex generator arrays in fin-and-tube heat exchangers, *International Journal of Heat and Mass Transfer* **55**(21–22), 5449–5458.

HEATRIC LTD. (2012) Typical diffusion-bonded heat exchanger characteristics (online), `http://www.heatric.com/typical_characteristics.html`, accessed: 26 August 2012.

Heggemann M., Hirschberg S., Spiegel L. and Bachmann C. (2007) CFD simulation and experimental validation of fluid flow in liquid distributors, *Chemical Engineering Research and Design* **85**(1), 59–64.

Hewitt G. (Ed.) (1998) *Heat Exchanger Design Handbook*, Begell House, Inc., Redding, CT, USA.

Hewitt G., Shires G. and Bott T. (1994) *Process Heat Transfer*, CRC Press, LLC, Boca Raton, FL, USA.

Hájek J. (2008) Computational fluid dynamic simulations in thermal waste treatment technology – design, optimisation and troubleshooting, *Energy* **33**(6), 930–941.

Houdek P. (2007) Flow instabilities in heat exchangers, Ph.D. thesis, Czech Technical University in Prague.

Idelchik I. (1986) *Handbook of Hydraulic Resistance*, Hemisphere Publishing Corporation, Washington, DC, USA, 2nd edn.

Islam M., Oyakawa K., Yaga M. and Kubo I. (2009) The influence of channel height on heat transfer enhancement of a co-angular type rectangular finned surface in narrow channel, *International Journal of Thermal Sciences* **48**(8), 1639–1648.

Jafari Nasr M., Habibi Khalaj A. and Mozaffari S. (2010) Modeling of heat transfer enhancement by wire coil inserts using artificial neural network analysis, *Applied Thermal Engineering* **30**(2–3), 143–151.

Jecha D., Dudeková M., Bébar L. and Stehlík P. (2008) Balances of contaminants in flue gas from industrial waste incineration plant, in *Proceedings of the 18th International Congress of Chemical and Process Engineering CHISA 2008, Prague, Czech Republic, 24 – 28 August 2008*, paper ID 1232/P5.124.

Jegla Z. (2008) Optimum arrangement of tube coil in radiation type of tubular furnace, *Heat Transfer Engineering* **29**(6), 546–555.

Jegla Z., Kilkovský B. and Stehlík P. (2010) Calculation tool for particulate fouling prevention of tubular heat transfer equipment, *Heat Transfer Engineering* **31**(9), 757–765.

Jones G. and Lior N. (1994) Flow distribution in manifolded solar collectors with negligible buoyancy effects, *Solar Energy* **52**(3), 289–300.

Kee R., Korada P., Walters K. and Pavol M. (2002) A generalized model of the flow distribution in channel networks of planar fuel cells, *Journal of Power Sources* **109**(1), 148–159.

Kemp I. (2006) *Pinch Analysis and Process Integration: A User Guide on Process Integration for the Efficient Use of Energy*, Butterworth-Heinemann, Inc., Burlington, MA, USA, 2nd edn.

Khadamakar H., Patwardhan A., Padmakumar G. and Vaidyanathan G. (2011) Flow distribution in the inlet plenum of steam generator, *Nuclear Engineering and Design* **241**(10), 4165–4180.

KHANI F., RAJI M. and NEJAD H. (2009) Analytical solutions and efficiency of the nonlinear fin problem with temperature-dependent thermal conductivity and heat transfer coefficient, *Communications in Nonlinear Science and Numerical Simulation* **14**(8), 3327–3338.

KILKOVSKÝ B., PAVLAS M., JEGLA Z. and STEHLÍK P. (2007) Database HGA: Common and specific types of heat exchangers for hot gas applications, in *Proceedings of the 3rd International Conference on Heat Transfer in Components and Systems for Sustainable Energy Technologies Heat-SET 2007, Chambéry, France, 18 – 20 April 2007*, pp. 463–470, paper ID 51.

KILKOVSKÝ B., TUREK V., JEGLA Z. and STEHLÍK P. (2011) Aspects of fouling in case of heat exchangers with polluted gas, in *Proceedings of the 8th International Conference on Heat Transfer, Fluid Mechanics and Thermodynamics HEFAT2011, Pointe Aux Piments, Mauritius, 11 – 13 July 2011*, pp. 220–229, paper ID HXX.7.

KIM N., KIM D. and BYUN H. (2011) Effect of inlet configuration on the refrigerant distribution in a parallel flow minichannel heat exchanger, *International Journal of Refrigeration* **34**(5), 1209–1221.

KIM N., LEE E. and BYUN H. (2012) Two-phase refrigerant distribution in a parallel flow minichannel heat exchanger having horizontal headers, *International Journal of Heat and Mass Transfer*, **in press**, DOI: 10.1016/j.ijheatmasstransfer.2012.07.082.

KIM S., CHOI E. and CHO Y. (1995) The effect of header shapes on the flow distribution in a manifold for electronic packaging applications, *International Communications in Heat and Mass Transfer* **22**(3), 329–341.

KLEMEŠ J., BULATOV I. and KOPPEJAN J. (2009) Novel energy saving technologies evaluation tool, *Computers & Chemical Engineering* **33**(3), 751–758.

KLEMEŠ J. and LAM H. (2011) Process integration for energy saving and pollution reduction, *Energy* **36**(8), 4586–4587.

KLEMEŠ J. and VARBANOV P. (2012) Heat integration including heat exchangers, combined heat and power, heat pumps, separation processes and process control, *Applied Thermal Engineering* **43**, 1–6.

KOCH HEAT TRANSFER COMPANY, LP (2012) Improving flow (online), `http://www.kochheattransfer.com/component/content/article/4-twisted-tube/29-improving-flow/`, accessed: 16 August 2012.

KOH J., SEO H., LEE C., YOO Y. and LIM H. (2003) Pressure and flow distribution in internal gas manifolds of a fuel-cell stack, *Journal of Power Sources* **115**(1), 54–65.

KRÁL D., STEHLÍK P., VAN DER PLOEG H. and MASTER B. (1996) Helical baffles in shell-and-tube heat exchangers, part I: Experimental verification, *Heat Transfer Engineering* **17**(1), 93–101.

KUKULKA D. and DEVGUN M. (2007) Fluid temperature and velocity effect on fouling, *Applied Thermal Engineering* **27**(16), 2732–2744.

KULKARNI A., ROY S. and JOSHI J. (2007) Pressure and flow distribution in pipe and ring spargers: Experimental measurements and CFD simulation, *Chemical Engineering Journal* **133**(1–3), 173–186.

Kumaraguruparan G., Kumaran R., Sornakumar T. and Sundararajan T. (2011) A numerical and experimental investigation of flow maldistribution in a micro-channel heat sink, *International Communications in Heat and Mass Transfer* **38**(10), 1349–1353.

Kundu B. and Lee K. (2012) Analytic solution for heat transfer of wet fins on account of all nonlinearity effects, *Energy* **41**(1), 354–367.

Lambert A., Cuevas S., del Río J. and López de Haro M. (2009) Heat transfer enhancement in oscillatory flows of Newtonian and viscoelastic fluids, *International Journal of Heat and Mass Transfer* **52**(23–24), 5472–5478.

Laukkanen T., Tveit T. and Fogelholm C. (2012) Simultaneous heat exchanger network synthesis for direct and indirect heat transfer inside and between processes, *Chemical Engineering Research and Design* **90**(9), 1129–1140.

Liang S. and Wong T. (2010) Experimental validation of model predictions on evaporator coils with an emphasis on fin efficiency, *International Journal of Thermal Sciences* **49**(1), 187–195.

Liu H., Li P. and Van Lew J. (2010a) CFD study on flow distribution uniformity in fuel distributors having multiple structural bifurcations of flow channels, *International Journal of Hydrogen Energy* **35**(17), 9186–9198.

Liu H., Li P., Van Lew J. and Juarez-Robles D. (2012) Experimental study of the flow distribution uniformity in flow distributors having novel flow channel bifurcation structures, *Experimental Thermal and Fluid Science* **37**, 142–153.

Liu X., Chen Q., Wang M., Pan N. and Guo Z. (2010b) Multi-dimensional effect on optimal network structure for fluid distribution, *Chemical Engineering and Processing: Process Intensification* **49**(10), 1038–1043.

Lotfi R., Rashidi A. and Amrollahi A. (2012) Experimental study on the heat transfer enhancement of MWNT-water nanofluid in a shell and tube heat exchanger, *International Communications in Heat and Mass Transfer* **39**(1), 108–111.

Lu F., Luo Y. and Yang S. (2008) Analytical and experimental investigation of flow distribution in manifolds for heat exchangers, *Journal of Hydrodynamics, Ser. B* **20**(2), 179–185.

Lunsford K. (1996) Advantages of brazed aluminium heat exchangers, *Hydrocarbon Processing* **75**(7), 55–63.

Maharudrayya S., Jayanti S. and Deshpande A. (2005) Flow distribution and pressure drop in parallel-channel configurations of planar fuel cells, *Journal of Power Sources* **144**(1), 94–106.

Manadilli G. (1997) Replace implicit equations with signomial functions, *Chemical Engineering* **104**(8), 129–132.

Maplesoft (2012) *Maple User Manual*, Waterloo Maple, Inc., Waterloo, ON, Canada.

MARCHITTO A., FOSSA M. and GUGLIELMINI G. (2012) The effect of the flow direction inside the header on two-phase flow distribution in parallel vertical channels, *Applied Thermal Engineering* **36**, 245–251.

MARTÍNEZ M., PALLARES J., LÓPEZ J., LÓPEZ A., ALBERTOS F., GARCÍA M., CUESTA I. and GRAU F. (2012) Numerical simulation of the liquid distribution in a trickle-bed reactor, *Chemical Engineering Science* **76**, 49–57.

MATHWORKS, INC. (2012) *MATLAB User's Guide*, MathWorks, Inc., Natick, MA, USA.

MELOUN M. and MILITKÝ J. (2004) *Statistická analýza experimentálních dat [Statistical analysis of experimental data]*, Academia, Prague, Czech Republic, 2nd edn., in Czech.

MIAO Z. and XU T. (2006) Single phase flow characteristics in the headers and connecting tube of parallel tube platen systems, *Applied Thermal Engineering* **26**(4), 396–402.

MINITAB, INC. (2006) *Minitab Statistical Software, Release 15 for Windows*, Minitab, Inc., State College, PA, USA.

MÜLLER-STEINHAGEN H., MALAYERI M. and WATKINSON A. (2005) Fouling of heat exchangers – new approaches to solve an old problem, *Heat Transfer Engineering* **26**(1), 1–4.

MOZDIANFARD M. and BEHRANVAND E. (2012) A field study of fouling in CDU preheaters at Esfahan refinery, *Applied Thermal Engineering*, **in press**, DOI: 10.1016/j.applthermaleng.2012.08.025.

NAPHON P. and SUCHANA T. (2011) Heat transfer enhancement and pressure drop of the horizontal concentric tube with twisted wires brush inserts, *International Communications in Heat and Mass Transfer* **38**(2), 236–241.

NGOMA G. and GODARD F. (2005) Flow distribution in an eight level channel system, *Applied Thermal Engineering* **25**(5–6), 831–849.

NIE J. and CHEN Y. (2010) Numerical modeling of three-dimensional two-phase gas-liquid flow in the flow field plate of a PEM electrolysis cell, *International Journal of Hydrogen Energy*, **35**(8), 3183–3197.

NOIE S., HERIS S., KAHANI M. and NOWEE S. (2009) Heat transfer enhancement using Al_2O_3/water nanofluid in a two-phase closed thermosyphon, *International Journal of Heat and Fluid Flow* **30**(4), 700–705.

OOSTHUIZEN P. and CARSCALLEN W. (2003) *Compressible Fluid Flow*, McGraw-Hill, Inc., New York, NY, USA.

PATANKAR S. (1980) *Numerical Heat Transfer and Fluid Flow*, Hemisphere Publishing Corporation, Washington, DC, USA.

PAVLAS M., BÉBAR L., DUDEKOVÁ M. and STEHLÍK P. (2007) Energy recovery systems in thermal processing of wastes, in *Proceedings of the 3rd International Conference on Heat Transfer in Components and Systems for Sustainable Energy Technologies Heat-SET 2007, Chambéry, France, 18 – 20 April 2007*, pp. 101–110, paper ID 9.

Pařízek T. (2009) Redukce emisí škodlivých látek u jednotek pro termické zpracování odpadů [Reduction of harmful emissions in units for thermal processing of wastes], Ph.D. thesis, Brno University of Technology, in Czech.

Perić M. (2004) Flow simulation using control volumes of arbitrary polyhedral shape, *European Research Community on Flow, Turbulence and Combustion (ERCOFTAC) Bulletin* **62**, 25–29.

Pethkool S., Eiamsa-ard S., Kwankaomeng S. and Promvonge P. (2011) Turbulent heat transfer enhancement in a heat exchanger using helically corrugated tube, *International Communications in Heat and Mass Transfer* **38**(3), 340–347.

Polley G., Morales-Fuentes A. and Wilson D. (2009) Simultaneous consideration of flow and thermal effects of fouling in crude oil preheat trains, *Heat Transfer Engineering* **30**(10–11), 815–821.

Pustylnik L., Barnea D. and Taitel Y. (2010) Adiabatic flow distribution of gas and liquid in parallel pipes – effect of additional restrictions, *Chemical Engineering Science* **65**(8), 2552–2557.

Rahimi M., Shabanian S. and Alsairafi A. (2009) Experimental and CFD studies on heat transfer and friction factor characteristics of a tube equipped with modified twisted tape inserts, *Chemical Engineering and Processing: Process Intensification* **48**(3), 762–770.

Ravindran A., Ragsdell K. and Reklaitis G. (2006) *Engineering Optimization: Methods and Applications*, John Wiley & Sons, Inc., Hoboken, NJ, USA, 2nd edn.

Rebrov E., Ismagilov I., Ekatpure R., de Croon M. and Schouten J. (2007) Header design for flow equalization in microstructured reactors, *AIChE Journal* **53**(1), 28–38.

Rebrov E., Schouten J. and de Croon M. (2011) Single-phase fluid flow distribution and heat transfer in microstructured reactors, *Chemical Engineering Science* **66**(7), 1374–1393.

Romeo E., Royo C. and Monzón A. (2002) Improved explicit equations for estimation of the friction factor in rough and smooth pipes, *Chemical Engineering Journal* **86**(3), 169–374.

Sabbaghi S., Rezaii A., Shahri G. and Baktash M. (2011) Mathematical analysis for the efficiency of a semi-spherical fin with simultaneous heat and mass transfer, *International Journal of Refrigeration* **34**(8), 1877–1882.

Saber M., Commenge J. and Falk L. (2010) Microreactor numbering-up in multi-scale networks for industrial-scale applications: Impact of flow maldistribution on the reactor performances, *Chemical Engineering Science* **65**(1), 372–379.

Salmasi F., Khatibi R. and Ghorbani M. (2012) A study of friction factor formulation in pipes using artificial intelligence techniques and explicit equations, *Turkish Journal of Engineering and Environmental Sciences* **36**(2), 121–138.

Schorle B., Churchill S. and Shacham M. (1980) Comments on: "An explicit equation for friction factor in pipe", *Industrial & Engineering Chemistry Fundamentals* **19**(2), 228–230.

SENGUPTA T. and POINSOT T. (Eds.) (2010) *Instabilities of Flows: With and Without Heat Transfer and Chemical Reaction, CISM Courses and Lectures*, vol. 517, Springer-Verlag, Inc., New York, NY, USA.

SERGHIDES T. (1984) Estimate friction factor accurately, *Chemical Engineering* **91**(5), 63–64.

SHARQAWY M., MOINUDDIN A. and ZUBAIR S. (2012) Heat and mass transfer from annular fins of different cross-sectional area. Part I. Temperature distribution and fin efficiency, *International Journal of Refrigeration* **35**(2), 365–376.

SHEIK ISMAIL L., VELRAJ R. and RANGANAYAKULU C. (2010) Studies on pumping power in terms of pressure drop and heat transfer characteristics of compact plate-fin heat exchangers – A review, *Renewable and Sustainable Energy Reviews* **14**(1), 478–485.

SMITH N. (1965) The difference between c_p and c_v for liquids and solids, *Journal of Chemical Education* **42**(12), 654.

STEHLÍK P. (2011) Conventional versus specific types of heat exchangers in the case of polluted flue gas as the process fluid – A review, *Applied Thermal Engineering* **31**(1), 1–13.

SUNDAR L. and SHARMA K. (2010) Heat transfer enhancements of low volume concentration Al_2O_3 nanofluid and with longitudinal strip inserts in a circular tube, *International Journal of Heat and Mass Transfer* **53**(19–20), 4280–4286.

TAN X., ZHU D., ZHOU G. and ZENG L. (2012) Heat transfer and pressure drop performance of twisted oval tube heat exchanger, *Applied Thermal Engineering*, **in press**, DOI: 10.1016/j.applthermaleng.2012.06.037.

TANG X. and ZHU D. (2012) Experimental and numerical study on heat transfer enhancement of a rectangular channel with discontinuous crossed ribs and grooves, *Chinese Journal of Chemical Engineering* **20**(2), 220–230.

THE CARBON TRUST (2012) Heat recovery: A guide to key systems and applications (online), `http://www.carbontrust.com/media/31715/ctg057_heat_recovery.pdf`, accessed: 13 August 2012.

TIMOFEEVA E., MORAVEK M. and SINGH D. (2011) Improving the heat transfer efficiency of synthetic oil with silica nanoparticles, *Journal of Colloid and Interface Science* **364**(1), 71–79.

TOH K., CHEN X. and CHAI J. (2002) Numerical computation of fluid flow and heat transfer in microchannels, *International Journal of Heat and Mass Transfer* **45**(26), 5133–5141.

TONDEUR D., FAN Y. and LUO L. (2009) Constructal optimization of arborescent structures with flow singularities, *Chemical Engineering Science* **64**(18), 3968–3982.

TONDEUR D. and LUO L. (2004) Design and scaling laws of ramified fluid distributors by the constructal approach, *Chemical Engineering Science* **59**(8–9), 1799–1813.

TONG J., SPARROW E. and ABRAHAM J. (2009) Geometric strategies for attainment of identical outflows through all of the exit ports of a distribution manifold in a manifold system, *Applied Thermal Engineering* **29**(17–18), 3552–3560.

Torabi M. and Aziz A. (2012) Thermal performance and efficiency of convective-radiative t-shaped fins with temperature dependent thermal conductivity, heat transfer coefficient and surface emissivity, *International Communications in Heat and Mass Transfer* **39**(8), 1018–1029.

Tubular Exchanger Manufacturers Association, Inc. (2007) *Standards of the Tubular Exchanger Manufacturers Association*, Tubular Exchanger Manufacturers Association, Inc., Tarrytown, NY, USA, 9th edn.

Tucker R. and Ward J. (2012) Identifying and quantifying energy savings on fired plant using low cost modelling techniques, *Applied Energy* **89**(1), 127–132.

Walker M., Safari I., Theregowda R., Hsieh M., Abbasian J., Arastoopour H., Dzombak D. and Miller D. (2012) Economic impact of condenser fouling in existing thermoelectric power plants, *Energy* **44**(1), 429–437.

Wang J. (2008) Pressure drop and flow distribution in parallel-channel configurations of fuel cells: U-type arrangement, *International Journal of Hydrogen Energy* **33**(21), 6339–6350.

Wang J. (2010) Pressure drop and flow distribution in parallel-channel configurations of fuel cells: Z-type arrangement, *International Journal of Hydrogen Energy* **35**(11), 5498–5509.

Wang J., Gao Z., Gan G. and Wu D. (2001) Analytical solution of flow coefficients for a uniformly distributed porous channel, *Chemical Engineering Journal* **84**(1), 1–6.

Wang J. and Wang H. (2012) Discrete approach for flow field designs of parallel channel configurations in fuel cells, *International Journal of Hydrogen Energy* **37**(14), 10881–10897.

Wang X. and Yu P. (1989) Isothermal flow distribution in header systems, *International Journal of Solar Energy* **7**(3), 159–169.

Wang Y., Smith R. and Kim J. (2012) Heat exchanger network retrofit optimization involving heat transfer enhancement, *Applied Thermal Engineering* **43**, 7–13.

Wetter M. and Wright J. (2004) A comparison of deterministic and probabilistic optimization algorithms for nonsmooth simulation-based optimization, *Building and Environment* **39**(8), 989–999.

White F. (1991) *Viscous Fluid Flow*, McGraw-Hill, Inc., New York, NY, USA, 2nd edn.

White F. (1998) *Fluid Mechanics*, McGraw-Hill, Inc., New York, NY, USA, 4th edn.

Wolfram Research, Inc. (2010) *Mathematica Edition: Version 8.0*, Wolfram Research, Inc., Champaign, IL, USA.

Wongcharee K. and Eiamsa-ard S. (2011a) Enhancement of heat transfer using CuO/water nanofluid and twisted tape with alternate axis, *International Communications in Heat and Mass Transfer* **38**(6), 742–748.

Wongcharee K. and Eiamsa-ard S. (2011b) Heat transfer enhancement by twisted tapes with alternate-axes and triangular, rectangular and trapezoidal wings, *Chemical Engineering and Processing: Process Intensification* **50**(2), 211–219.

YIN J., YANG G. and LI Y. (2012) The effects of wavy plate phase shift on flow and heat transfer characteristics in corrugated channel, *Energy Procedia* **14**, 1566–1573.

YUAN P., JIANG G., HE Y., YI X. and TAO W. (2012) Experimental study on the performance of a novel structure for two-phase flow distribution in parallel vertical channels, *International Journal of Multiphase Flow*, **in press**, DOI: 10.1016/j.ijmultiphaseflow.2012.05.006.

ZHANG L., GAO G., SUI H., LI H. and LI X. (2011) CFD simulation and experimental validation of fluid flow in pre-distributor, *Chinese Journal of Chemical Engineering* **19**(5), 815–820.

ZHANG N., SMITH R., BULATOV I. and KLEMEŠ J. (2012) Sustaining high energy efficiency in existing processes with advanced process integration technology, *Applied Energy*, **in press**, DOI: 10.1016/j.apenergy.2012.02.037.

ZHANG T., WEN J., JULIUS A., PELES Y. and JENSEN M. (2011) Stability analysis and maldistribution control of two-phase flow in parallel evaporating channels, *International Journal of Heat and Mass Transfer* **54**(25–26), 5298–5305.

ZHANG W., HU P., LAI X. and PENG L. (2009) Analysis and optimization of flow distribution in parallel-channel configurations for proton exchange membrane fuel cells, *Journal of Power Sources* **194**(2), 931–940.

ZHU X., ZANFIR M. and KLEMEŠ J. (2000) Heat transfer enhancement for heat exchanger network retrofit, *Heat Transfer Engineering* **21**(2), 7–18.

Nomenclature

Acronyms

CFD	computational fluid dynamics
CPU	central processing unit
CSV	comma-separated values
HP	high pressure
HRSG	heat recovery steam generator
HVAC	heating, ventilation, and air conditioning
IP	intermediate pressure
LAN	local area network
LP	low pressure
PC	personal computer
PCDD/F	polychlorinated dibenzo-p-dioxins and dibenzofurans
PTFE	polytetrafluoroethylene
PVC-C	chlorinated polyvinyl chloride
PWG	process waste gas
SIMPLE	semi-implicit method for pressure-linked equations
WAN	wide area network
WTE	waste-to-energy

Latin letters

AD	Anderson-Darling statistic	[–]
b	cross-section width	[m]
c_p	specific heat capacity at constant pressure	$[\mathrm{J\,kg^{-1}\,K^{-1}}]$
c_v	specific heat capacity at constant volume	$[\mathrm{J\,kg^{-1}\,K^{-1}}]$
C_d	discharge coefficient	[–]
C_r	coefficient of static regain	[–]
d	tube diameter	[m]
D	manifold diameter	[m]
$D_{1-\alpha}$	critical value of Anderson-Darling statistic	[–]
D_h	hydraulic diameter	[m]
e	Euler's number	[–]
E	tube exsertion length	[m]
f	Darcy friction factor	[–]
$\hat{f}$	value obtained with regression model	[–]
g	standard gravity	$[\mathrm{m\,s^{-2}}]$
h	manifold cross-section height	[m]
H	enthalpy	[J]
l	length	[m]
m	molar mass	$[\mathrm{kg\,mol^{-1}}]$
$\dot{m}$	mass flow rate	$[\mathrm{kg\,s^{-1}}]$
n	total number of branches	[–]
N	number of observations	[–]
p	pressure	[Pa]
$\dot{q}$	heat flux density	$[\mathrm{W\,m^{-2}}]$
r	residual	[–]

R	specific gas constant	$[\mathrm{J\,kg^{-1}\,K^{-1}}]$
$\bar{R}$	universal gas constant	$[\mathrm{J\,mol^{-1}\,K^{-1}}]$
R^2	coefficient of determination	[–]
R_H	radius of curvature of top manifold wall	[m]
R_W	radius of curvature of side manifold walls	[m]
Re	Reynolds number	[–]
s	branch cross-sectional area	$[\mathrm{m^2}]$
S	manifold cross-sectional area	$[\mathrm{m^2}]$
SS	sum of squares	[–]
t	temperature	[°C]
$\hat{t}$	simulated time	[s]
T	thermodynamic temperature	[K]
U	channel circumference	[m]
v	flow velocity	$[\mathrm{m\,s^{-1}}]$
w	discharge velocity	$[\mathrm{m\,s^{-1}}]$
x	mole fraction	[–]
y	observed value	[–]
$\bar{y}$	estimate of mean of observed values	[–]
z	elevation above reference plane	[m]

Greek letters

α	statistical significance	[–]
β	angle of inclination	[°]
γ	heat capacity ratio	[–]
δ	flow distribution uniformity indicator	[%]
Δx	spatial step	[m]

ϵ	absolute roughness	[m]
ζ	coefficient of hydraulic resistance	[–]
θ	discharge angle	[°]
κ	variable used during calculation of coefficient of static regain	[–]
μ	dynamic viscosity	[Pa s]
π	ratio of a circle's circumference to its diameter	[–]
ρ	density	[kg m^{-3}]
τ	sub-term of coefficient of static regain	[–]
φ	Golden ratio	[–]
ω	vorticity magnitude	[s^{-1}]
$\vec{\omega}$	vorticity	[s^{-1}]
Ω	sum of volume integrals of vorticity magnitude	[m^3 s^{-1}]

Subscripts

abs	absolute value
b	related to manifold cross-section width
CO	closed to open end
da	dry air
h	related to manifold cross-section height
i	manifold section, branch
id	ideal
in	at inlet
man	manifold
opt	optimum
out	at outlet
res	residual

S	related to cross-sectional area
tot	total
w	wall
wv	water vapour

Superscripts

a	axial
any	for constant or linearly variable manifold cross-section
avg	average
B	at/through branch
const	for constant manifold cross-section
D	just downstream
diff	difference from average value
fr	due to friction
M	in the middle of manifold section
ovr	overall
r	radial
rat	ratio
U	just upstream
var	for linearly variable manifold cross-section

A tilde (~) placed above an identifier denotes an estimate. Capital letters A and B, used in subscripts, superscripts, or directly, indicate auxiliary variables.

Appendices

A

Synthesis of Heat Exchanger Networks

Raw materials, intermediate products, and finished products flow through process plants in so called process streams. These streams may either be “hot”, or “cold”, depending on their need to be cooled or heated during a production process. It is clear that a sole use of hot utilities (e.g. steam or hot water) and cold utilities (e.g. cooling water, air, or various refrigerants) to increase or lower temperatures of process streams is not only uneconomic, but also a waste of energy in some sense. Since well-designed heat exchanger network (HEN) can bring substantial energy and financial savings, there is a lot of effort devoted to this topic. The design process consists of the three main steps described below.

Targeting, that is, a preliminary technical-economic analysis determining optimum heat recovery. As Kemp (2006, Sec. 2.4.1) stated, higher values of minimum allowed temperature difference between hot and cold process streams, ΔT_{min}, give higher hot and cold utility requirements whereas lower values give larger and more costly heat exchangers. Since the right value of ΔT_{min} in fact depends on the actual target, we can approach this particular issue in many different ways – e.g. by supertargeting (Wan Alwi et al., 2012a) we find ΔT_{min} corresponding to the minimum total annual cost (see Figure A.1). Other approaches include utility targeting (Castier, 2012), total site targeting (Klemeš et al., 1997; Varbanov et al., 2012), minimum outsourced electricity targeting in hybrid power systems (Wan Alwi et al., 2012b), or even multi-criteria targeting (Serna-González and Ponce-Ortega, 2011). General information on this subject can be found for example in (Klemeš et al., 2010).

Synthesis. During this step an optimum heat exchanger network layout is found (see further).

Detailed design of individual units, i.e., selection of suitable heat exchanger types to be used and their design in terms of required heat duties, allowed pressure drops, necessary

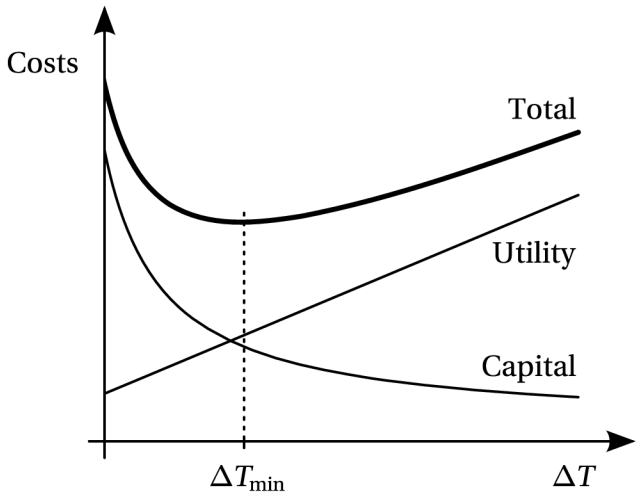

Figure A.1. Supertargeting: determining $\Delta T_{\min}$

compatibility of media with materials that exchanger parts are made of (see e.g. Gillham and Sennik, 1984), fouling (Jegla et al., 2010; Markowski et al., 2012; Ojaniemi et al., 2012), etc.

In this chapter, we will focus on a brief description of optimization models for heat exchanger network synthesis. The topic was introduced into the literature by Ten Broeck (1944) while the first grassroot HEN synthesis was presented by Hwa (1965). Nevertheless, a rigorous definition of this problem did not appear until the very end of the 1960s (Masso and Rudd, 1969). Later, many sequential algorithms were developed. These divided the task into a set of sub-problems solved successively in order of decreasing significance and therefore computational demand was reduced. The most well-known example is pinch analysis (Kemp, 2006, Chap. 2), a sequential heuristic technique developed in late 1978 by Ph.D. student Bodo Linnhoff. This method and many other approaches based on it (e.g. Klemeš and Ptáčník, 1985; Ptáčník and Klemeš, 1988) have been used widely in engineering practice due to their simplicity. The downside, however, is that these usually yield "nearly optimal" solutions only (Floudas et al., 1986; Linnhoff and Hindmarsh, 1983). This fact led to the development of simultaneous synthesis algorithms, first of which were presented by Yee and Grossmann (1990) and Ciric and Floudas (1991). Such algorithms do not perform any decomposition and, obviously, produce computationally much more intensive tasks. As a consequence, various simplifying assumptions need to be made even though the growth in available computing power is faster than exponential (Moravec, 1998). Recent simultaneous models include, for example, the ones presented by Drobež et al. (2012), Laukkanen and Fogelholm (2011), or Xiao et al. (2010). A simultaneous graphical tool for HEN synthesis was proposed by Wan Alwi and Manan (2010). The objective of the majority of available models is minimization of total annual cost, but sometimes also other factors are considered – see e.g. (López-Maldonado et al., 2011) where both cost and environmental impact are taken into account. Synthesis of networks with unconstrained topology was investigated for example by Toffolo (2009). As for networks with inter-process heat exchange being possible, these were studied by Laukkanen et al. (2012a). There also are a few articles dealing with phase changes of media inside heat exchangers (for instance Hasan et al., 2009; Ponce-Ortega et al., 2008), but construction of efficient optimization models supporting this is still a live research topic. Additionally, many of the models mentioned so far do not guarantee finding global optima due to the highly

combinatorial non-convex nature of HEN synthesis problems. Still, some global models are available (see for example Adjiman et al., 1997; Björk and Westerlund, 2002; Bogataj and Kravanja, 2012).

Aside from pure simultaneous synthesis, various other approaches can be employed to obtain optimum HEN layouts – e.g. interval-based synthesis (Isafiade and Fraser, 2010), stage-wise models (Huang et al., 2012), genetic algorithms (Fieg et al., 2009; Luo et al., 2009), particle swarm optimization (Silva et al., 2009), randomization (Gupta and Ghosh, 2010), or synthesis using a p-graph (Heckl et al., 2005; Nagy et al., 2001). Interactive methods (Laukkanen et al., 2010, 2012b), tools for computer-aided synthesis (see e.g. Centre for Process Integration, University of Manchester, UK, 2012), and models for synthesis of heat and mass exchanger networks (Azeez et al., 2012; Liu et al., 2012) exist as well.

Considering HEN retrofits, a method suitable for optimization of large scale networks was proposed by Pan et al. (2012b) while models including measures for enhanced heat transfer were provided for instance by Pan et al. (2012a), Wang et al. (2012), or Zhu et al. (2000). A model including detailed equipment design was proposed by Ravagnani and Silva (2012). There even are models taking fouling into account (Coletti et al., 2011). The approaches employed in case of retrofits include not only the mentioned simultaneous methods, but also hybrid genetic algorithms (Liu et al., 2011; Rezaei and Shafiei, 2009; Soltani and Shafiei, 2011) or stage-wise methods (Kovač Kralj, 2010). General guidelines for HEN retrofits were presented by Smith et al. (2010) while debottlenecking was discussed by Varbanov and Klemeš (2000). Issues related to HEN reliability, availability, and maintenance were investigated by Sikos and Klemeš (2010).

Furman and Sahinidis (2001) showed that synthesis of a heat exchanger network is an NP-hard problem (non-deterministic polynomial-time hard; see Atallah and Blanton, 2009) and thus a computationally efficient polynomial algorithm yielding exact solutions cannot be constructed. What is more, they demonstrated that HEN synthesis is NP-hard in the strong sense (definition of strong NP-hardness can, again, be found in Atallah and Blanton, 2009). With respect to these results, Errico et al. (2007) proposed a deterministic algorithm suitable for synthesis of structurally simple – albeit possibly large – heat exchanger networks. This algorithm will be used here as a basis for the sample models described further in the text.

A.1 General Representation of Network Structure

Let us consider the problem once again: a robust yet efficient enough (in terms of computational demand) optimization model must be built such that it would allow for virtually any reasonable HEN structure. A general way to represent a wide range of networks is to use superstructures consisting of one or more "repetitive units" proposed by Yee and Grossmann (1990) (see Figure A.2). Horizontal lines and their numbered vertical couplings constitute process streams and heat exchangers, respectively. Elements at the ends of streams represent utility heat exchangers. Layout of a repetitive unit (including stream splitting) is given by the number of hot and cold process streams.

Stream splitting can in some cases improve overall performance of a heat exchanger network. However, it also increases costs and network complexity which, in consequence, can lead to higher vulnerability of the entire structure. Splitting is therefore avoided if possible and in such a case the layout of repetitive units can be slightly simplified. This results in superstructures similar to the one in Figure A.3.

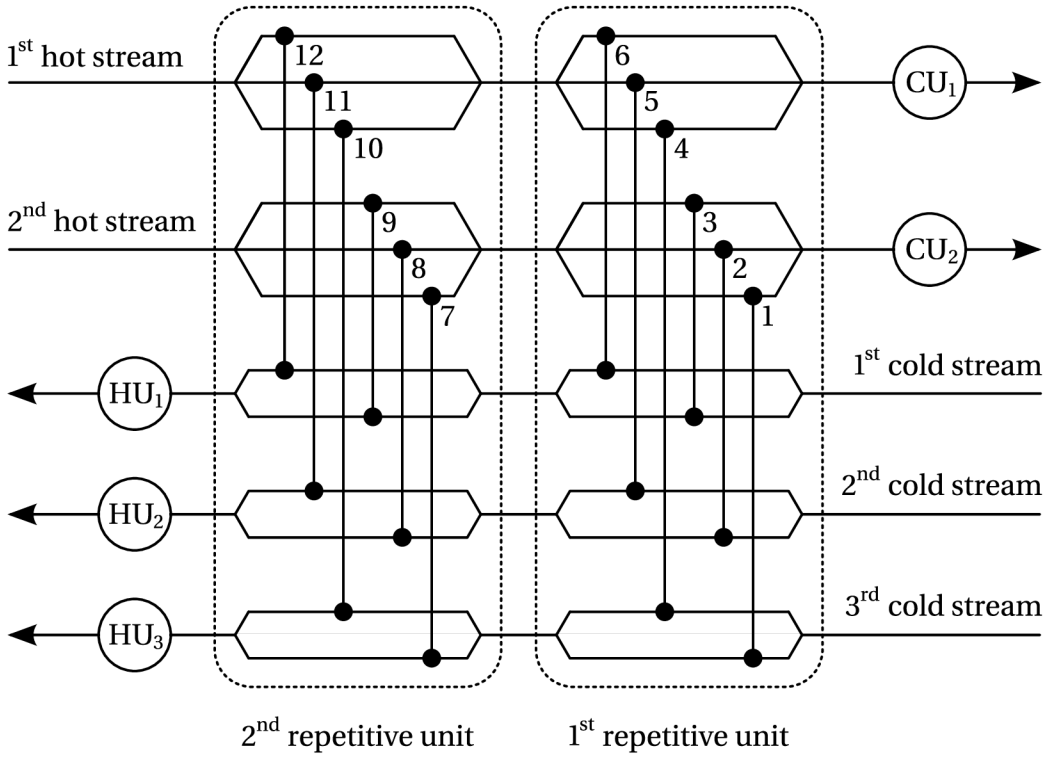

Figure A.2. General HEN superstructure proposed by Yee and Grossmann (1990)

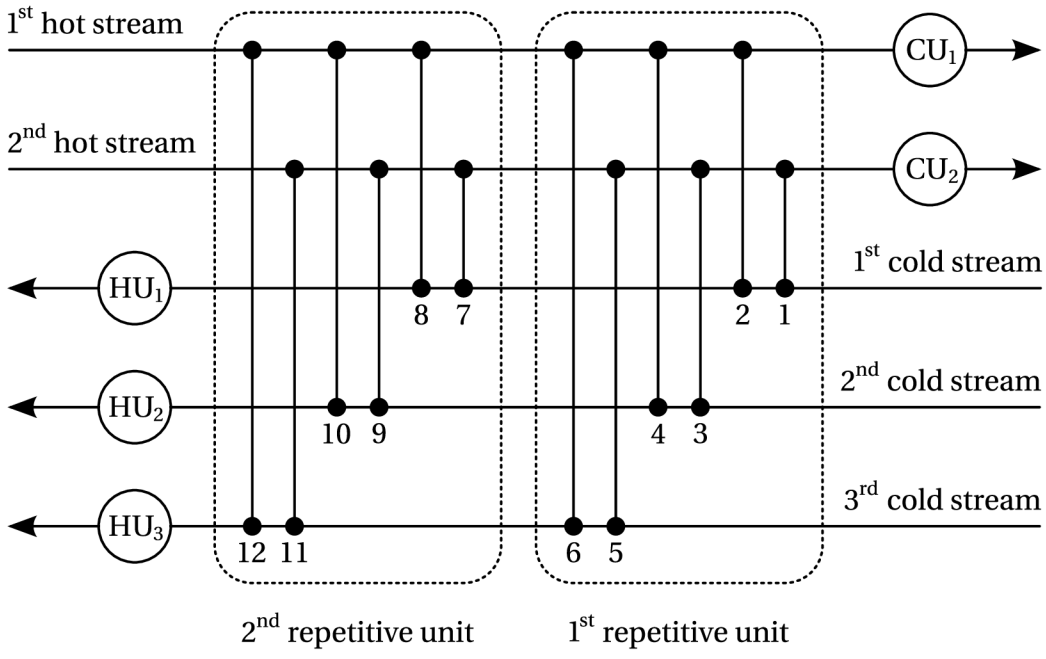

Figure A.3. Simplified HEN superstructure

The advantage of superstructure representation of heat exchanger networks is that it can be used regardless of properties of the actual heat exchange units. In other words, no matter which types of heat exchangers (shell-and-tube, plate, spiral, etc.) are chosen in the end, models based on this representation will still be valid.

A.2 Optimization Models

Typically, one of the following optimization criteria is used:

- maximum energy recovery (MER), or
- minimum total heat exchange area, or
- minimum number of heat exchange units, or
- minimum total annual cost (TAC) in case of maximum energy recovery.

Although Mastromanno et al. (2006) or Trivedi et al. (1997) argue that reaching MER may lead to sub-optimal network designs, this can be remedied by finding more solutions instead of a single one and implementing additional mechanisms – for example the driving force plot (Linnhoff and Vredeveld, 1984) (see Section A.3).

In this section we will discuss two basic global optimization models that should, at least for relatively simple synthesis problems, yield suitable HEN designs with much less effort and in significantly shorter times than are necessary in case of conventional methods such as pinch analysis. The first model is a MILP (mixed-integer linear programming) one and maximizes energy recovery. Due to its linearity, it does not support stream splitting or any other feature requiring non-linear constraints, however, global solutions are always reached quickly.

Let us consider a heat exchanger network with n_{H} hot streams and n_{C} cold streams represented by a superstructure similar to the one in Figure A.3. Let the superstructure consist of n_{R} repetitive units. Then the total number of heat exchangers in the general representation of the network is $n_{\mathrm{E}} = n_{\mathrm{H}} n_{\mathrm{C}} n_{\mathrm{R}}$ and there are n_{C} hot utility units and n_{H} cold utility units. Let also E_{ijk}, $i = 1,\ldots,n_{\mathrm{H}}$, $j = 1,\ldots,n_{\mathrm{C}}$, $k = 1,\ldots,n_{\mathrm{R}}$, denote heat duties of common heat exchangers (a particular exchanger E_{ijk} matches ith hot stream with jth cold stream in kth repetitive unit), U_j^{H} hot utility unit on jth cold stream, and U_i^{C} cold utility unit on ith hot stream. Each exchanger will then be assigned a number such that the one with $n_{ijk} = 1$ is closest to cold utilities and the one with $n_{ijk} = n_{\mathrm{E}}$ is closest to hot utilities. Additionally, the following input parameters will be necessary:

- source, $T_i^{\mathrm{H,S}}$, and target, $T_i^{\mathrm{H,T}}$, temperatures of hot streams;
- source, $T_j^{\mathrm{C,S}}$, and target, $T_j^{\mathrm{C,T}}$, temperatures of cold streams;
- flowing heat capacities of hot, $C_{\mathrm{p},i}^{\mathrm{H}}$, and cold, $C_{\mathrm{p},j}^{\mathrm{C}}$, streams (these will be considered constant);
- minimum required temperature difference, ΔT_{min}, between hot and cold streams;
- minimum required temperature difference, $\Delta T_{\mathrm{min}}^{\mathrm{U}}$, for utility units;

- maximum, $E_{ijk}^{\max}$, and minimum, $E_{ijk}^{\min}$, allowed heat duties of common heat exchangers;
- maximum, $U_j^{\mathrm{H,max}}$, and minimum, $U_j^{\mathrm{H,min}}$, allowed heat duties of hot utility units;
- maximum, $U_i^{\mathrm{C,max}}$, and minimum, $U_i^{\mathrm{C,min}}$, allowed heat duties of cold utility units;
- maximum allowed total heat duty, $U_{\mathrm{tot}}^{\mathrm{H,max}}$, of hot utility units;
- maximum allowed total heat duty, $U_{\mathrm{tot}}^{\mathrm{C,max}}$, of cold utility units;
- maximum common heat exchanger count, $n_{\max}$;
- types of common heat exchangers, i.e., countercurrent or concurrent;
- inlet and outlet temperatures of hot and cold media flowing through the respective utility heat exchangers[1];
- heat transfer coefficients for common heat exchangers;
- maximum allowed heat exchange area of a single common heat exchanger; and
- number of solutions that the solver should return.

Existence of a common heat exchanger will be denoted by $\delta_{ijk}=1$ (otherwise $\delta_{ijk}=0$). Hot and cold utility units will be treated analogously using δ_j^{H} and δ_i^{C}, respectively.

The below set of equations constitutes the most basic deterministic model. First, there are heat duties necessary to cool hot streams down from their source to target temperatures,

$$C_{\mathrm{p},i}^{\mathrm{H}}\left(T_i^{\mathrm{H,S}}-T_i^{\mathrm{H,T}}\right)=\sum_{j=1}^{n_{\mathrm{C}}}\sum_{k=1}^{n_{\mathrm{R}}}E_{ijk}+U_i^{\mathrm{C}}\qquad i=1,\ldots,n_{\mathrm{H}} \tag{A.1}$$

and heat duties necessary to heat cold streams up,

$$C_{\mathrm{p},j}^{\mathrm{C}}\left(T_j^{\mathrm{C,T}}-T_j^{\mathrm{C,S}}\right)=\sum_{i=1}^{n_{\mathrm{H}}}\sum_{k=1}^{n_{\mathrm{R}}}E_{ijk}+U_j^{\mathrm{H}}\qquad j=1,\ldots,n_{\mathrm{C}}. \tag{A.2}$$

The following constraints then allow us to find inlet and outlet stream temperatures for each heat exchanger. Usually, these are not included into the model, but we will need them later during construction of composite curves and driving force plots. For each $i=1,\ldots,n_{\mathrm{H}}$, $j=1,\ldots,n_{\mathrm{C}}$, $k=1,\ldots,n_{\mathrm{R}}$, we have:

$$T_{ijk}^{\mathrm{H,in}}=T_i^{\mathrm{H,T}}+\frac{1}{C_{\mathrm{p},i}^{\mathrm{H}}}\left(U_i^{\mathrm{C}}+\sum_{\substack{s=1\\ n_{ist}\le n_{ijk}}}^{n_{\mathrm{C}}}\sum_{t=1}^{n_{\mathrm{R}}}E_{ist}\right), \tag{A.3}$$

$$T_{ijk}^{\mathrm{H,out}}=T_i^{\mathrm{H,T}}+\frac{1}{C_{\mathrm{p},i}^{\mathrm{H}}}\left(U_i^{\mathrm{C}}+\sum_{\substack{s=1\\ n_{ist}<n_{ijk}}}^{n_{\mathrm{C}}}\sum_{t=1}^{n_{\mathrm{R}}}E_{ist}\right), \tag{A.4}$$

[1]While these may seem superfluous, they will be utilized during construction of driving force plots for each of the obtained solutions.

$$T_{ijk}^{\mathrm{C,in}} = T_j^{\mathrm{C,S}} + \frac{1}{C_{\mathrm{p},j}^{\mathrm{C}}} \sum_{\substack{r=1 \\ n_{rjt}<n_{ijk}}}^{n_{\mathrm{H}}} \sum_{t=1}^{n_{\mathrm{R}}} E_{rjt}, \tag{A.5}$$

$$T_{ijk}^{\mathrm{C,out}} = T_j^{\mathrm{C,S}} + \frac{1}{C_{\mathrm{p},j}^{\mathrm{C}}} \sum_{\substack{r=1 \\ n_{rjt}\le n_{ijk}}}^{n_{\mathrm{H}}} \sum_{t=1}^{n_{\mathrm{R}}} E_{rjt}, \tag{A.6}$$

where $T_{ijk}^{\mathrm{H,in}}$, $T_{ijk}^{\mathrm{H,out}}$, $T_{ijk}^{\mathrm{C,in}}$, and $T_{ijk}^{\mathrm{C,out}}$ denote inlet and outlet temperatures of hot and cold streams for each common heat exchanger E_{ijk}, respectively. Temperature differences at hot and cold sides of these heat exchangers are then given by the following relations:

$$\Delta T_{ijk}^{\mathrm{H}} = \begin{cases} T_{ijk}^{\mathrm{H,in}} - T_{ijk}^{\mathrm{C,out}} & \text{if } \mathrm{E}_{ijk} \text{ is countercurrent} \\ T_{ijk}^{\mathrm{H,in}} - T_{ijk}^{\mathrm{C,in}} & \text{if } \mathrm{E}_{ijk} \text{ is concurrent} \qquad \text{and} \end{cases} \tag{A.7}$$

$$\Delta T_{ijk}^{\mathrm{C}} = \begin{cases} T_{ijk}^{\mathrm{H,out}} - T_{ijk}^{\mathrm{C,in}} & \text{if } \mathrm{E}_{ijk} \text{ is countercurrent} \\ T_{ijk}^{\mathrm{H,out}} - T_{ijk}^{\mathrm{C,out}} & \text{if } \mathrm{E}_{ijk} \text{ is concurrent,} \end{cases} \tag{A.8}$$

while the allowed temperature changes of streams inside heat exchangers are guaranteed by

$$T_{ijk}^{\mathrm{H,out}} \le T_{ijk}^{\mathrm{H,in}} \qquad \text{and} \tag{A.9}$$

$$T_{ijk}^{\mathrm{C,out}} \ge T_{ijk}^{\mathrm{C,in}}. \tag{A.10}$$

Inequality constraints ensure that minimum and maximum heat duties, maximum exchanger count, and minimum temperature differences are met. A large enough negative value $\alpha \ll 0$ is necessary so that constraints are valid even if some exchangers do not exist. For $i = 1,\ldots,n_{\mathrm{H}}$, $j = 1,\ldots,n_{\mathrm{C}}$, and $k = 1,\ldots,n_{\mathrm{R}}$, we have:

$$E_{ijk} \ge \delta_{ijk} E_{ijk}^{\min}, \tag{A.11}$$

$$E_{ijk} \le \delta_{ijk} E_{ijk}^{\max} \tag{A.12}$$

$$U_j^{\mathrm{H}} \ge \delta_j^{\mathrm{H}} U_j^{\mathrm{H,min}}, \tag{A.13}$$

$$U_j^{\mathrm{H}} \le \delta_j^{\mathrm{H}} U_j^{\mathrm{H,max}}, \tag{A.14}$$

$$U_i^{\mathrm{C}} \ge \delta_i^{\mathrm{C}} U_i^{\mathrm{C,min}}, \tag{A.15}$$

$$U_i^{\mathrm{C}} \le \delta_i^{\mathrm{C}} U_i^{\mathrm{C,max}}, \tag{A.16}$$

$$U_{\mathrm{tot}}^{\mathrm{H,max}} \ge \sum_{j=1}^{n_{\mathrm{C}}} U_j^{\mathrm{H}}, \tag{A.17}$$

$$U_{\mathrm{tot}}^{\mathrm{C,max}} \ge \sum_{i=1}^{n_{\mathrm{H}}} U_i^{\mathrm{C}}, \tag{A.18}$$

$$\Delta T^{\mathrm{H}}_{ijk} \geq \Delta T_{\min} + \left(1 - \delta_{ijk}\right) \alpha, \tag{A.19}$$

$$\Delta T^{\mathrm{C}}_{ijk} \geq \Delta T_{\min} + \left(1 - \delta_{ijk}\right) \alpha, \tag{A.20}$$

$$\frac{U^{\mathrm{H}}_j}{C^{\mathrm{C}}_{\mathrm{p},j}} \geq \Delta T^{\mathrm{U}}_{\min} + \left(1 - \delta^{\mathrm{H}}_j\right) \alpha, \tag{A.21}$$

$$\frac{U^{\mathrm{C}}_i}{C^{\mathrm{H}}_{\mathrm{p},i}} \geq \Delta T^{\mathrm{U}}_{\min} + \left(1 - \delta^{\mathrm{C}}_i\right) \alpha, \qquad \text{and} \tag{A.22}$$

$$n_{\max} \geq \sum_{i=1}^{n_{\mathrm{H}}} \sum_{j=1}^{n_{\mathrm{C}}} \sum_{k=1}^{n_{\mathrm{R}}} \delta_{ijk}. \tag{A.23}$$

Since the MILP model maximizes energy recovery, its most basic version can be written as follows:

$$\begin{aligned} &\max \sum_{i=1}^{n_{\mathrm{H}}} \sum_{j=1}^{n_{\mathrm{C}}} \sum_{k=1}^{n_{\mathrm{R}}} E_{ijk} \\ &\quad \text{such that} \\ &\quad (A.1) - (A.23) \\ &\quad E_{ijk} \geq 0,\ U^{\mathrm{C}}_i \geq 0,\ U^{\mathrm{H}}_j \geq 0; \quad i = 1, \ldots, n_{\mathrm{H}},\ j = 1, \ldots, n_{\mathrm{C}},\ k = 1, \ldots, n_{\mathrm{R}}. \end{aligned} \tag{A.24}$$

Nonetheless, the actual optimization model – written for example in GAMS (GAMS Development Corporation, Inc., 2012) – might include a lot more. It could check all possible networks with the number of repetitive units between one and their maximum allowed count and, to avoid non-linearities, verify feasibility of heat transfer areas using an external application. This approach is necessary because heat transfer equation containing the non-linear logarithmic mean temperature difference (LMTD) is required for this to be done. It should also be noted here that the formula for LMTD can give wrong results when temperature differences at hot and cold sides of heat exchangers are close and finite arithmetic is used (error can commonly be as high as 30–50 %; see Gomiz, 2006). Although Akman et al. (2002) and Pettersson (2008) demonstrated that it is possible to construct LMTD-free MILP models, either the complexity of such approaches or the introduced imprecision were considerable. Using Gomiz's formally rewritten (but still non-linear) formula for LMTD therefore seems to be the best choice as far as relatively simple optimization models such as this one are concerned. Finally, driving force plots for all remaining feasible solutions could be generated by the very same external application.

The second, MINLP (mixed-integer non-linear programming) model is similar. However, because it supports stream splitting, we must also perform flowing heat capacity balances for every split stream in every repetitive unit and calculate temperatures of streams leaving each repetitive unit (due to mixing of sub-streams) – hence the non-linearity. If we wanted, we might even introduce lower limit on split stream fractions, upper limit on the number of splits, and so on. For the sake of brevity, we will not provide all the necessary equations here, but at least some of them are mentioned below.

As we are working with the superstructure from Figure A.2, $\delta_{ijk} = 1$ now denotes existence of the heat exchanger connecting jth sub-stream of ith hot stream with ith sub-stream of jth

cold stream in kth repetitive unit. Should $\delta_{ijk}=0$ then such an exchanger is not present in the network. Balances of flowing heat capacities can therefore be written as

$$C^{\mathrm{H}}_{\mathrm{p},i}=\sum_{j=1}^{n_{\mathrm{C}}} C^{\mathrm{H}}_{\mathrm{p},ijk} \qquad i=1,\ldots,n_{\mathrm{H}},\ k=1,\ldots,n_{\mathrm{R}} \tag{A.25}$$

$$C^{\mathrm{C}}_{\mathrm{p},j}=\sum_{i=1}^{n_{\mathrm{H}}} C^{\mathrm{C}}_{\mathrm{p},ijk} \qquad j=1,\ldots,n_{\mathrm{C}},\ k=1,\ldots,n_{\mathrm{R}}, \tag{A.26}$$

where, for kth repetitive unit, $C^{\mathrm{H}}_{\mathrm{p},ijk}$ is the flowing heat capacity of jth sub-stream of ith hot stream and $C^{\mathrm{C}}_{\mathrm{p},ijk}$ is the flowing heat capacity of ith sub-stream of jth cold stream. Similarly, with $F_{\min}\in(0;1)$ being the minimum allowed split stream fraction, $i=1,\ldots,n_{\mathrm{H}}$, $j=1,\ldots,n_{\mathrm{C}}$, $k=1,\ldots,n_{\mathrm{R}}$, and

$$C^{\mathrm{H}}_{\mathrm{p},ijk}\leq\delta_{ijk}C^{\mathrm{H}}_{\mathrm{p},i} \tag{A.27}$$

$$C^{\mathrm{H}}_{\mathrm{p},ijk}\geq\delta_{ijk}F_{\min}C^{\mathrm{H}}_{\mathrm{p},i} \tag{A.28}$$

$$C^{\mathrm{C}}_{\mathrm{p},ijk}\leq\delta_{ijk}C^{\mathrm{C}}_{\mathrm{p},j} \tag{A.29}$$

$$C^{\mathrm{C}}_{\mathrm{p},ijk}\geq\delta_{ijk}F_{\min}C^{\mathrm{C}}_{\mathrm{p},j} \tag{A.30}$$

we would make sure that sub-streams exist only if the related heat exchangers exist and that in such a case the sub-streams are large enough. Maximum number of splits, $S_{\max}$, could be enforced for example with

$$\begin{aligned} S_{\max}\geq\sum_{k=1}^{n_{\mathrm{R}}}\Bigg[&\sum_{i=1}^{n_{\mathrm{H}}}\left(1-\prod_{j=1}^{n_{\mathrm{C}}}\left(1-\delta_{ijk}\right)\right)\left(\sum_{j=1}^{n_{\mathrm{C}}}\delta_{ijk}-1\right)+\\ &+\sum_{j=1}^{n_{\mathrm{C}}}\left(1-\prod_{i=1}^{n_{\mathrm{H}}}\left(1-\delta_{ijk}\right)\right)\left(\sum_{i=1}^{n_{\mathrm{H}}}\delta_{ijk}-1\right)\Bigg]. \end{aligned} \tag{A.31}$$

Right hand side of the equation above yields the number of sub-streams necessary in addition to the main streams. In other words, if we considered only a single stream in a single repetitive unit and one sub-stream was present, that is, if splitting was not necessary, then we would get zero. If two sub-streams were required then one split would have to be made and thus we would get one and so on.

Obviously, if we wanted to minimize total annual cost then cost coefficients[2] would be necessary. In such case, however, we might want to opt for a two-stage implementation. Maximum possible energy recovery would first be determined using the previously mentioned MILP model. Subsequently, a HEN design with minimum total annual cost ensuring MER would be found by the MINLP model. Due to its non-linearity, this model is suitable for rather

[2]For instance, to estimate total cost of a shell-and-tube heat exchanger, the model might use the formula presented in (Ahmad et al., 1990), i.e., Cost = (fixed cost) + (cost of 1 m^2) $\cdot$ (heat transfer area)$^{\text{(area cost exponent)}}$. Besides this one there are many other relations available for many different types of heat exchangers; see for example (Couper et al., 1990), (Hall et al., 1990), (Peters et al., 2002), or (Kilkovský, 2008).

small networks, e.g. in waste-to-energy plants, but can directly incorporate the heat transfer area feasibility check. Obtained solutions could, by all means, be again passed to an external application for post-processing.

A.3 Post-Processing of Solutions

Ideally, stream temperatures on both sides of a heat exchanger plotted into composite curves should constitute vertical lines. Considering a network of heat exchangers, this "verticality" of heat transfer ensures minimum heat exchange area with corresponding minimum number of units. However, in practice this leads to a prohibitively large number of matches and thus the designs usually have near minimum number of exchangers and are expected only to approach – rather than meet exactly – the ideal temperature differences (see Ahmad and Smith, 1989). These authors also noted that a match of process streams with excess driving force may itself require a low number of units and low area, but will cause subsequent matches to have small temperature differences, leading to a net increase in number of heat exchangers and area for the network. Since heat transfer verticality can be evaluated using a driving force plot (DFP; see Linnhoff and Vredeveld, 1984), we will describe this technique now.

Having created hot and cold composite curves, DFP can be obtained by simply plotting the data into $T^{\mathrm{C}}_{\mathrm{cc}} - (T^{\mathrm{H}}_{\mathrm{cc}} - T^{\mathrm{C}}_{\mathrm{cc}})$ axes, where $T^{\mathrm{H}}_{\mathrm{cc}}$ and $T^{\mathrm{C}}_{\mathrm{cc}}$ denote temperatures on hot and cold composite curve, respectively. To draw a trapezoid representing a heat exchanger into the driving force plot, one uses inlet and outlet temperatures of the corresponding hot and cold streams flowing through that particular exchanger. Ratio of the area of this trapezoid and the area under DFP curve in the same interval of $T^{\mathrm{C}}_{\mathrm{cc}}$ indicates how well that particular exchanger is placed. The closer it is to unity the better. Figure A.4 shows sample composite curves of a certain heat exchanger network and Figure A.5 the corresponding driving force plot with three trapezoids representing heat exchangers. It seems that a simple sum of absolute values of $\log_{10}$(exchanger indicator) related to all exchangers in a particular network is a suitable overall heat transfer verticality indicator for that network. Results closer to zero indicate better HEN designs.

In addition to driving force plot construction and subsequent heat transfer verticality check, any other required task can be performed by the respective external application. What is more, since the application can be called on-the-fly from within the implemented model and return data back, there can be more of them called as necessary at any point to perform tasks involving operations that the modelling system might not handle well.[3]

A.4 Sample HEN Synthesis Problem

Let us consider a sample HEN synthesis problem specified in Table A.1 with $\Delta T_{\mathrm{min}} = 20\,^{\circ}\mathrm{C}$. Limiting the maximum allowed number of repetitive units to two and maximum allowed number of heat exchangers to five, MILP model returns the solution in Figure A.6 as the best

[3] In GAMS, for example, larger numbers of accesses to individual elements of matrices produce significant delay. Even though data exchange between GAMS and an external applications via GDX I/O API (GAMS Data Exchange I/O Application Programming Interface; see documentation available at [GAMS installation folder]\apifiles\gdx\) takes some time, this is amply compensated by the time saved by performing the task outside the modelling system.

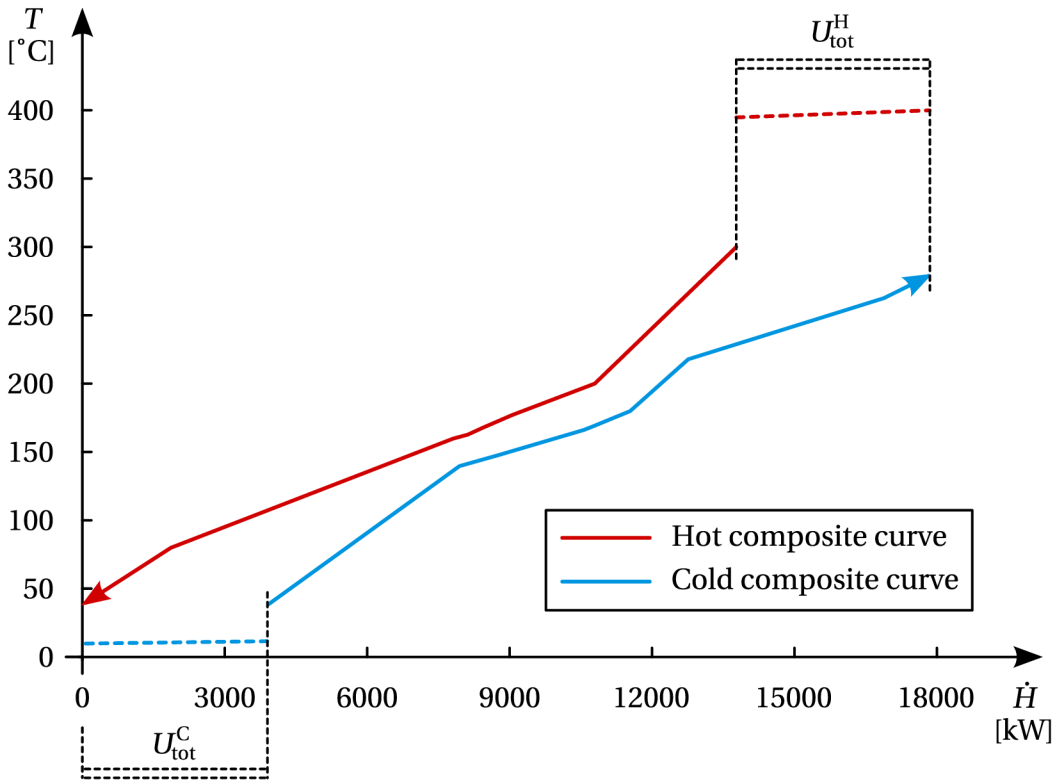

Figure A.4. Composite curves; dashed parts of curves represent utility heat exchangers

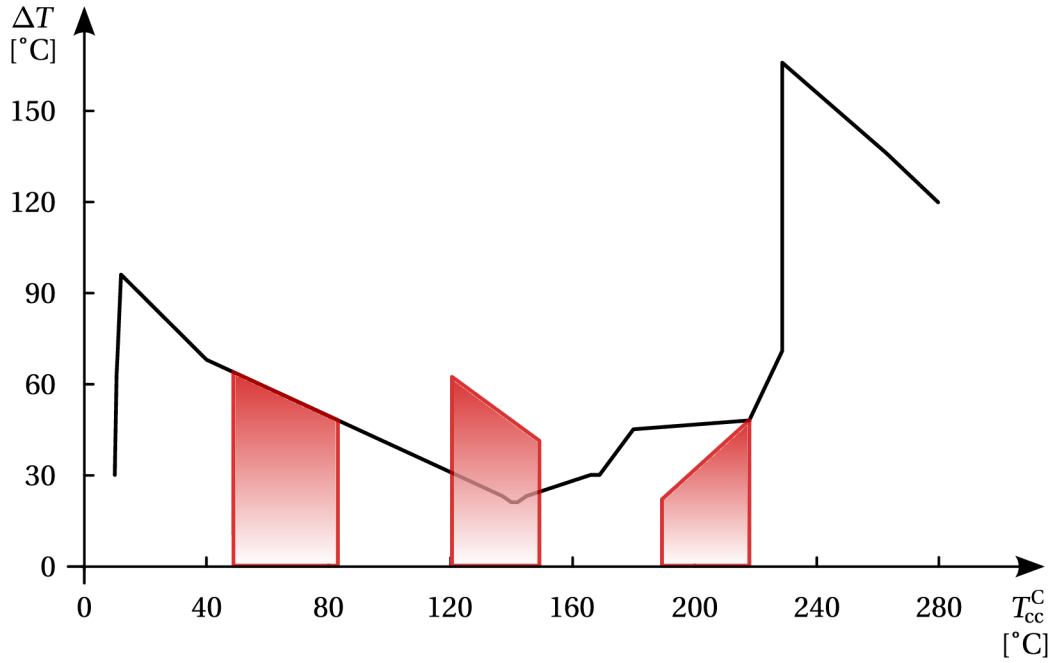

Figure A.5. Driving force plot for composite curves in Figure A.4. The left trapezoid represents a well placed heat exchanger while the middle and the right one represent exchangers that use excess and deficit driving force, respectively.

Table A.1. Stream parameters for the sample HEN synthesis problem

Stream	Stream No.	Source temperature [°C]	Target temperature [°C]	Flowing heat capacity [kW/°C]
hot	1	300	80	30
	2	200	40	45
cold	1	40	180	40
	2	140	280	60

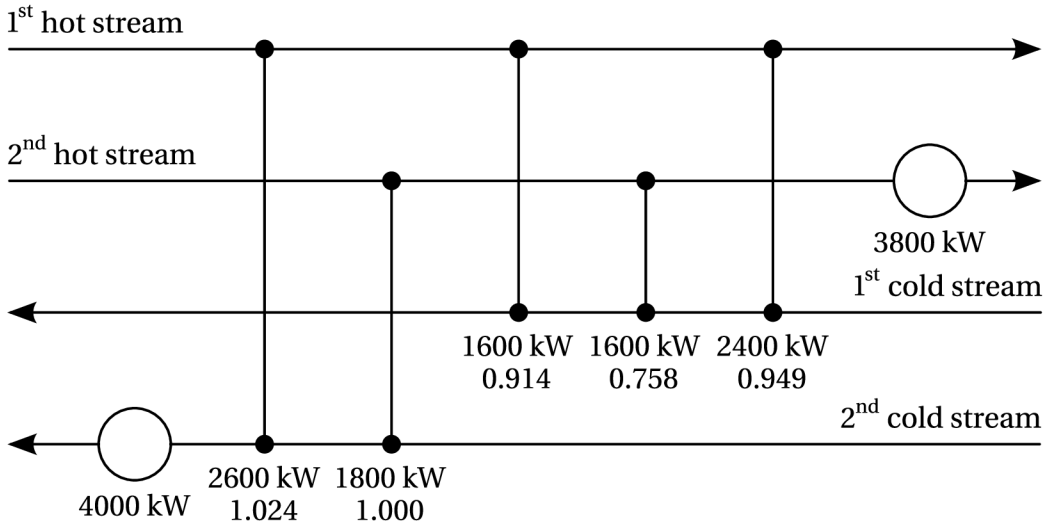

Figure A.6. Grid diagram of the best solution to the sample problem obtained with the MILP optimization model. Numbers below heat exchanger duties denote individual heat transfer verticality indicators.

one in mere eight seconds on a PC with an old single-core AMD Athlon 3200+ CPU. Energy recovery is 10 MW and the overall heat transfer verticality indicator is 0.192.

Following the heuristic rules of pinch analysis, one gets the solution in Figure A.7. It can be easily seen that energy recovery is identical and that left parts of the grid diagrams are essentially the same. Nevertheless, this may not always be the case. Although there are four common heat exchangers now, the number of utility units has increased by one. The main difference, however, is in the verticality of heat transfer (the overall heat transfer verticality indicator is 0.279). Considering the two rightmost common exchangers in the grid diagram obtained with the MILP model, it is much closer to the ideal case.

The solution in Figure A.8 with a slightly lower energy recovery (9.84 MW) is obtained when running the same problem through the MINLP model. This decrease is due to the different superstructure configuration – when stream splitting is allowed, one must increase the maximum feasible number of repetitive units to get a solution with energy recovery at least the same as the one yielded by the MILP model. The solution is the best one in terms of energy recovery, total annual costs (1.082 million USD), and overall heat transfer verticality indicator (0.428). Optimization time ranges from a few minutes to half an hour depending

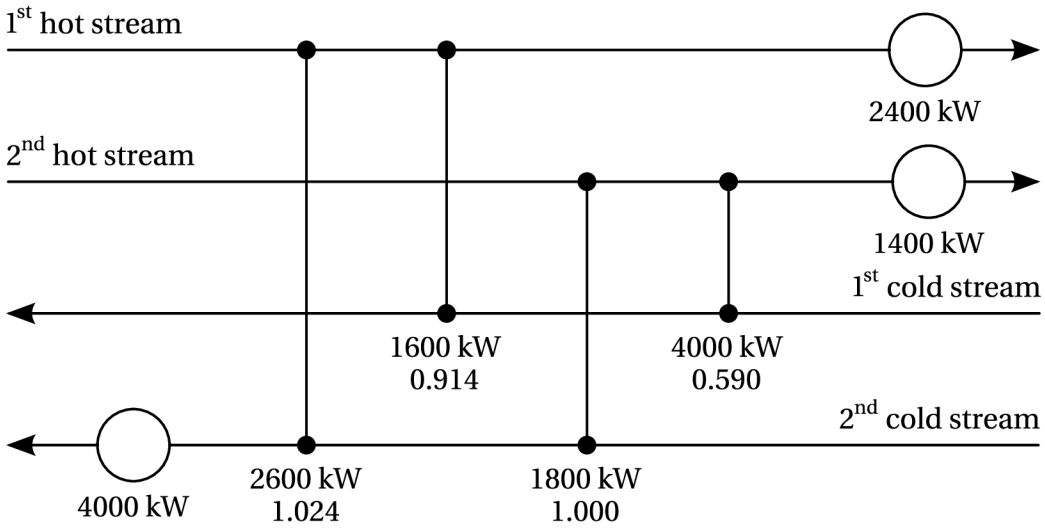

Figure A.7. Grid diagram of the solution to the sample problem obtained with pinch analysis. Numbers below heat exchanger duties denote individual heat transfer verticality indicators.

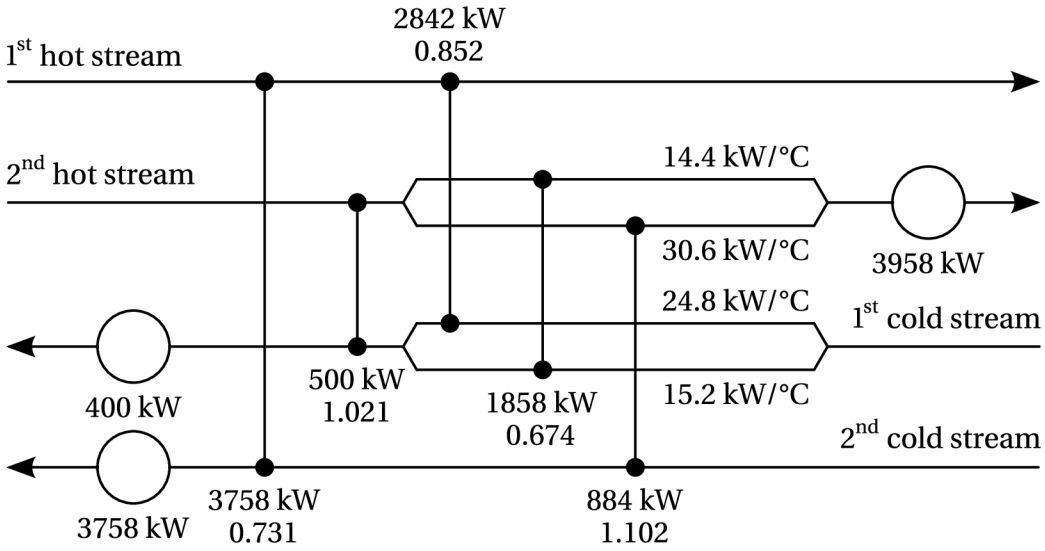

Figure A.8. Grid diagram of the best solution to the sample problem obtained with the MINLP optimization model. Numbers below heat exchanger duties denote individual heat transfer verticality indicators.

on how well the variable space is initially constrained, i.e., whether intervals for variables are provided and, if so, how short these are.

Using the same cost coefficients, total annual cost would in the first two cases be 1.003 million USD (MILP model) and 1.036 million USD (pinch analysis). These values suggest that solutions without split streams are better in this particular case. However, the cost coefficients might not have been accurate enough in this particular example. One should always verify them before making a final decision.

Clearly, the advantage of the optimization approach over pinch analysis is that once a model is built, HEN synthesis and construction of driving force plots are effortless tasks. More than one solution with the same energy recovery is usually available due to the combinatorial nature of the problem and comparing them manually might be laborious. Adding an algorithm that would sort feasible solutions according to our set of criteria is therefore beneficial.

A.5 Summary

The purpose of the presented simple optimization models is to perform automated synthesis of heat exchanger networks based on given input values. Since there can be many solutions matching optimization criteria (e.g. maximum energy recovery) while varying in quality, algorithm selecting the best possible HEN design from the obtained ones should be a part of the models as well. A relaxation mechanism – e.g. one of those presented by Kocis and Grossmann (1987), Björk and Westerlund (2002), or Bergamini et al. (2008, 2007) – might improve optimization times. Also, adding support for media phase changes would considerably broaden the applicability of the models.

Bibliography

ADJIMAN C., ANDROULAKIS I. and FLOUDAS C. (1997) Global optimization of MINLP problems in process synthesis and design, *Computers & Chemical Engineering* **21**(Supplement 1), S445–S450.

AHMAD S., LINNHOFF B. and SMITH R. (1990) Cost optimum heat exchanger networks – 2. Targets and design for detailed capital cost models, *Computers & Chemical Engineering* **14**(7), 751–767.

AHMAD S. and SMITH R. (1989) Targets and design for minimum number of shells in heat exchanger networks, *Chemical Engineering Research & Design* **67**(5), 481–494.

AKMAN U., UYGUN K., UZTÜRK D. and KONUKMAN A. (2002) HEN optimizations without using logarithmic-mean-temperature difference, *AIChE Journal* **48**(3), 596–606.

ATALLAH M. and BLANTON M. (2009) *Algorithms and Theory of Computation Handbook*, CRC Press, LLC, Boca Raton, FL, USA, 2nd edn.

AZEEZ O., ISAFIADE A. and FRASER D. (2012) Supply and target based superstructure synthesis of heat and mass exchanger networks, *Chemical Engineering Research and Design* **90**(2), 266–287.

BERGAMINI M., GROSSMANN I., SCENNA N. and AGUIRRE P. (2008) An improved piecewise outer-approximation algorithm for the global optimization of MINLP models involving concave and bilinear terms, *Computers & Chemical Engineering* **32**(3), 477–493.

BERGAMINI M., SCENNA N. and AGUIRRE P. (2007) Global optimal structures of heat exchanger networks by piecewise relaxation, *Industrial & Engineering Chemistry Research* **46**(6), 1752–1763.

Björk K. and Westerlund T. (2002) Global optimization of heat exchanger network synthesis problems with and without the isothermal mixing assumption, *Computers & Chemical Engineering* **26**(11), 1581–1593.

Bogataj M. and Kravanja Z. (2012) An alternative strategy for global optimization of heat exchanger networks, *Applied Thermal Engineering* **43**, 75–90.

Castier M. (2012) Rigorous multiple utility targeting in heat exchanger networks, *Energy Conversion and Management* **59**, 74–85.

Centre for Process Integration, University of Manchester, UK (2012) SPRINT – Simulation, optimisation, control and flexibility of heat exchanger networks (online), `http://www.ceas.manchester.ac.uk/research/centres/centreforprocessintegration/software/packages/sprint/`, accessed: 26 August 2012.

Ciric A. and Floudas C. (1991) Heat exchanger network synthesis without decomposition, *Computers & Chemical Engineering* **15**(6), 385–396.

Coletti F., Macchietto S. and Polley G. (2011) Effects of fouling on performance of retrofitted heat exchanger networks: A thermo-hydraulic based analysis, *Computers & Chemical Engineering* **35**(5), 907–917.

Couper J., Penney W., Fair J. and Walas S. (1990) *Chemical Process Equipment: Selection and Design*, Butterworth-Heinemann, Burlington, MA, USA.

Drobež R., Pintarič Z., Pahor B. and Kravanja Z. (2012) Simultaneous synthesis of a biogas process and heat exchanger network, *Applied Thermal Engineering* **43**, 91–100.

Errico M., Maccioni S., Tola G. and Zuddas P. (2007) A deterministic algorithm for the synthesis of maximum energy recovery heat exchanger network, *Computers & Chemical Engineering* **31**(7), 773–781.

Fieg G., Luo X. and Jeżowski J. (2009) A monogenetic algorithm for optimal design of large-scale heat exchanger networks, *Chemical Engineering and Processing: Process Intensification* **48**(11–12), 1506–1516.

Floudas C., Ciric A. and Grossmann I. (1986) Automatic synthesis of optimum heat exchanger network configurations, *AIChE Journal* **32**(2), 276–290.

Furman K. and Sahinidis N. (2001) Computational complexity of heat exchanger network synthesis, *Computers & Chemical Engineering* **25**(9–10), 1371–1390.

GAMS Development Corporation, Inc. (2012) *GAMS – A User's Guide*, GAMS Development Corporation, Inc., Washington, DC, USA.

Gillham M. and Sennik L. (1984) Selecting elastomers for plate heat exchanger gaskets, *Materials & Design* **5**(4), 181–185.

Gomiz A. (2006) Computation of the logarithmic mean temperature difference, *Journal of Heat Transfer* **128**(1), 84–86.

GUPTA A. and GHOSH P. (2010) A randomized algorithm for the efficient synthesis of heat exchanger networks, *Computers & Chemical Engineering* **34**(10), 1632–1639.

HALL S., AHMAD S. and SMITH R. (1990) Capital cost targets for heat exchanger networks comprising mixed materials of construction, pressure ratings and exchanger types, *Computers & Chemical Engineering* **14**(3), 319–335.

HASAN M., KARIMI I. and ALFADALA H. (2009) Synthesis of heat exchanger networks involving phase changes, in ALFADALA H., REKLAITIS G. and EL-HALWAGI M. (Eds.) *Proceedings of the 1st Annual Gas Processing Symposium, Doha, Qatar, 10 – 12 January 2009*, pp. 185–192, Elsevier.

HECKL I., FRIEDLER F. and FAN L. (2005) Integrated synthesis of optimal separation and heat exchanger networks involving separations based on various properties, *Heat Transfer Engineering* **26**(5), 25–41.

HUANG K., AL-MUTAIRI E. and KARIMI I. (2012) Heat exchanger network synthesis using a stagewise superstructure with non-isothermal mixing, *Chemical Engineering Science* **73**, 30–43.

HWA C. (1965) Mathematical formulation and optimization of heat exchanger networks using separable programming, in *AIChE-IChemE Symposium Series 4*, pp. 101–106, American Institute of Chemical Engineers.

ISAFIADE A. and FRASER D. (2010) Interval based MINLP superstructure synthesis of heat exchanger networks for multi-period operations, *Chemical Engineering Research and Design* **88**(10), 1329–1341.

JEGLA Z., KILKOVSKÝ B. and STEHLÍK P. (2010) Calculation tool for particulate fouling prevention of tubular heat transfer equipment, *Heat Transfer Engineering* **31**(9), 757–765.

KEMP I. (2006) *Pinch Analysis and Process Integration: A User Guide on Process Integration for the Efficient Use of Energy*, Butterworth-Heinemann, Inc., Burlington, MA, USA, 2nd edn.

KILKOVSKÝ B. (2008) Modelování zařízení pro výměnu tepla v procesech termického zpracování [Modelling of equipment for heat exchange in thermal treatment processes], Ph.D. thesis, Brno University of Technology, in Czech.

KLEMEŠ J., DHOLE V., RAISSI K., PERRY S. and PUIGJANER L. (1997) Targeting and design methodology for reduction of fuel, power and CO_2 on total sites, *Applied Thermal Engineering* **17**(8–10), 993–1003.

KLEMEŠ J., FRIEDLER F., BULATOV I. and VARBANOV P. (2010) *Sustainability in the Process Industry: Integration and Optimization*, McGraw-Hill, Inc., New York, NY, USA.

KLEMEŠ J. and PTÁČNÍK R. (1985) Computer-aided synthesis of heat exchange network, *Journal of Heat Recovery Systems* **5**(5), 425–435.

KOCIS G. and GROSSMANN I. (1987) Relaxation strategy for the structural optimization of process flow sheets, *Industrial & Engineering Chemistry Research* **26**(9), 1869–1880.

Kovač Kralj A. (2010) Optimization of an industrial retrofitted heat exchanger network, using a stage-wise model, *Energy* **35**(12), 4748–4753.

Laukkanen T. and Fogelholm C. (2011) A bilevel optimization method for simultaneous synthesis of medium-scale heat exchanger networks based on grouping of process streams, *Computers & Chemical Engineering* **35**(11), 2389–2400.

Laukkanen T., Tveit T. and Fogelholm C. (2012a) Simultaneous heat exchanger network synthesis for direct and indirect heat transfer inside and between processes, *Chemical Engineering Research and Design* **90**(9), 1129–1140.

Laukkanen T., Tveit T., Ojalehto V., Miettinen K. and Fogelholm C. (2010) An interactive multi-objective approach to heat exchanger network synthesis, *Computers & Chemical Engineering* **34**(6), 943–952.

Laukkanen T., Tveit T., Ojalehto V., Miettinen K. and Fogelholm C. (2012b) Bilevel heat exchanger network synthesis with an interactive multi-objective optimization method, *Applied Thermal Engineering* **48**, 301–316.

Linnhoff B. and Hindmarsh E. (1983) The pinch design method for heat exchanger networks, *Chemical Engineering Science* **38**(5), 745–763.

Linnhoff B. and Vredeveld R. (1984) Pinch technology has come of age, *Chemical Engineering Progress* **80**(7), 33–40.

Liu L., Du J., El-Halwagi M., Ponce-Ortega J. and Yao P. (2012) A simultaneous synthesis method for combined heat and mass exchange networks, in Karimi I. and Srinivasan R. (Eds.) *Computer Aided Chemical Engineering*, vol. 31, pp. 185–189.

Liu L., Du J., Xiao F., Chen L. and Yao P. (2011) Direct heat exchanger network synthesis for batch process with cost targets, *Applied Thermal Engineering* **31**(14–15), 2665–2675.

López-Maldonado L., Ponce-Ortega J. and Segovia-Hernández J. (2011) Multiobjective synthesis of heat exchanger networks minimizing the total annual cost and the environmental impact, *Applied Thermal Engineering* **31**(6–7), 1099–1113.

Luo X., Wen Q. and Fieg G. (2009) A hybrid genetic algorithm for synthesis of heat exchanger networks, *Computers & Chemical Engineering* **33**(6), 1169–1181.

Markowski M., Trafczynski M. and Urbaniec K. (2012) Identification of the influence of fouling on the heat recovery in a network of shell and tube heat exchangers, *Applied Energy*, **in press**, DOI: 10.1016/j.apenergy.2012.08.038.

Masso A. and Rudd D. (1969) The synthesis of system designs. II. Heuristic structuring, *AIChE Journal* **15**(1), 10–17.

Mastromanno S., Petrucci J. and Sciubba E. (2006) HENEA-3: A second law based expert assistant for the synthesis of heat exchanger networks, in *Proceedings of the 8th Biennial ASME Conference on Engineering Systems Design and Analysis, Torino, Italy, 4 – 7 July 2006*, American Society of Mechanical Engineers, paper ID ESDA2006-95765.

MORAVEC H. (1998) When will computer hardware match the human brain?, *Journal of Evolution and Technology* **1**(1), 1–12.

NAGY A., ADONYI R., HALASZ L., FRIEDLER F. and FAN L. (2001) Integrated synthesis of process and heat exchanger networks: algorithmic approach, *Applied Thermal Engineering* **21**(13–14), 1407–1427.

OJANIEMI U., RIIHIMÄKI M., MANNINEN M. and PÄTTIKANGAS T. (2012) Wall function model for particulate fouling applying XDLVO theory, *Chemical Engineering Science* **84**, 57–69.

PAN M., BULATOV I., SMITH R. and KIM J. (2012a) Novel MILP-based iterative method for the retrofit of heat exchanger networks with intensified heat transfer, *Computers & Chemical Engineering* **42**, 263–276.

PAN M., BULATOV I., SMITH R. and KIM J. (2012b) Optimisation for the retrofit of large scale heat exchanger networks with different intensified heat transfer techniques, *Applied Thermal Engineering*, **in press**, DOI: 10.1016/j.applthermaleng.2012.04.038.

PETERS M., TIMMERHAUS K. and WEST R. (2002) *Plant Design and Economics for Chemical Engineers*, McGraw-Hill, Inc., New York, NY, USA, 5th edn.

PETTERSSON F. (2008) Heat exchanger network design using geometric mean temperature difference, *Computers & Chemical Engineering* **32**(8), 1726–1734.

PONCE-ORTEGA J., JIMÉNEZ-GUTIÉRREZ A. and GROSSMANN I. (2008) Optimal synthesis of heat exchanger networks involving isothermal process streams, *Computers & Chemical Engineering* **32**(8), 1918–1942.

PTÁČNÍK R. and KLEMEŠ J. (1988) An application of mathematical optimization methods in heat-exchange network synthesis, *Computers & Chemical Engineering* **12**(2–3), 231–235.

RAVAGNANI M. and SILVA A. (2012) Retrofit of heat exchanger networks including the detailed equipment design, in KARIMI I. and SRINIVASAN R. (Eds.) *Computer Aided Chemical Engineering*, vol. 31, pp. 235–239.

REZAEI E. and SHAFIEI S. (2009) Heat exchanger networks retrofit by coupling genetic algorithm with NLP and ILP methods, *Computers & Chemical Engineering* **33**(9), 1451–1459.

SERNA-GONZÁLEZ M. and PONCE-ORTEGA J. (2011) Total cost target for heat exchanger networks considering simultaneously pumping power and area effects, *Applied Thermal Engineering* **31**(11–12), 1964–1975.

SIKOS L. and KLEMEŠ J. (2010) Reliability, availability and maintenance optimisation of heat exchanger networks, *Applied Thermal Engineering* **30**(1), 63–69.

SILVA A., RAVAGNANI M., BISCAIA E. and CABALLERO J. (2009) Optimal heat exchanger network synthesis using particle swarm optimization, *Optimization and Engineering* **11**(3), 459–470.

SMITH R., JOBSON M. and CHEN L. (2010) Recent development in the retrofit of heat exchanger networks, *Applied Thermal Engineering* **30**(16), 2281–2289.

Soltani H. and Shafiei S. (2011) Heat exchanger networks retrofit with considering pressure drop by coupling genetic algorithm with LP (linear programming) and ILP (integer linear programming) methods, *Energy* **36**(5), 2381–2391.

Ten Broeck H. (1944) Economic selection of exchanger sizes, *Industrial & Engineering Chemistry* **36**(1), 64–67.

Toffolo A. (2009) The synthesis of cost optimal heat exchanger networks with unconstrained topology, *Applied Thermal Engineering* **29**(17–18), 3518–3528.

Trivedi K., O'Neill B., Roach J. and Wood R. (1997) A best-first search strategy for energy relaxation in MER heat exchanger networks, *Engineering Optimization* **16**(3), 165–189.

Varbanov P., Fodor Z. and Klemeš J. (2012) Total site targeting with process specific minimum temperature difference ($\Delta T_{\min}$), *Energy* **44**(1), 20–28.

Varbanov P. and Klemeš J. (2000) Rules for paths construction for HENs debottlenecking, *Applied Thermal Engineering* **20**(15–16), 1409–1420.

Wan Alwi S. and Manan Z. (2010) STEP – A new graphical tool for simultaneous targeting and design of a heat exchanger network, *Chemical Engineering Journal* **162**(1), 106–121.

Wan Alwi S., Manan Z. and Nam S. (2012a) A new method to determine the optimum heat exchanger network approach temperature, in Karimi I. and Srinivasan R. (Eds.) *Computer Aided Chemical Engineering*, vol. 31, pp. 190–194.

Wan Alwi S., Mohammad Rozali N., Manan Z. and Klemeš J. (2012b) A process integration targeting method for hybrid power systems, *Energy* **44**(1), 6–10.

Wang Y., Smith R. and Kim J. (2012) Heat exchanger network retrofit optimization involving heat transfer enhancement, *Applied Thermal Engineering* **43**, 7–13.

Xiao F., Du J., Liu L., Luan G. and Yao P. (2010) Simultaneous optimization of synthesis and scheduling of cleaning in flexible heat exchanger networks, *Chinese Journal of Chemical Engineering* **18**(3), 402–411.

Yee T. and Grossmann I. (1990) Simultaneous optimization models for heat integration – II. Heat exchanger network synthesis, *Computers & Chemical Engineering* **14**(10), 1165–1184.

Zhu X., Zanfir M. and Klemeš J. (2000) Heat transfer enhancement for heat exchanger network retrofit, *Heat Transfer Engineering* **21**(2), 7–18.

Nomenclature

Acronyms

CPU	central processing unit
CU	cold utility heat exchanger

DFP	driving force plot
E	common heat exchanger
HEN	heat exchanger network
HU	hot utility heat exchanger
LMTD	logarithmic mean temperature difference
MER	maximum energy recovery
MILP	mixed-integer linear programming
MINLP	mixed-integer non-linear programming
PC	personal computer
TAC	total annual cost

Latin letters

C_p	flowing heat capacity	[W/°C]
E	heat duty of common heat exchanger	[W]
F_{min}	minimum allowed split stream fraction	[–]
$\dot{H}$	temporal change of enthalpy of media	[W]
n	identification number of common heat exchanger	[–]
n_C	number of cold process streams	[–]
n_E	total number of heat exchangers in general HEN representation	[–]
n_H	number of hot process streams	[–]
n_{max}	maximum allowed number of common heat exchangers	[–]
n_R	number of repetitive units	[–]
S_{max}	maximum allowed number of stream splits	[–]
T	temperature	[°C]
T_{cc}	temperature on composite curve	[°C]
U	heat duty of utility heat exchanger	[W]

Greek letters

α	large enough negative value	[–]
δ	binary variable denoting existence of heat exchange unit	[–]
$\Delta T_{\min}$	minimum allowed temperature difference between hot and cold process streams	[°C]
$\Delta T_{\min}^{\mathrm{U}}$	minimum allowed temperature difference for utility units	[°C]

Subscripts

i, r	hot process stream
j, s	cold process stream
k, t	repetitive unit
tot	total

Superscripts

C	related to cold stream, cold utility, or cold composite curve
H	related to hot stream, hot utility, or hot composite curve
in	at stream inlet
max	maximum allowed value
min	minimum allowed value
out	at stream outlet
S	source
T	target

B

Contents of the CD

The attached CD contains

- PDF version of this thesis;
- multi-platform Java application “Distributor” including the source code with its documentation (see Section 3.4.1);
- Maple worksheet with pseudo-1D model of a parallel flow system (see Section 3.4.2); and
- multi-platform Java application “U-tube exchanger module” including the Quick start guide and source code with its documentation (see Section 3.4.3).

Each of the three tools mentioned above comes bundled with a “Readme.txt” file containing installation instructions and with a file specifying licensing conditions.

C

List of Author's Publications

Journals with Impact Factor

Turek V., Hájek J., Jegla Z. and Stehlík P. (2011) Optimum design of distribution systems in heat exchangers, *Asia-Pacific Journal of Chemical Engineering* **6**(5), 750–759.

Journals without Impact Factor

Turek V., Bělohradský P. and Jegla Z. (2012) Geometry optimization of a gas preheater inlet region – a case study, *Chemical Engineering Transactions* **29**(2), 1339–1344.

Turek V. and Jegla Z. (2010) Modified deterministic algorithm for automated HEN design in waste-to-energy applications, *Chemical Engineering Transactions* **21**(2), 847–852.

Turek V., Jegla Z. and Stehlík P. (2011) Alternative approach to modelling of fluid distribution in a parallel flow system, *Chemical Engineering Transactions* **25**(1), 237–242.

Turek V., Kohoutek J., Jegla Z. and Stehlík P. (2009) Contribution to analytical calculation methods for prediction of uniform fluid flow dividing in tubular distributor, *Chemical Engineering Transactions* **18**(2), 809–814.

Conference Papers

Kilkovský B., Turek V., Jegla Z. and Stehlík P. (2011) Aspects of fouling in case of heat exchangers with polluted gas, in *Proceedings of the 8th International Conference on Heat Transfer, Fluid Mechanics and Thermodynamics HEFAT2011, Pointe Aux Piments, Mauritius, 11 – 13 July 2011*, pp. 220–229, paper ID HXX.7.

Turek V., Jegla Z. and Kunc V. (2009a) Automatizovaný návrh výměníkové sítě pomocí modifikovaného deterministického modelu [Automated design of a heat exchanger network using a modified deterministic model], in *Proceedings of the 56th National Conference of Chemical and Process Engineering CHISA 2009, Srní, Czech Republic, 19 – 22 October 2009*, paper ID 33/V052, in Czech.

Turek V., Kohoutek J., Hájek J. and Jegla Z. (2010) Optimum design of distributor and collector in a specific U-tube heat exchanger, in *Proceedings of the 19th International Congress of Chemical and Process Engineering CHISA 2010, Prague, Czech Republic, 28 August – 1 September 2010*, paper ID 344/P7.253.

Turek V., Kohoutek J. and Jegla Z. (2009b) Příspěvek k řešení rovnoměrného rozdělení toku v trubkovém distributoru [A note on uniform flow distribution in a tubular manifold], in *Proceedings of the 56th National Conference of Chemical and Process Engineering CHISA 2009, Srní, Czech Republic, 19 – 22 October 2009*, paper ID 58/V053, in Czech.

Research Reports

Turek V., Kohoutek J. and Jegla Z. (2009) Optimální tvar distributoru s nekonstantním obdélníkovým příčným průřezem [Optimum geometry of a distributor having variable rectangular cross-section], report ID NPV2-V001-09-01, Institute of Process and Environmental Engineering, Faculty of Mechanical Engineering, Brno University of Technology, in Czech.